NASA Technical Memorandum 84609

Beaufort/Bering 1979 Microwave Remote Sensing Data Catalog Report - March 14-24, 1979

William S. Hirstein, Harold F. Hennigar,
Sally K. Schaffner, Victor E. Delnore,
and William L. Grantham

MAY 1983

25th Anniversary
1958-1983

NASA

NASA Technical Memorandum 84609

Beaufort/Bering 1979 Microwave Remote Sensing Data Catalog Report - March 14-24, 1979

William S. Hirstein
Bionetics Corporation
Hampton, Virginia

Harold F. Hennigar
Deepsea Ventures, Inc.
Gloucester Point, Virginia

Sally K. Schaffner
OAO Corporation
Hampton, Virginia

Victor E. Delnore
Kentron Technical Center
Kentron International, Inc.
Hampton, Virginia

William L. Grantham
Langley Research Center
Hampton, Virginia

NASA

National Aeronautics
and Space Administration

Scientific and Technical
Information Branch

1983

CONTENTS

SUMMARY

This report catalogs the airborne microwave remote sensing measurements obtained by the Langley Research Center in support of the 1979 Sea-Ice Radar Experiment (SIRE) in the Beaufort and Bering Seas. The remote sensing objective of SIRE was to define correlations between both active and passive microwave signatures and ice phenomena associated with practical applications in the Arctic. The instruments used by Langley during SIRE include the stepped frequency microwave radiometer (SFMR), the airborne microwave scatterometer (AMSCAT), the precision radiation thermometer (PRT-5), and metric aerial photography. Remote sensing data are inventoried and cataloged in a user-friendly format. The data catalog is presented as time-history plots of when and where data were obtained as well as the sensor configuration. All data are available on 9-track computer tapes in card-image format upon request to the National Technical Information Service (NTIS).

INTRODUCTION

This report catalogs the airborne remote sensing data sets obtained by the NASA Langley Research Center in support of the 1979 Sea-Ice Radar Experiment (SIRE). The remote sensing objective of SIRE was the determination of the correlations between both active and passive microwave signatures and ice phenomena, both surface and subsurface, associated with practical applications in the Arctic. The long-range goal of SIRE is the development of remote measurement techniques and sensor combinations capable of determining ice properties at the appropriate temporal and spatial frequencies.

Five flights were conducted during March 1979: three over the Beaufort Sea and two over the Bering Sea/Norton Sound. All flights were staged from Elmendorf AFB, Alaska, with refueling stops at Galena and King Salmon Air Stations, Alaska, and at Inuvik, N.W.T. All flights were made with the NASA C-130 aircraft (fig. 1) which was then assigned to Johnson Space Center as NASA 929 but is now assigned to Ames Research Center as NASA 707.

Figure 2 is a map of the waters surrounding Alaska, with flight lines indicated. A summary of data flight days is given in table I.

NASA Langley sensors onboard the C-130 aircraft were the 14.6-GHz airborne microwave scatterometer (AMSCAT) and the 4.5- to 7.2-GHz stepped frequency microwave radiometer (SFMR). Also, a thermal infrared radiometer (PRT-5), two Zeiss 6-inch focal length metric cameras, and a downward-looking altimetric laser were aboard. Another instrument, the 13.9-GHz radiometer/scatterometer (RADSCAT) (ref. 1) was onboard the C-130, but its data are not included in this report. These instruments are described in the next section.

DATA ORGANIZATION

The primary objective of this report is to present the remote sensing data collected on the mission in a user-friendly format. Data are organized by flight day and are referenced to Greenwich mean time (GMT). Data catalogs are presented as time-line plots indicating when and where the data were obtained as well as the sensor configuration. Photographic data are detailed in appendix A. All data have been inspected and time corrected, where appropriate, and are available on 9-track computer tapes in card-image format upon request to the National Technical Information Service (NTIS). (See appendix B.) Upon inspection of the time-line plots, a user can access a specific data segment by searching the tapes for the appropriate start and stop times. Selection of data for detailed analysis will depend upon the requirements of the user. The data have been organized so that selection is easiest if the user has a particular sensor configuration in mind or is interested in a particular geographic location. No detailed analysis has been attempted in this report, and users are urged to apply their own methods of analysis to the data. It is hoped that by making these data available, many alternative methods of analysis will be developed and applied. A bibliography is included which lists publications of general interest as well as those dealing specifically with NASA Langley instrumentation and the SIRE experiment.

SENSOR DESCRIPTIONS

Stepped Frequency Microwave Radiometer

The stepped frequency microwave radiometer (SFMR) is a precision, nadir-looking, circular polarized radiometer designed, developed, and fabricated by the Langley Research Center. The SFMR is believed to be the first variable-frequency microwave radiometer controlled by a digital microprocessor, which provides both radiometer control functions and real-time data processing. The radiometer antenna, microwave section, and signal processor are shown in figure 3. The front panel of the digital controller is shown in figure 4.

The SFMR is capable of operating at frequencies between 4.5 GHz and 7.2 GHz at intermediate frequency (IF) bandwidths of 10, 50, 250, or 1000 MHz and integration times from 0.2 to 20 s. The frequency can be varied in incremental steps from approximately 0.2 to 5 times the bandwidth per integration time. Several different frequencies and integration periods were used during the SIRE mission. The three ways in which frequency was varied were

1. Single-frequency runs: Only a single frequency was recorded. Frequencies of 5570, 5586, 6594, and 7186 MHz were used in this mission for single-frequency runs. Calibration factors for 5570, 5586, and 7186 MHz were obtained from laboratory calibrations. The calibration factor for 6594 MHz was obtained from a field "anchor point" calibration by using water at the ice edge as a reference.

2. Double-frequency runs: Two frequencies were alternated within a run. The two frequencies used in this mission for double-frequency runs were 5586 and 6594 MHz.

3. Multiple-frequency runs: The SFMR steps through nine frequencies within a run. These frequencies are determined according to the formula:

$$F = 5522 + \sum_{n=0}^{8} 32n$$

where F is given in megahertz.

Five different integration periods were used: 0.2, 0.5, 1.0, 2.0, and 5.0 s. Various combinations of frequency and integration time were used.

Analysis has shown that the SFMR exhibits an absolute precision of better than 2.0 K. Removal of absolute instrument bias was accomplished through comparison of the physical sea surface temperature calculated from the brightness temperature observed by the SFMR at the ice edge with the in situ sea surface temperature. Wind speed and sea surface salinity were taken into account in the calculation of sea surface temperature from brightness temperature. The ideal radiometer brightness temperature sensitivity of the instrument varies between 0.012 K and 1.25 K depending on the bandwidth and integration time selected for the SFMR. The measured radiometer sensitivity at 6.6 GHz was between 0.69 K and 0.88 K with 90-percent confidence and between 0.65 K and 0.94 K with 99-percent confidence. The ideal radiometer sensitivity at 6.6 GHz was 0.25 K. The radiometer was operating with a 50-MHz predetection filter bandwidth, a 0.2-s postdetection integration time, with five samples averaged during postflight data reduction to achieve a sample period of 1 s.

The SFMR is a balanced Dicke-switched square-wave correlated radiometer. The radiometer utilizes a closed-loop Type I noise feedback circuit to add noise to the received antenna noise and thereby balances to the Dicke reference noise. The microwave portion of the radiometer, including the broadband tunnel-diode low-noise amplifier, is maintained in a constant temperature enclosure at the Dicke reference temperature within ±0.10 K. A block diagram of the radiometer is shown in figure 5.

The antenna consists of a corrugated-wall broadband horn with a 10-dB beam width of approximately 20.5°. The antenna has a meander line polarizer to provide reception to circular polarization only. An 11-layer fiberglass honeycomb-sandwich radome is used as a pressure seal over the polarizing radome. The feed of the antenna is located within the constant-temperature enclosure, as is the noise injection circuit, which consists of a solid-state noise diode, isolator, PIN diode switch, and 20-dB directional coupler. The Dicke switch is a broadband latching circulator.

The receiver portion of the radiometer consists of a homodyne mixer, YIG-tuned local oscillator, and 1- to 1000-MHz IF amplifier. The microwave frequency of the radiometer is controlled by an 8-bit digital word from the digital subsystem that is converted to 0 to 10 V dc. This signal controls the voltage-tuned microwave oscillator. The frequency can be changed every 200 ms in steps of 16 MHz or greater over the frequency range from 4.018 GHz to 8.098 GHz. However, the antenna limits the usable frequency range to 4.500 GHz to 7.200 GHz. The bandwidth of the radiometer is selected by the digital subsystem using one of four paths through the filter bank.

The 1- to 1000-MHz constant-power-level noise signal is transformer coupled into a hot-carrier diode square-law detector in the analog signal processor. The detected noise signal is amplified and synchronously detected with the Dicke switching frequency. The resultant error signal is fed to a true integrator. The output of the integrator is filtered to remove the effect of the Dicke switching frequency and used to control the pulse train output of a voltage-to-frequency (V/F) converter.

The V/F converter provides a variable-duty-cycle 70-μs-pulse train. The pulse repetition frequency, from 0 to 10 000 pulses per second, varies linearly with the dc output voltage of the integrator. This pulse train is applied to the noise-injection PIN diode switch and controls the number of injected constant-amplitude, constant-width noise pulses, which are added to signals from the antenna. The digital subsystem measures the duty cycle of the pulse train to determine the noise added to the antenna noise.

The digital subsystem provides control functions to the radiometer, data processing of the output signal from the radiometer, and physical temperature measurements of several locations in the radiometer. It also provides front panel control functions and real-time displays for the operator. The radiometer data are formatted along with time, temperatures, and other operational data, and are recorded on a digital tape recorder. A parameter proportional to brightness temperature is computed by the microprocessor and displayed to the operator (ref. 2). The integration time of the radiometer is determined by the count periods of the injection time counters which compute the duty cycle of the radiometer output. The integration time of the closed-loop radiometer noise feedback is several times faster than the minimum integration time allowed by the digital subsystem.

Airborne Microwave Scatterometer

The airborne microwave scatterometer, AMSCAT (formerly known as SUS), is an active microwave remote sensor that was developed at the Langley Research Center to measure the normalized radar cross section of ocean, ice, and land targets. The scatterometer operates in a "long-pulse," or interrupted continuous wave, mode at a center frequency of 14.6 GHz. A simplified block diagram is shown in figure 6. AMSCAT is separated into three major assemblies: gimbal assembly, transmitter-receiver assembly, and rack-mounted electronics.

The gimbal assembly consists of a dual-linear polarized parabolic antenna (3.5° beam width), a two-axis servo-controlled pedestal (to provide independent elevation and azimuth positioning), and a multilayer fiberglass honeycomb radome. For SIRE, this assembly was mounted on the underside of the fuselage beneath the vertical stabilizer (tail section) of the NASA C-130 aircraft (fig. 7).

The transmitter-receiver assembly (fig. 8) consists of all the microwave hardware including circulator switches, a 1-W and a 20-W traveling wave tube (TWT) power amplifier, low-noise tunnel-diode amplifier, and a solid-state microwave source for generating the transmitter and receiver local oscillator signals. The system operation is digitally controlled by commands generated in the rack-mounted equipment (fig. 9).

The rack-mounted electronics (fig. 9) consists of power supplies, the gimbal controller, the signal processor, digital controller and data system, and an analog strip chart recorder. The signal processor (fig. 6) has two overlapping channels that provide a received power dynamic range of greater than 40 dB. A programmable attenuator is used as a coarse gain control to provide an additional 60-dB range. In each channel, the signals are square-law detected, integrated for 500 ms, and then analog-to-digital (A/D) converted and recorded with a 7-track digital recorder. The digital controller and data system is a microprocessor that generates the precise timing and control logic needed by the scatterometer to form radio frequency (RF) pulses, operate switches and range gates, and A/D convert scatterometer integrator voltages. The processor also formats aircraft parameters and radar data for recording. The use of this processor enables considerable flexibility in the selection of AMSCAT operating characteristics (table II) via an interactive programming mode. Table III lists the scatterometer processor statistics for both channels.

In making scatterometer measurements, the quantity of interest is the scattering coefficient σ^o. This quantity is independent of the type of radar performing the measurement and is defined from the radar equation as

$$\sigma^o = \frac{P_r}{P_t} \frac{(4\pi)^3 R^4}{G^2 \lambda^2 A_T L_s} \tag{1}$$

where

P_r	received power
P_t	transmitted power
G	antenna gain
R	slant range
L_s	miscellaneous losses due to couplers, waveguide, etc.
λ	free-space wavelength
A_T	effective antenna footprint on surface

For the AMSCAT case of beam-limited conditions,

$$A_T = \frac{\pi}{4} \frac{(\beta_{eq} R)^2}{\cos\,\theta} \tag{2}$$

where β_{eq} is the effective pencil-beam antenna width (approximately equal to the half-power antenna beam width) in radians and θ is the incidence angle. The scattering coefficient thus becomes

$$\sigma^o = \frac{P_r}{P_t} \frac{(16\pi)^2 R^2 \cos\,\theta}{G^2 \lambda^2 \beta_{eq}^2 L_s} \tag{3}$$

Refer to the block diagram of figure 6. The ratio P_r/P_t is measured in two steps. A sample of the transmitter power, attenuated by a known value GXR, when switched into the receiver produces a "calibration" output voltage V_{cal} proportional to P_t in each receiver channel. When the transmitter is connected to the antenna, an output voltage V_{sur} proportional to P_r is obtained in a particular channel. Solving for the received-to-transmitted power ratio (in terms of the voltage from a particular channel) yields

$$\frac{P_r}{P_t} = \frac{V_{sur}}{V_{cal}} \frac{(GXR)\alpha_{cal}}{\alpha_{sur}} \tag{4}$$

where

V	output voltage of integrator
α	programmable attenuator value
GXR	receiver calibration loop attenuation

and the subscripts denote

cal	during calibration
sur	during surface observation

Finally, in terms of the AMSCAT transfer function, the expression for σ^o is

$$\sigma^o = (16\pi)^2 \frac{H^2 V_{sur} \alpha_{cal} (GXR)}{\lambda^2 V_{cal} \alpha_{sur} G^2 \beta_{eq}^2 L_s \cos\theta} \tag{5}$$

where H is the altitude of the aircraft (antenna).

The σ^o value from equation (5) is in error because of inaccuracies in the determination of the instrument transfer coefficients (G, α, L_s, GXR, and β_{eq}) and the variables (H, θ, and V). This error can be separated into a bias and a random component. The accuracy of this bias determination is better than ±1 dB.

The major contributor to the random component of σ^o is V_{sur}. Because of Rayleigh fading of the received power from the surface, V_{sur} is an imperfect estimate of the mean received power used in the σ^o calculation (eq. (1)). The normalized standard deviation of the cross section is approximately

$$\frac{\Delta\sigma^o}{\sigma^o} = \frac{1}{\sqrt{N}} \tag{6}$$

The number of independent samples N is

$$N = \sqrt{\beta_d \tau} \tag{7}$$

where τ is integration time and β_d, Doppler bandwidth of received power, is

$$\beta_d = \frac{2V_{gr} f}{c}(\sin\theta_{max} - \sin\theta_{min}) \tag{8}$$

where

V_{gr}	aircraft ground speed
f	radar frequency
c	speed of light

For the SIRE mission, $\Delta\sigma^o/\sigma^o$ was less than ±0.5 dB.

Precision Radiation Thermometer

The precision radiation thermometer, referred to as the PRT-5, is a nadir-looking infrared radiometer used to remotely measure the physical temperature. The output of the PRT-5 is available on the 9-track digital tapes as surface temperature in degrees Celsius. Table IV summarizes the operating characteristics of the instrument used during the SIRE mission. Some of the PRT-5 data may not be usable, since temperatures lower than its minimum measurable range were encountered during SIRE. The user should consult reference 3 for a complete description of the instrument.

SENSOR GEOMETRY

To use the data obtained during the 1979 SIRE mission, sensor geometry and its effects on temporal and spatial alignment of the data must be understood. Figure 10 illustrates the arrangement of sensors onboard the C-130 aircraft during the SIRE mission. The stepped frequency microwave radiometer (SFMR), PRT-5, and aerial cameras are nadir-looking instruments; hence, the footprints of these instruments were directly beneath the aircraft. The airborne microwave scatterometer (AMSCAT), however, operated at a variety of incidence angles from 0^o to 54^o and was aimed behind the aircraft. For an incidence angle of 0^o, the AMSCAT was nadir looking; however, as the incidence angle increases, the AMSCAT footprint is translated backward along the flight line. Therefore, the SFMR, PRT-5, and aerial cameras will image an area before the AMSCAT. As stated previously, all sensors have been referenced to Greenwich mean time (GMT). This requires that a temporal correction be applied by the user to the AMSCAT data in order to align the data from all sensors on the same target. This correction is as follows:

$$\text{AMSCAT time (GMT)} = \text{NADIR time (GMT)} + \Delta t$$

where Δt is a function of aircraft altitude H, ground speed V_{gr}, and incidence angle θ of the AMSCAT. The temporal offset (Δt) can be calculated from the following equation:

$$\Delta t = \frac{H \tan \theta}{V_{gr}}$$

Altitude and ground speed must be in the same units (i.e., altitude in meters; ground speed in meters per second). Location of footprints on the aerial photography requires the calculation of the distance offset between the AMSCAT and the nadir-looking instruments. For the AMSCAT, the time recorded with a σ^o value indicates the centroid of the smeared footprint rather than instantaneous footprint. With the variables just described, the distance offset can be calculated from

$$\text{Distance offset} = H \tan \theta$$

The distance offset can be applied to the photography by converting to distance on the aerial photography by using the scale of the aerial photograph. For the 152.4-mm focal length camera used during SIRE,

$$\text{Photographic scale} = \frac{H}{\text{Focal length}}$$

For example, at an altitude of 1600 m the scale of the aerial photograph is 1:10500. At this scale, 1 cm on the photograph equals 105 m on the ground.

Footprint sizes of the instruments vary, with the aerial cameras having the largest footprints and the SFMR, AMSCAT, and PRT-5 having successively smaller footprints, all of which are contained within the camera footprint (i.e., photograph). Calculation of footprint sizes for the various sensors is described in the following paragraphs.

Instantaneous footprints of all sensors at nadir would be nearly circular, except that there is a smearing of the footprint in the direction of the flight line due to sensor data integration times. For example, the instantaneous 10-dB footprint (Beam width = 20.5^o = 0.37 rad) of the SFMR can be calculated from

$$\text{SFMR footprint diameter} = 0.37H$$

At an aircraft altitude of 1000 m, the SFMR instantaneous footprint would be a circle with a diameter of 370 m. The footprint is smeared, however, along the flight line by the distance the aircraft traveled during the signal integration time τ. At an aircraft ground speed of 114 m/s, the aircraft would have traveled 57 m over a 0.5-s integration period. Therefore, the SFMR footprint would approximate an ellipse (fig. 11) with the major axis along the flight line and the minor axis perpendicular to the flight line. For the SFMR, the time recorded with a data value indicates the centroid of the smeared footprint rather than the instantaneous footprint. Referring to figure 10, the footprint dimension perpendicular to the flight line A is

$$A = 0.37H$$

whereas the footprint dimension along the flight line B is

$$B = A + \tau V_{gr}$$

For an altitude of 1000 m, an integration time of 0.5 sec, and a ground speed of 114 m/s, footprint dimensions are as follows:

$$A = 370 \text{ m}$$

$$B = 427 \text{ m}$$

Footprints of the PRT-5, for all practical purposes, are circular since the integration time was less than 0.03 s.

For the PRT-5, footprint dimensions are

$$A = B = 0.035H$$

For an altitude of 1000 m and an aircraft ground speed of 114 m/s, footprint dimensions are

$$A = B = 35 \text{ m}$$

Calculation of footprint size for the AMSCAT is slightly different because, in addition to smearing along the flight line, the instrument is not nadir looking. The AMSCAT instantaneous footprint dimensions perpendicular to flight line A and along flight line B are given by

$$A = \frac{0.0612H}{\cos\theta}$$

$$B = \frac{A}{\cos\theta}$$

where θ is incidence angle. (The antenna 3.5-dB beam width expressed in radians is 0.0612.)

Again, for an aircraft in motion, there is smearing along the flight line and B becomes

$$B = \frac{A}{\cos\theta} + \tau V_{gr}$$

For an altitude of 1000 m, an aircraft ground speed of 114 m/s, and an incidence angle of 45°, the AMSCAT footprint size is

$$A = 86.5 \text{ m}$$

$B = 179.3$ m

It is important to consider that time recorded for each photograph indicates the position of the aircraft over the center of the photograph. If photography were obtained at the same time as a nadir-looking sensor recorded data, the sensor footprints would be located over the exact center of the aerial photograph. This will not always prove to be true and an adjustment must be made. Given the time of the aerial photograph ($t = 0$ s) and the time the nadir-looking instruments recorded data ($t = +1$ s), the sensor footprints will be located ahead of the center of the aerial photograph, relative to the direction of travel. At a speed of 114 m/s, the center of the nadir-looking sensor footprints would be approximately 114 m ahead of the center of the photograph. At a photographic scale of 1:10500, the footprint would be approximately 1.1 cm ahead of the center of the photograph for a 1-s time difference. Likewise, for photograph time = 0 and sensor time = -1 s, the sensor footprint would be located 114 m behind the center of the photograph, again relative to the direction of travel.

After the centers of the nadir-looking sensors have been located on the aerial photograph, the AMSCAT footprints may be located by using the distance and time offsets as calculated in this section.

After footprint sizes have been calculated for the various sensors at the appropriate altitudes, ground speeds, incidence angles, and integration times, templates of the footprints may be drawn at the scale of the photography for that section and transferred to clear acetate sheets. The acetate sheets can then be overlaid on the appropriate aerial photograph and used to locate footprints.

In summary, the process of locating microwave footprints on an aerial photograph is as follows:

1. Calculate time and distance offsets for AMSCAT relative to SFMR and PRT-5 (AMSCAT time = Nadir time + Δt)

2. Calculate footprint sizes for SFMR, PRT-5, and AMSCAT

3. Draw template of sensor footprints at scale of appropriate photography

4. Locate center of photograph

5. Determine if nadir-looking sensor footprints (SFMR and PRT-5) are located behind or ahead of center of photograph

6. Calculate distance offset between center of aerial photograph and sensor footprint

7. Center footprint templates for SFMR and PRT-5 along the flight line

8. Use distance offset calculated for AMSCAT to locate AMSCAT footprint behind SFMR and PRT-5 footprints

9. Identify ice types within each footprint and correlate with remote sensing data

SIRE DATA CATALOG

This section catalogs all the remote sensing data obtained by NASA Langley Research Center during the 1979 Sea-Ice Radar Experiment (SIRE). These data are available on photographs (appendix A), and on digital computer tapes (appendix B).

Data were obtained for 5 days during the period of March 14 to 24, 1979, and are referenced by Julian Day. Flight line plots are presented for each day in appendix C.

Time-line plots, referenced to Greenwich mean time (GMT), for each day show when sensors were recording data; corresponding latitude and longitude are also shown. The plots enable selection of data for detailed analysis based upon the user's need for a particular sensor configuration and/or geographical location. For ease of access to data on the available digital tapes, all sensor data are referenced to Greenwich mean time (GMT). Nine variables are indicated on each time-line plot. A solid line indicates the presence of data; absence of a solid line indicates the absence of data. The scale of these plots is 120 s/in. Data gaps of less than 10 s are not indicated. The parameters shown for each time-line plot are labeled in figure 12 and described as follows:

A: Day 82 - The Julian Day during 1979 corresponding to the time-line plot. Julian Days and their corresponding calendar days are as follows:

Julian Day	Calendar day
73-74	March 14-15, 1979
75-76	March 16-17, 1979
77-78	March 18-19, 1979
79	March 20, 1979
82-83	March 23-24, 1979

B: Photography - Ellipses indicating when photographs were made. Stereo-coverage 9-in. black and white aerial photography was obtained for nearly all official flight lines. An ellipse indicates the most accurate estimate of when a photograph was taken. Because of the overlap on adjacent photographs, ground coverage is nearly continuous; however, during the middle of some flight lines, extensive cloud cover beneath the aircraft prevented the acquisition of usable photography. Since only a limited amount of film was carried onboard the aircraft, the camera operator manually turned the camera off over extensive cloud cover and turned it on again when openings appeared. Consequently, there are gaps in the photographic record of some flight lines. A complete inventory of all available aerial photography is presented in appendix A.

C: Flight lines - Solid line indicating whether data were obtained during an official flight line. The number (i.e., 1-3) refers to flight line 1 and run number 3. Geographic locations of the official flight lines for each day are plotted at the beginning of data for each day. Furthermore, aerial photography is inventoried (appendix A) for each day according to its flight line and run, as well as by GMT. Data obtained other than during an official flight line may not be usable. These data are presented herein for the sake of completeness and for their considerable value as an historical data base. (Flight lines which have no accompanying aerial photography are not listed on the time-line plots.)

D: PRT-5 - Solid line indicating when the infrared radiometer (radiation thermometer) was taking data. This instrument remotely senses the physical temperature of the Earth's surface.

E: SFMR - Solid line indicating whether the stepped frequency microwave radiometer acquired radiometric temperatures (T_A).

F: AMSCAT (XX polarization) - Solid lines showing whether the airborne microwave scatterometer was taking data and at what polarizations it was operating. For example, VH polarization indicates that AMSCAT transmitted at vertical polarization and received at horizontal polarization. Likewise, HH polarization indicates horizontal transmission and horizontal reception.

G: Greenwich mean time (hour:min:sec) - All data are referenced to GMT. Available computer tapes can be easily accessed by searching for the start and stop times of desired data segments.

H and I: Latitude and Longitude - Approximate latitude and longitude indicated in hundredths of a degree every 2 min along the flight line.

Langley Research Center
National Aeronautics and Space Administration
Hampton, VA 23665
April 13, 1983

APPENDIX A

AERIAL PHOTOGRAPHIC LOG AND ORDERING INFORMATION

Aerial photography obtained during 1979 SIRE may be purchased as 9- by 9-in. black and white contact prints from the EROS Data Center.

Requests for photographs should be addressed to

EROS Data Center
U.S. Geological Survey
Sioux Falls, SD 57198

When ordering photographs, supply the following information:

Mission number:	396
Film roll number:	(See table AI)
Start frame number:	(See table AI)
End frame number:	(See table AI)

As of March 1983, the cost is approximately $5.00 per 9- by 9-in. black and white contact print. Payment in the form of cash, check, money order, or purchase order must accompany request for data.

Selection of aerial photographs for purchase should be made in conjunction with inspection of the time-line plots. When a particular data segment has been selected for analysis, the flight line and run numbers obtained from the time-line plot can be referenced to the photographic log (table AI) to identify the first and last frame in that particular run and the film roll number.

For example, from figure 12, which was used to illustrate the use of time-line plots, one obtains the following information:

Day: 82
Flight line and run: 1-3

From the photographic inventory for day 82, line 1, run 3 in table AI, one obtains the following information:

Mission number:	396
Film roll number:	11
Start frame number:	298
End frame number:	525

This information should then be supplied to EROS Data Center to order photographs.

APPENDIX A

TABLE AI.- PHOTOGRAPHIC AERIAL PHOTO LOG

Day	Line	Run	Roll	Start frame	Start frame time	End frame	End frame time	Approximate photographic scale	Aircraft ground speed, knots
73	1	4	1	20	223533.0	112	224045.8	1:1050	211
	1	3	1	113	224713.0	179	225301.0	1:1050	199
	1	2	1	180	225722.8	232	230223.1	1:2500	223
	1	1	1	233	230856.8	325	231357.0	1:2500	232
	6	9	2	1	232335.8	203	233535.9	1:2500	206
	2	5	2	204	234852.4	305	235354.2	1:2200	199
	11	0	3	1	235855.9	73	000355.3	1:2000	215
	2	4	3	79	000934.0	95	001318.7	1:2000	199
	1	9	3	96	001751.0	205	002503.9	1:2000	192
75	6	1	4	1	210116.0	574	225455.3	1:2000	142
	6	12	3	206	225719.0	236	230015.2	1:2000	151
	6	2	5	1	230536.0	252	235435.8	1:1000	165
	1	1	5	253	000801.0	339	001343.1	1:2500	136
	2	1	5	340	001950.0	422	002453.1	1:2500	145
	3	1	5	423	003440.1	540	004029.3	1:2500	129
	4	1	3	237	004801.0	345	005323.5	1:2500	143
	5	1	6	1	010056.9	110	010623.1	1:2500	140
77	1	1	6	111	230111.4	577	233204.2	1:3000	133
	1	1	7	1	233329.3	150	234321.8	1:2100	133
	1	2	7	151	234633.5	576	002848.3	1:2100	139
	1	3	8	1	003237.9	435	011415.0	1:2100	142
	1	4	8	436	011419.8	582	012403.4	1:2500	140
	1	4	9	1	012529.1	411	015239.5	1:3000	154
	2	1	9	412	020312.3	446	020527.4	1:2100	130
	2	2	9	447	020806.4	489	021011.7	1:2100	154
79	1	4	10	1	214836.0	60	215328.8	1:2000	143
	1	5	10	61	215742.3	125	220300.1	1:2000	140
	1	6	10	126	220631.6	186	221129.5	1:2000	143
	1	7	10	187	221522.9	240	221946.0	1:2000	129
	1	8	10	241	222523.1	300	223015.9	1:2000	147
	1	9	10	301	223423.6	353	223929.3	1:2000	130
	11	0	10	354	224353.3	379	224844.3	1:1000	160
	11	1	10	380	225348.1	405	225846.0	1:1000	140
	3	1	10	406	230122.6	426	230959.1	1:1000	153
	2	1	10	427	231101.2	446	231447.6	1:1000	152
	2	2	10	447	232140.8	496	232544.1	1:2000	138
	2	3	10	497	232924.4	556	233404.8	1:2000	136
	2	4	11	1	233733.0	51	234141.5	1:2000	138
82	1	2	11	60	222706.5	297	231431.1	1:8000	131
	1	3	11	298	231812.0	525	235159.8	1:8000	169
	1	4	11	526	235612.9	568	000251.8	1:8000	126
	1	4	12	1	001435.3	165	003616.4	1:4000	126
	3	1	12	166	010526.0	186	010644.6	1:2500	178
	3	2	12	187	011335.0	209	011525.3	1:2500	123
	3	3	12	210	011816.2	215	011836.1	1:2300	160
	3	4	12	216	012150.2	236	012200.7	1:2300	127

APPENDIX B

SIRE DATA TAPE DOCUMENTATION

The NASA Langley SIRE Data Set is available on six 9-track tapes from the National Technical Information Service (NTIS). The first five tapes (one tape for each day of the SIRE mission) contain NERDAS parameters, camera control information, PRT-5 and environmental information, and AMSCAT information. The file structure for these tapes is as follows:

File portion	Variable	Meaning	Format
Header	MISS	Mission number	I10
	NDAY	Julian Day	I10
	NFILE	File number	I10
	NFEND	End file counter	I10
	NTSTRT	Start tape counter	I10
	NTEND	End tape counter	I10
	TSTRT	Start time, HHMMSS.S*	F10.2
	TEND	End time, HHMMSS.S	F10.2
SUBRECORD 1	GMT	Time, HHMMSS.S	F10.2
	SEC	Time, total seconds from start of year	F10.2
	XLAT	Latitude, deg	F10.2
	XLON	Longitude, deg	F10.2
	CTIM	Camera time, s (GMT)	F10.2
	NCP	Camera pulse	I5
	NFRAM	Camera frame number	I5
	NFCNT	File record counter	I10
	NTCNT	Tape record counter	I10
	NCP=1	If photograph was taken: otherwise NCP = Integer dummy value (-9999)	
SUBRECORD 2	ALT	Altitude, m	F8.2
	HEAD	Heading, deg	F8.2
	DRIFT	Drift, deg	F8.2
	ROLL	Roll, deg	F8.2
	PITCH	Pitch, deg	F8.2
	GRSP	Ground speed, m/s	F8.2
	WDSP	Wind speed, m/s	F8.2
	WDAN	Wind angle, deg	F8.2
	PRT	PRT temperature, °C	F8.2
	TAT	Total air temperature, °C	F8.2
SUBRECORD	SDB	Scattering coefficient, dB (see AMSCAT description)	F8.2
	THETA	Incidence angle, deg	F8.2
	PHI	Azimuth angle, deg	F8.2
	DPF	Depolarization factor	F8.4
	DFR	Doppler frequency, GHz	F8.4
	IPOL	Polarization: 0 = HH; 2 = VH; 1 = HV; 3 = VV	I8
	MODE	Mode	I8
	ISET	Set	I8
	ISTIM	Scatterometer timing	I8
	IREC	AMSCAT record number	I8

*HHMMSS.S indicates that the first two digits of the variable are hours, the next two digits are minutes, and the next three digits are seconds to the nearest tenth.

APPENDIX B

The time, latitude, and longitude records within a file are continuous with a sample rate of 0.5 s. Missing parameters are filled in with dummy variables. Real dummy values are 9999.99 or 99.9999. Integer dummy values are -9999. A FORTRAN program to read these tapes is as follows:

```
      PROGRAM REDTAP (INPUT, OUTPUT, TAPE1)
 10   READ (1, 101) MISS, NDAY, NFILE, NFEND, NTSTRT, NTEND, TSTRT, TEND
      IF (EOF (1).NE.0) STOP
 20   READ (1, 201) GMT, SEC, XLAT, XLON, CTIM, NCP, NFRAM, NFCNT, NTCNT
      IF (EOF (1).NE.0) GO TO 10
      READ (1, 202) ALT, HEAD, DRIFT, ROLL, PITCH, GRSP, WDSP, WDAN, PRT
     1TAT
      READ (1, 203) SDB, THETA, PHI, DPF, DFR, IPOL, MODE, ISET, ISTIM
     1IREC
      GO TO 20
101   FORMAT (6I10, 2F10.2)
201   FORMAT (5F10.2, 2I5, 2I10)
202   FORMAT (10F8.2)
203   FORMAT (3F8.2, 2F8.4, 5I8)
      END
```

The sixth tape in the set contains SFMR data for all 5 days of the SIRE mission. The file structure for this tape is

File portion	Variable	Meaning	Format
HEADER	MISS	Mission number	I10
	NDAY	Julian Day	I10
	NFILE	File number	I10
	NFEND	End file counter	I10
	NTSTRT	Start tape counter	I10
	NTEND	End tape counter	I10
	TSTRT	Start time, HHMMSS.S*	F10.2
	TEND	End time, HHMMSS.S	F10.2
SFMR RECORD	GMT	Time, HHMMSS.S	F10.2
	SEC	Time, seconds from beginning of year	F15.2
	TA	Radiometric temperature,† K	F10.2
	FREQ	Frequency, MHz	F10.2
	NFCNT	File record counter	I10
	NTCNT	Tape record counter	I10

*HHMMSS.S indicates that the first two digits of the variable are hours, the next two digits are minutes, and the next three digits are seconds to the nearest tenth.

†See reference 2.

APPENDIX B

The sample rate varies for these records and dummy values are listed as -99.99. A FORTRAN program to read this tape is as follows:

```
      PROGRAM REDTAP (INPUT, OUTPUT, TAPE1)
 10   READ (1, 101) MISS, NDAY, NFILE, NFEND, NTSTRT, NTEND, TSTRT, TEND
      IF (EOF (1).NE.0) STOP
 20   READ (1, 201) GMT, SEC, TA, FREQ, NFCNT, NTCNT
      IF (EOF (1).NE.0) GO TO 10
      GO TO 20
101   FORMAT (6I10, 2F10.2)
201   FORMAT (F10.2, F15.2, 2F10.2, 2I10)
      END
```

The following table lists tape numbers for the SIRE data set:

Julian Day	Calendar day	Tape number
73-74	March 14-15, 1979	NM0458
75-76	March 16-17, 1979	NM0459
77-78	March 18-19, 1979	NM0653
79	March 20, 1979	NM0654
82-83	March 23-24, 1979	NM0708
SFMR (all days)		NM0770

The following table lists start and stop times, tape counters, and the number of records for each file on the first six tapes in the set:

Day	File	Start time	Stop time	Number of records	Start tape counter	End tape counter
Tape number NM0458						
73-74	1	195224.0	200830.5	1934	1	1934
	2	203346.0	213738.5	7666	1935	9600
	3	215941.0	230332.0	7662	9601	17262
	4	230519.0	235558.0	6079	17263	23341
	5	235831.0	002453.5	3166	23342	26507
Tape number NM0459						
75-76	1	212953.0	214616.5	1968	1	1968
	2	220219.5	225727.0	6616	1969	8584
	3	230233.0	001420.5	8616	8585	17200
	4	001929.0	010621.5	5626	17201	22826

APPENDIX B

Day	File	Start time	Stop time	Number of records	Start tape counter	End tape counter
Tape number NM0653						
77-78	1	231844.0	234353.5	3019	1	3019
	2	234556.0	235959.5	1688	3020	4707
	3	000000.5	002010.0	2420	4708	7127
	4	004438.5	015303.5	8211	7128	15338
	5	020256.0	021004.0	857	15339	16195
Tape number NM0654						
79	1	204731.5	211206.5	2951	1	2951
	2	213113.5	222132.0	6038	2952	8989
	3	222423.5	231530.5	6135	8990	15125
	4	232054.5	234137.0	2486	15126	17610
Tape number NM0708						
82-83	1	202821.0	210748.0	4735	1	4735
	2	212910.0	215324.0	2908	4736	7643
	3	222130.0	235225.0	10910	7644	18553
	4	235552.0	003749.5	5036	18554	23589
	5	010444.0	020015.5	6664	23590	30253
Tape number NM0770						
73-74	1	202904.0	213206.0	1844	1	1844
	2	220020.0	225405.0	9994	1845	11838
	3	225816.0	233639.0	2723	11839	14561
	4	234938.0	002613.0	3378	14562	17939
75-76	1	214202.0	222619.0	1499	1	1499
	2	222630.0	230018.0	1994	1500	3493
	1	230548.4	003559.0	1551	1	1551
	2	003610.0	011722.0	1366	1552	2917
77-78	1	224835.0	235959.0	3788	1	3788
	2	000010.0	004340.1	4606	3789	8394
	3	004350.1	015244.0	10137	8395	18531
	4	015828.0	031842.0	4061	18532	22592
79	1	203922.0	211859.0	649	1	649
	2	211908.0	213307.0	700	650	1349
	3	213335.0	214258.0	713	1350	2062
	4	214328.0	214825.0	224	2063	2286
	5	214904.0	215003.0	116	2287	2402
	6	215014.0	220057.0	907	2403	3309
	7	220112.0	220131.0	38	3310	3347
	8	220147.0	233309.0	7507	3386	10854
	9	233337.0	234953.0	1242	10855	12096

Day	File	Start time	Stop time	Number of records	Start tape counter	End tape counter
Tape number NM0770 (Concluded)						
82-83	1	212932.0	215302.0	2751	1	2751
	2	222713.0	232014.0	5905	2752	8656
	3	232022.0	235959.0	4088	8657	12744
	4	000005.0	015825.0	13848	12745	26592

Copies of the digital tapes are available upon request to

National Technical Information Service (NTIS)
5285 Port Royal Road
Springfield, VA 22161

APPENDIX C

1979 SIRE FLIGHT LINES AND TIME-LINE PLOTS

APPENDIX C

Day 73-74

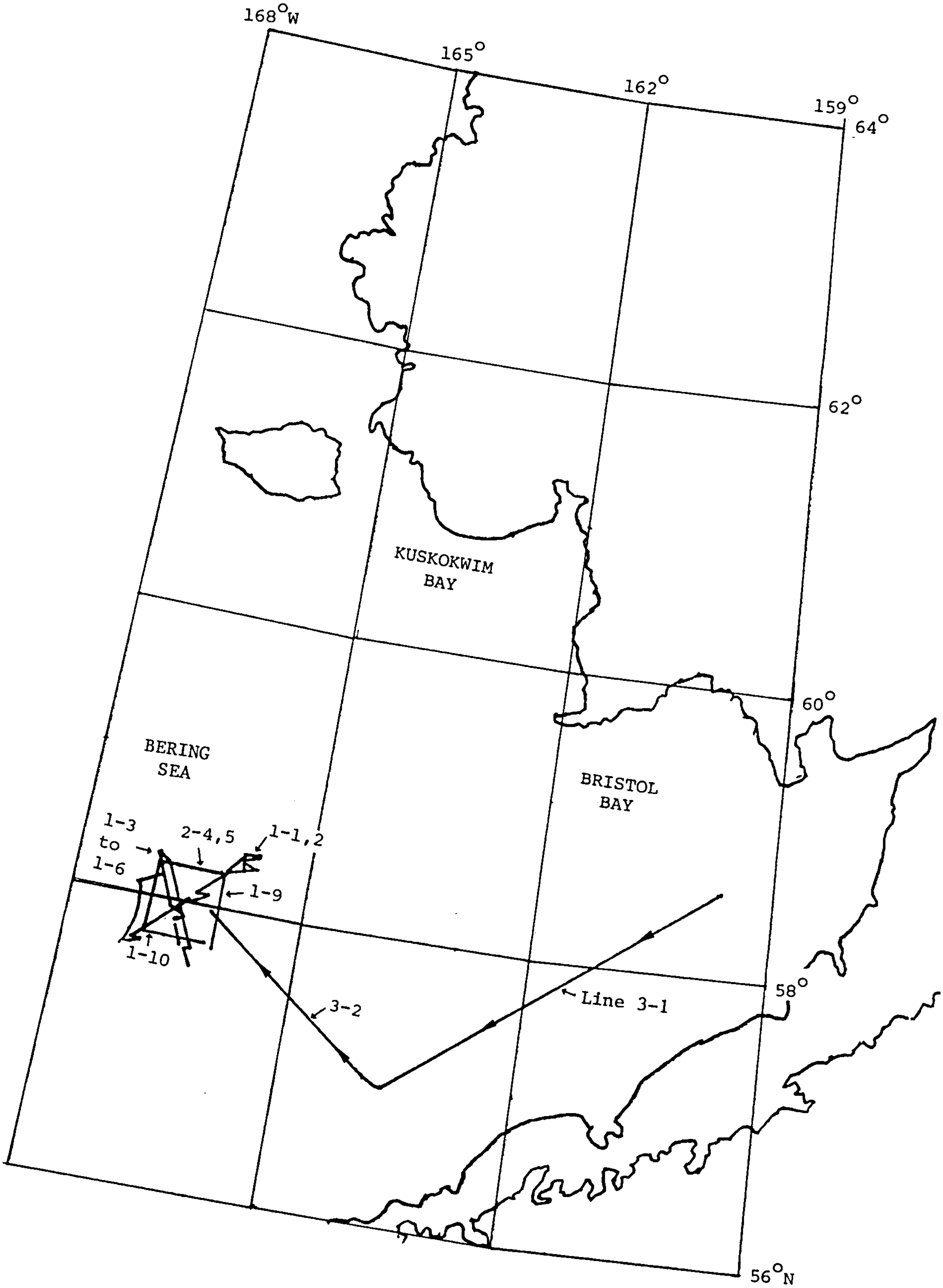

Flight lines for day 73-74

SIRE DATA SET SUMMARY
DAY 73

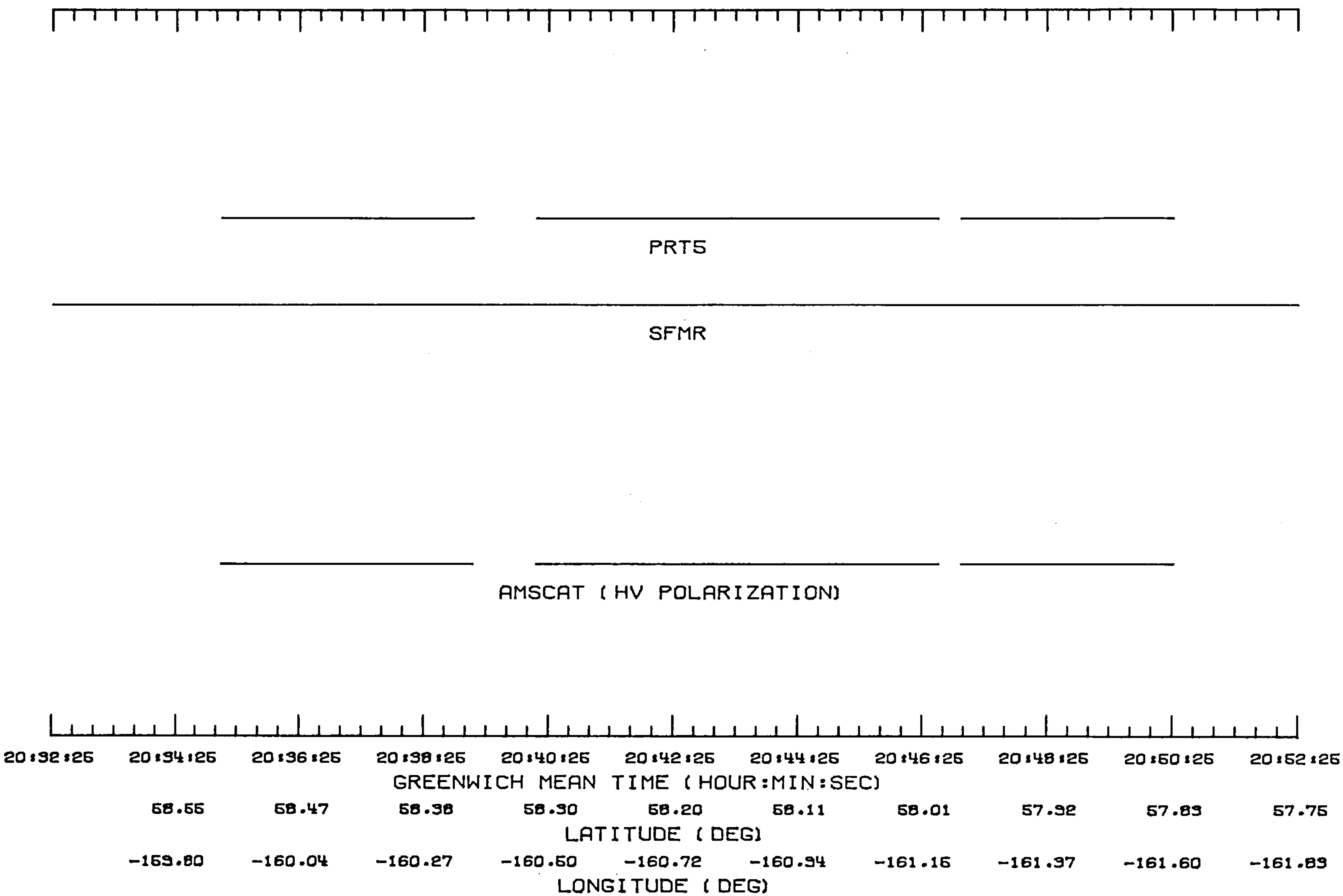

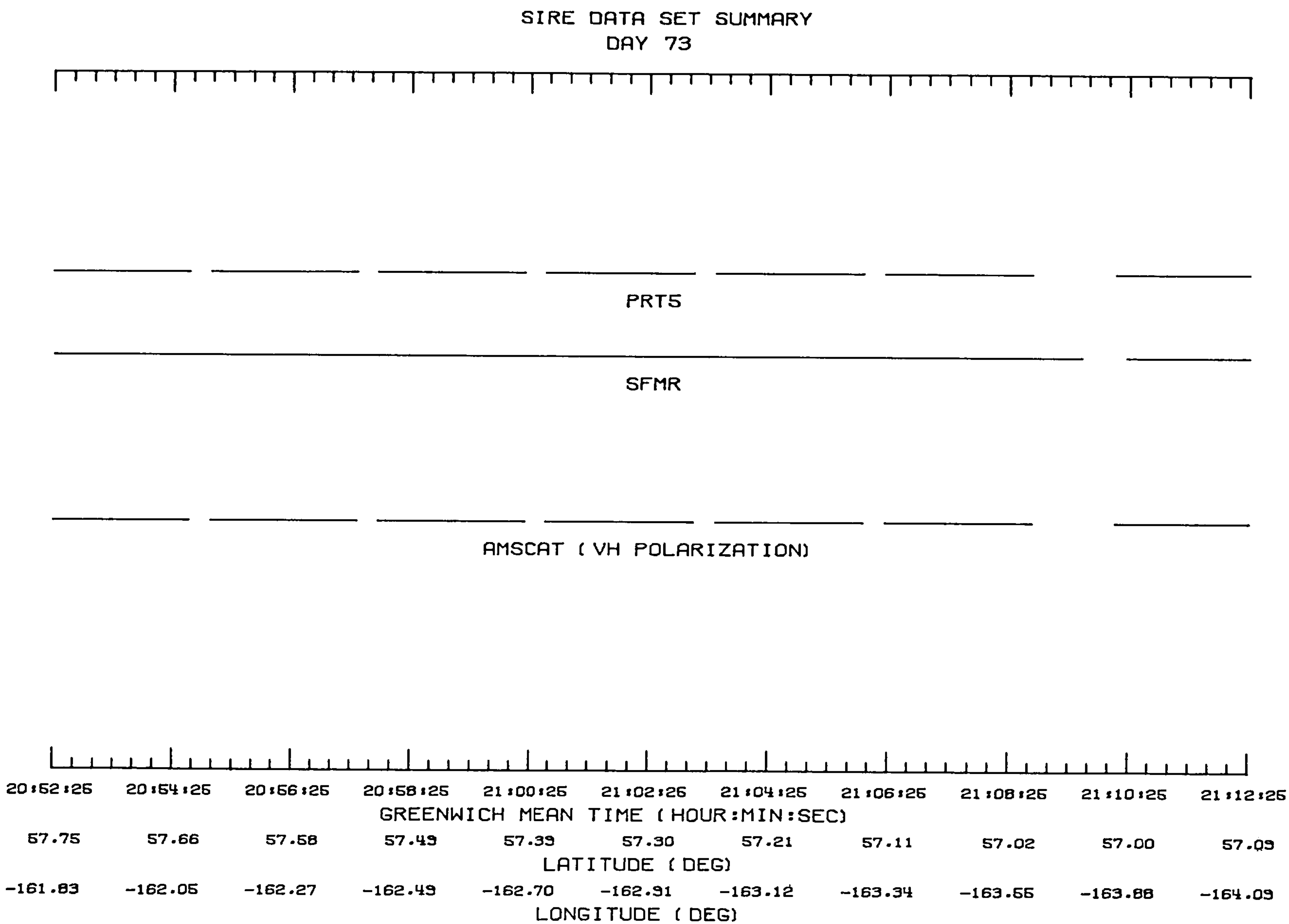
SIRE DATA SET SUMMARY
DAY 73
PRT5
SFMR
AMSCAT (VH POLARIZATION)
20:52:25
20:54:25
20:56:25
20:58:25
21:00:25
21:02:25
21:04:25
21:06:25
21:08:25
21:10:25
21:12:25
GREENWICH MEAN TIME (HOUR:MIN:SEC)
57.75
57.66
57.58
57.49
57.39
57.30
57.21
57.11
57.02
57.00
57.09
LATITUDE (DEG)
-161.83
-162.05
-162.27
-162.49
-162.70
-162.91
-163.12
-163.34
-163.55
-163.88
-164.09
LONGITUDE (DEG)

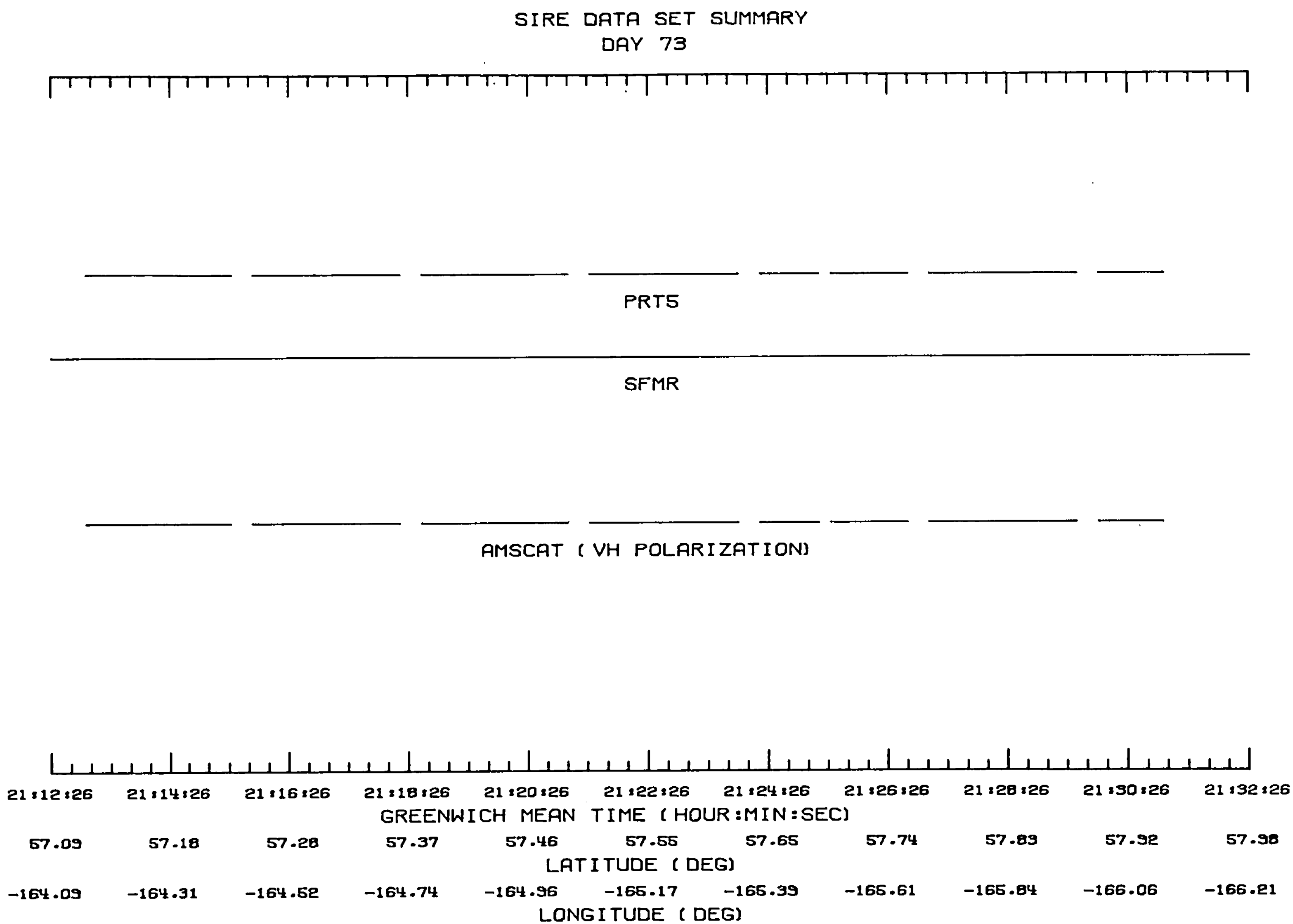
SIRE DATA SET SUMMARY
DAY 73
PRT5
SFMR
AMSCAT (VH POLARIZATION)
21:12:26 21:14:26 21:16:26 21:18:26 21:20:26 21:22:26 21:24:26 21:26:26 21:28:26 21:30:26 21:32:26
GREENWICH MEAN TIME (HOUR:MIN:SEC)
57.09 57.18 57.28 57.37 57.46 57.55 57.65 57.74 57.83 57.92 57.98
LATITUDE (DEG)
-164.09 -164.31 -164.52 -164.74 -164.96 -165.17 -165.39 -165.61 -165.84 -166.06 -166.21
LONGITUDE (DEG)

SIRE DATA SET SUMMARY
DAY 73

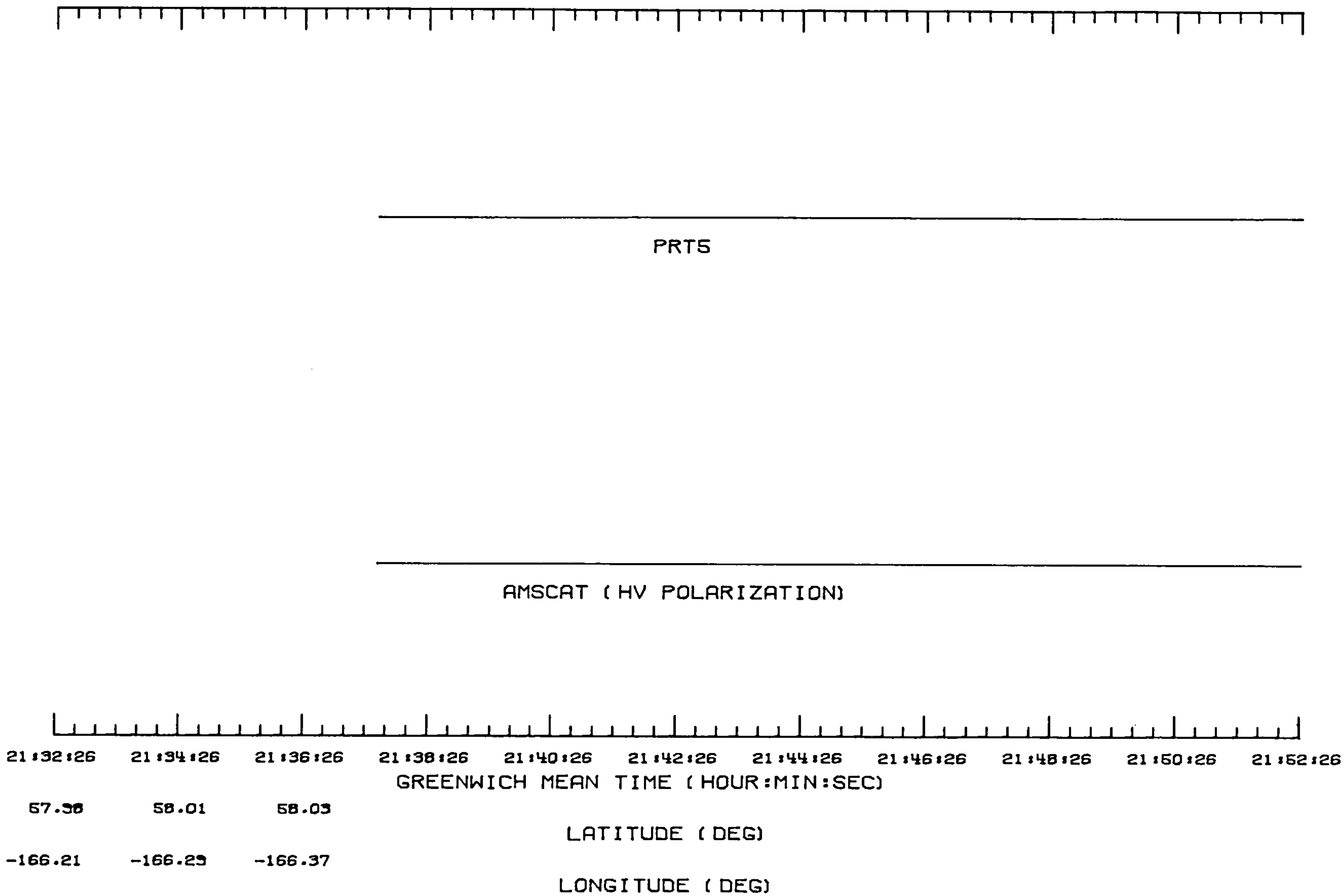

SIRE DATA SET SUMMARY
DAY 73

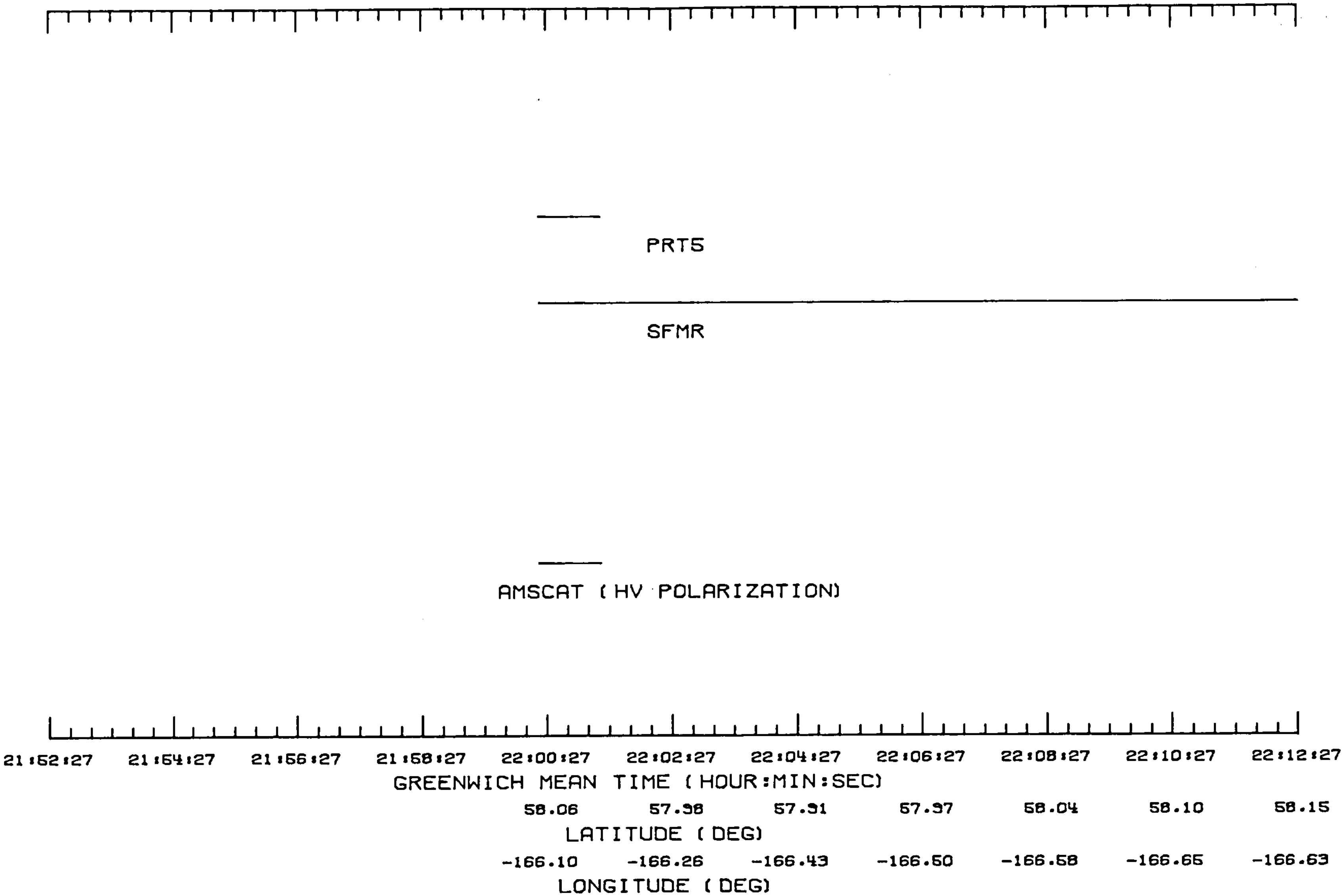

SIRE DATA SET SUMMARY
DAY 73

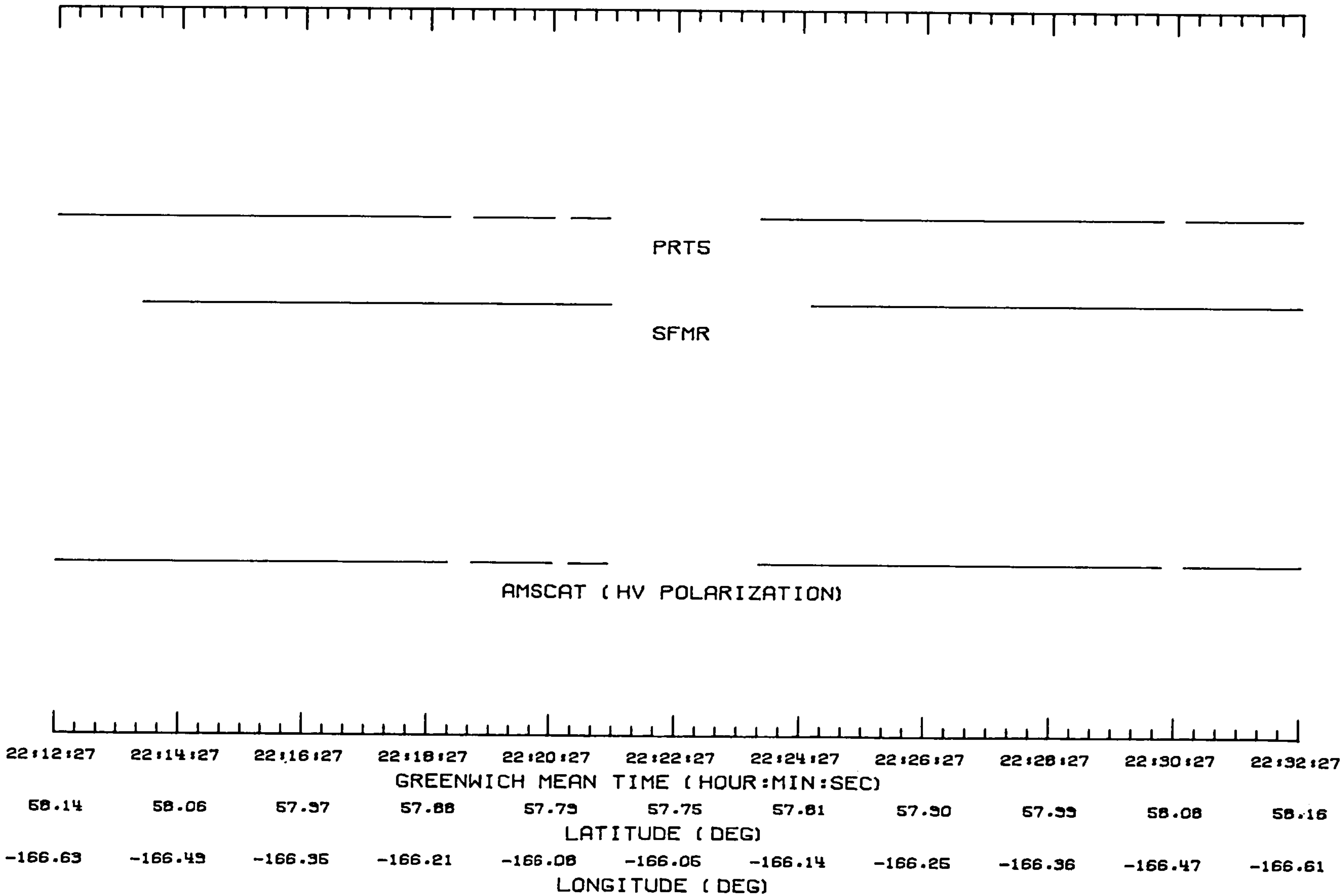

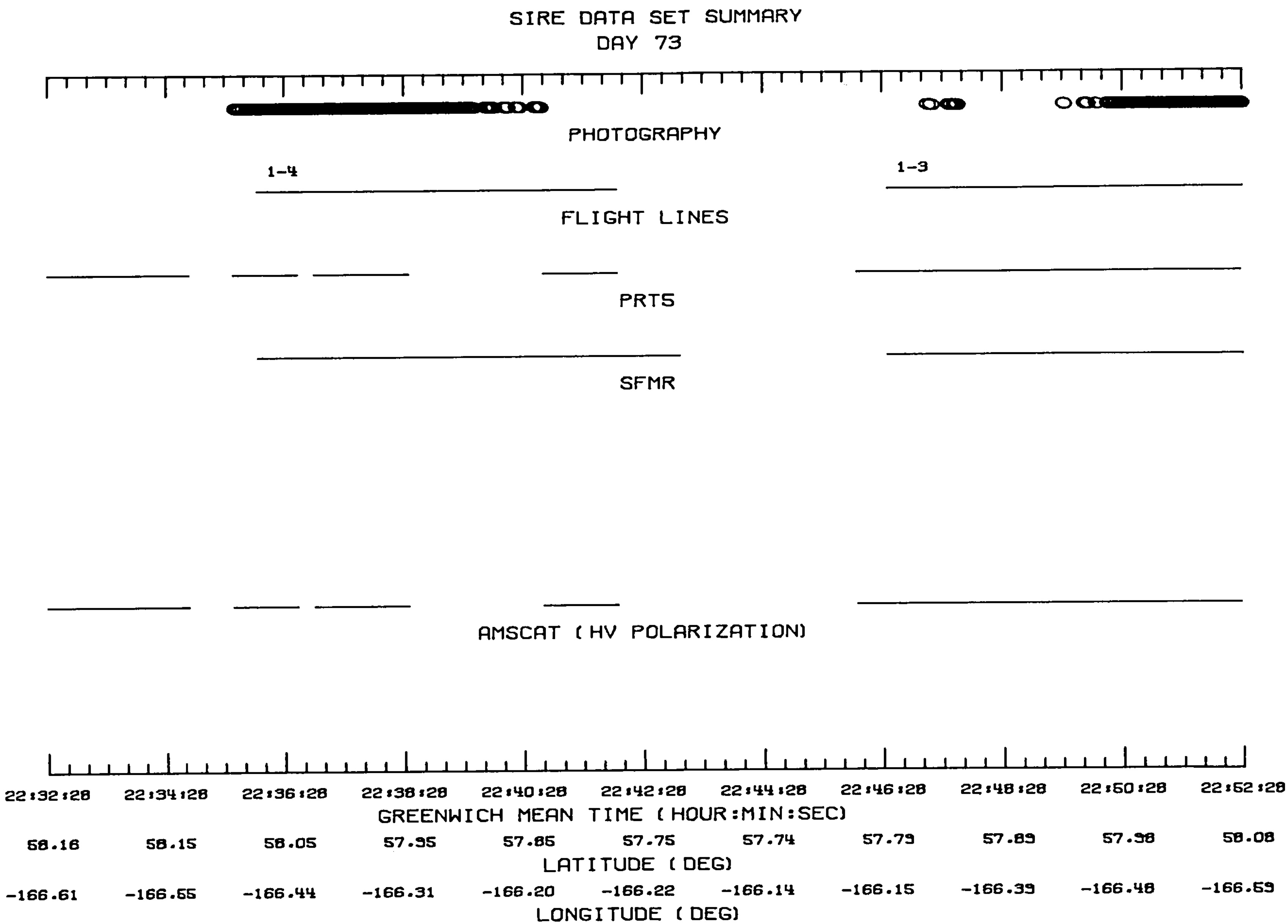

SIRE DATA SET SUMMARY
DAY 73
PHOTOGRAPHY
1-4
1-3
FLIGHT LINES
PRTS
SFMR
AMSCAT (HV POLARIZATION)
22:32:28
22:34:28
22:36:28
22:38:28
22:40:28
22:42:28
22:44:28
22:46:28
22:48:28
22:50:28
22:52:28
GREENWICH MEAN TIME (HOUR:MIN:SEC)
58.16
58.15
58.05
57.95
57.85
57.75
57.74
57.79
57.89
57.98
58.08
LATITUDE (DEG)
-166.61
-166.55
-166.44
-166.31
-166.20
-166.22
-166.14
-166.15
-166.39
-166.48
-166.59
LONGITUDE (DEG)

SIRE DATA SET SUMMARY
DAY 73

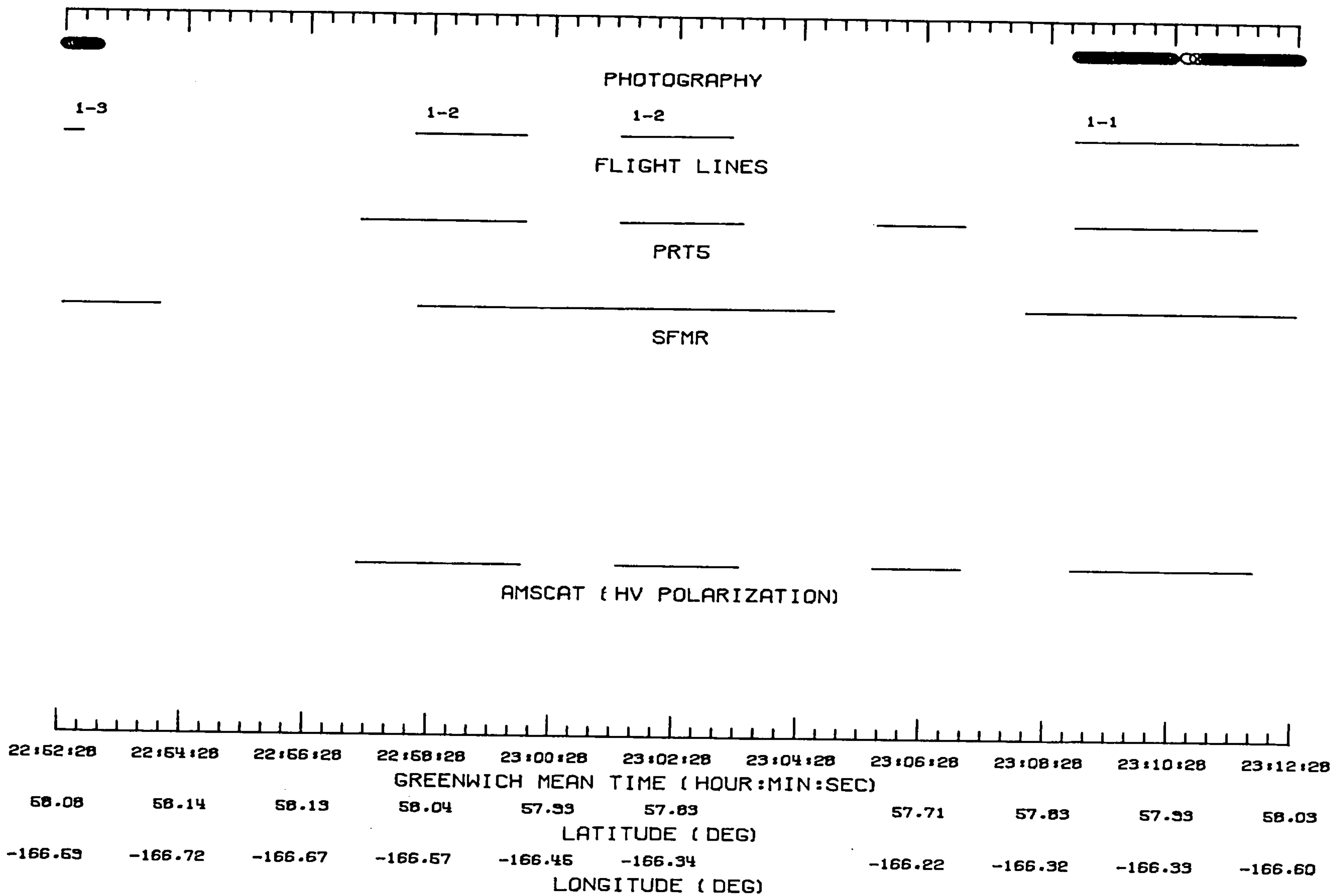

SIRE DATA SET SUMMARY
DAY 73

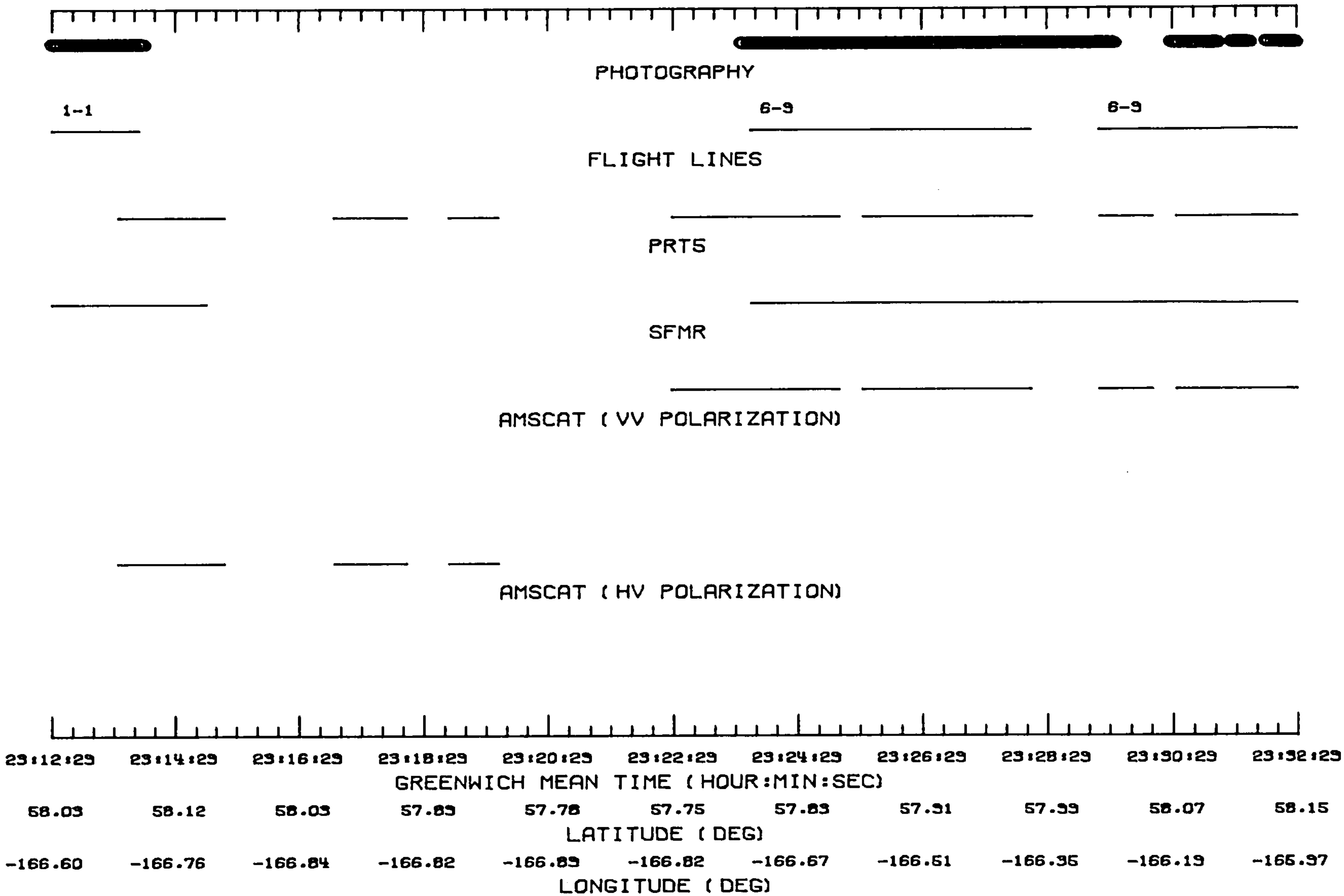

SIRE DATA SET SUMMARY
DAY 73

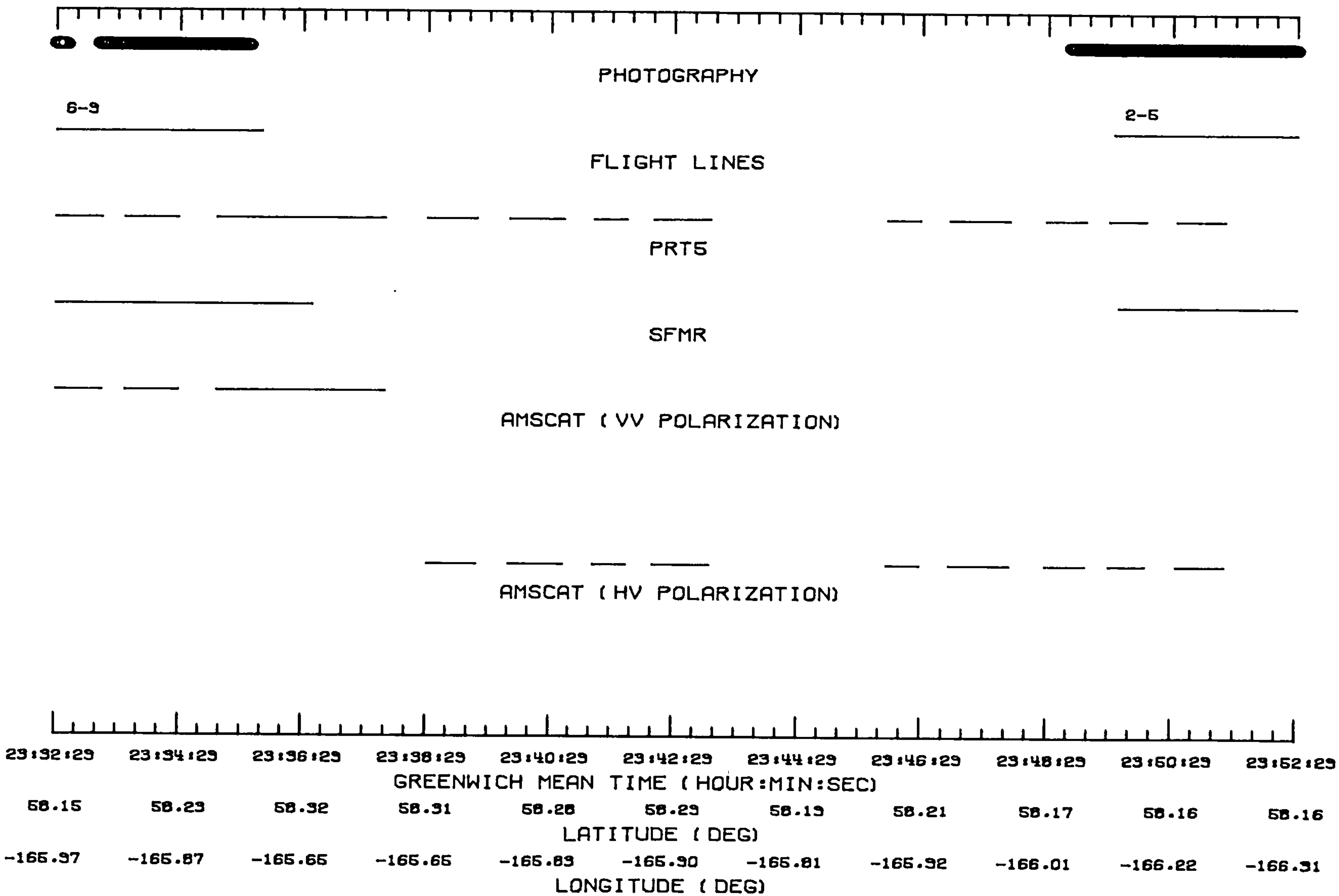

SIRE DATA SET SUMMARY
DAY 74

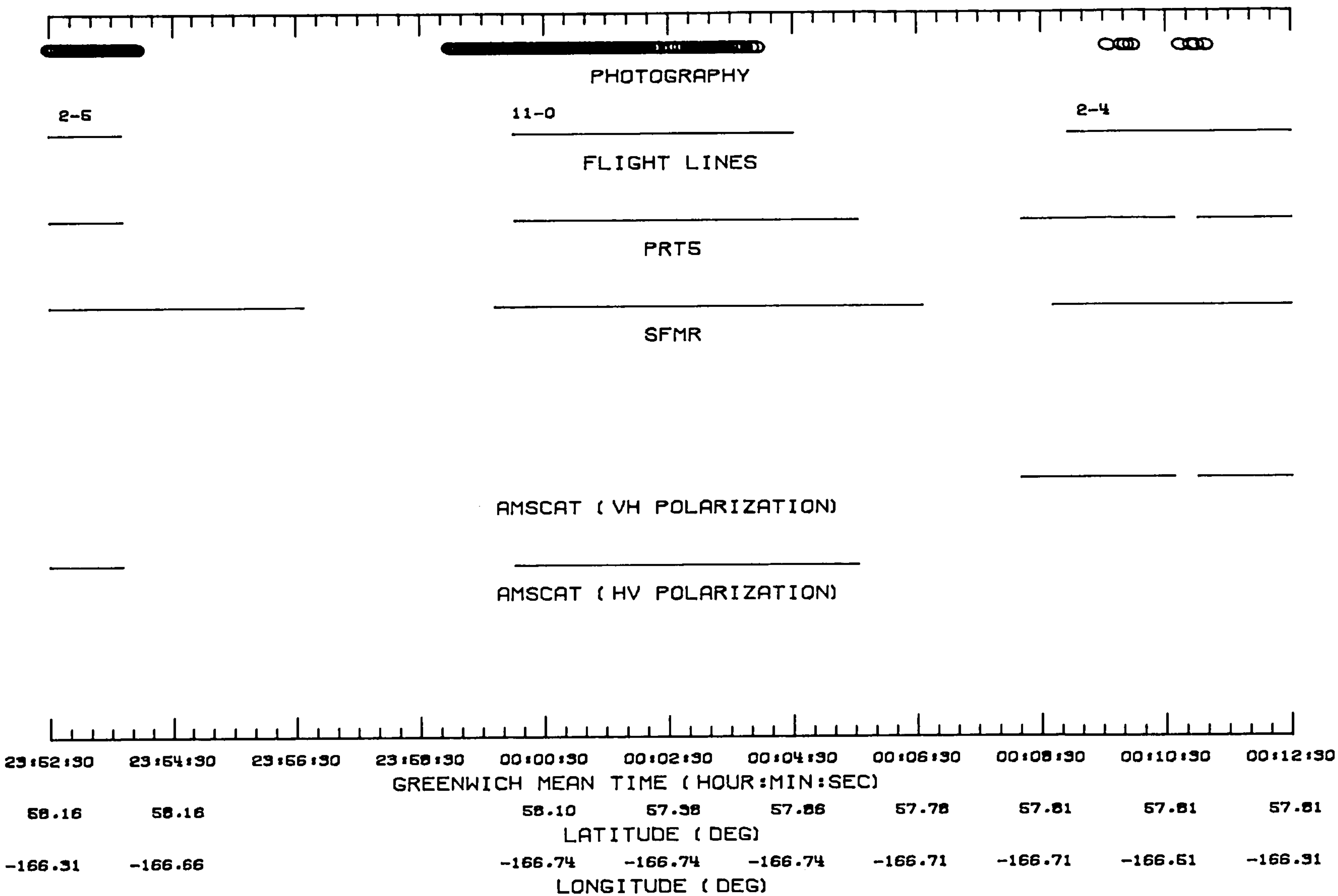

SIRE DATA SET SUMMARY
DAY 74

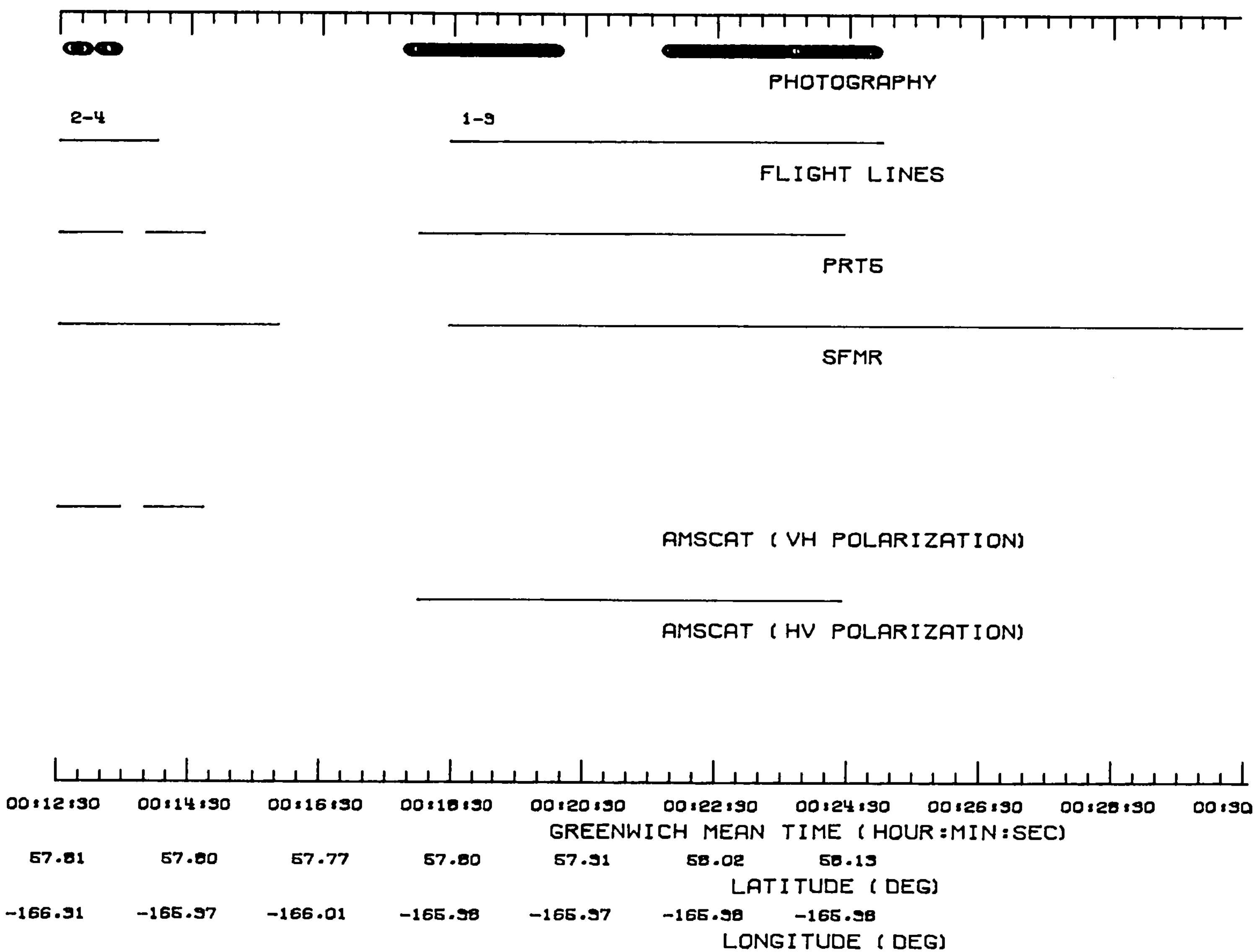

APPENDIX C

Day 75-76

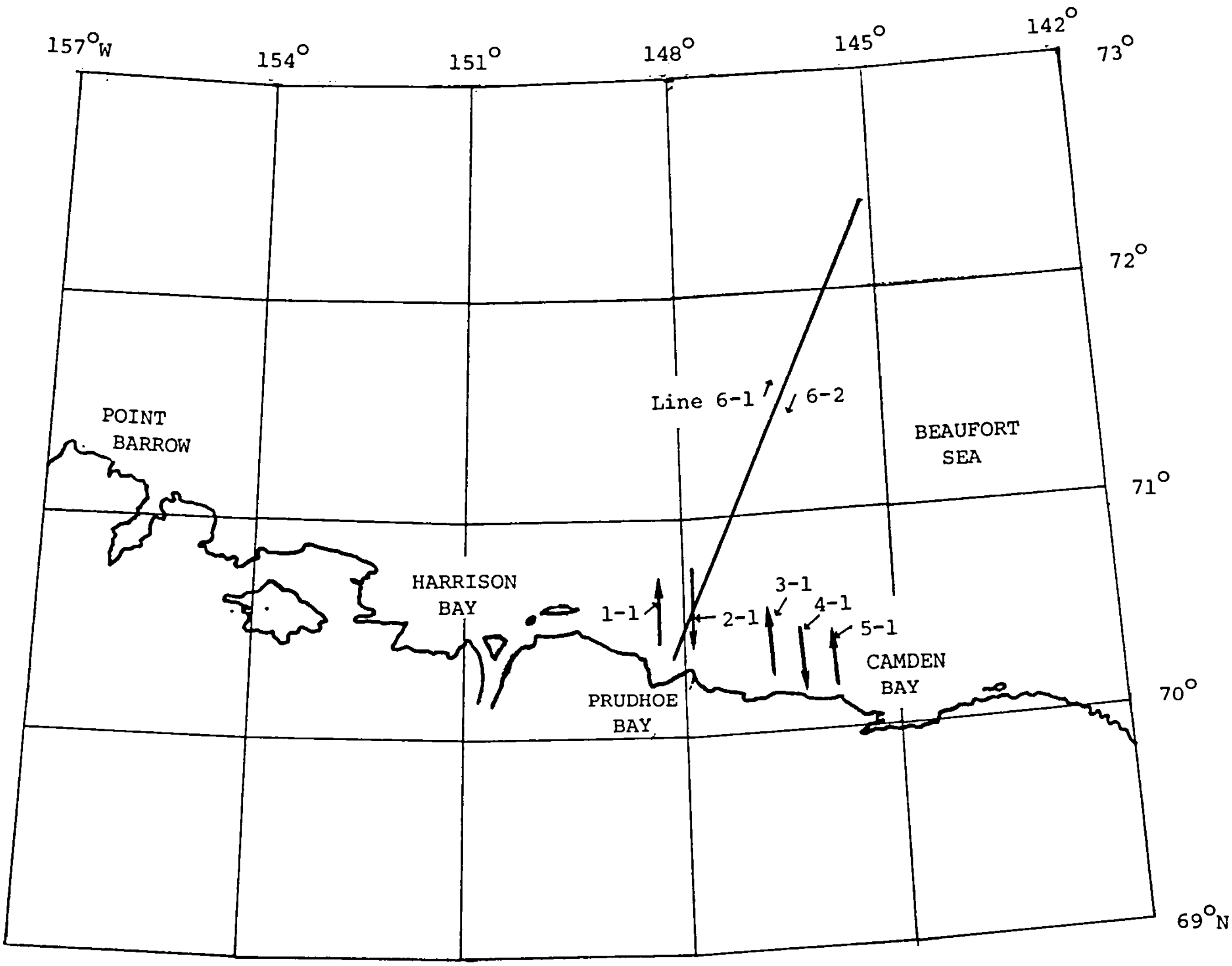

Flight lines for day 75-76

SIRE DATA SET SUMMARY
DAY 75

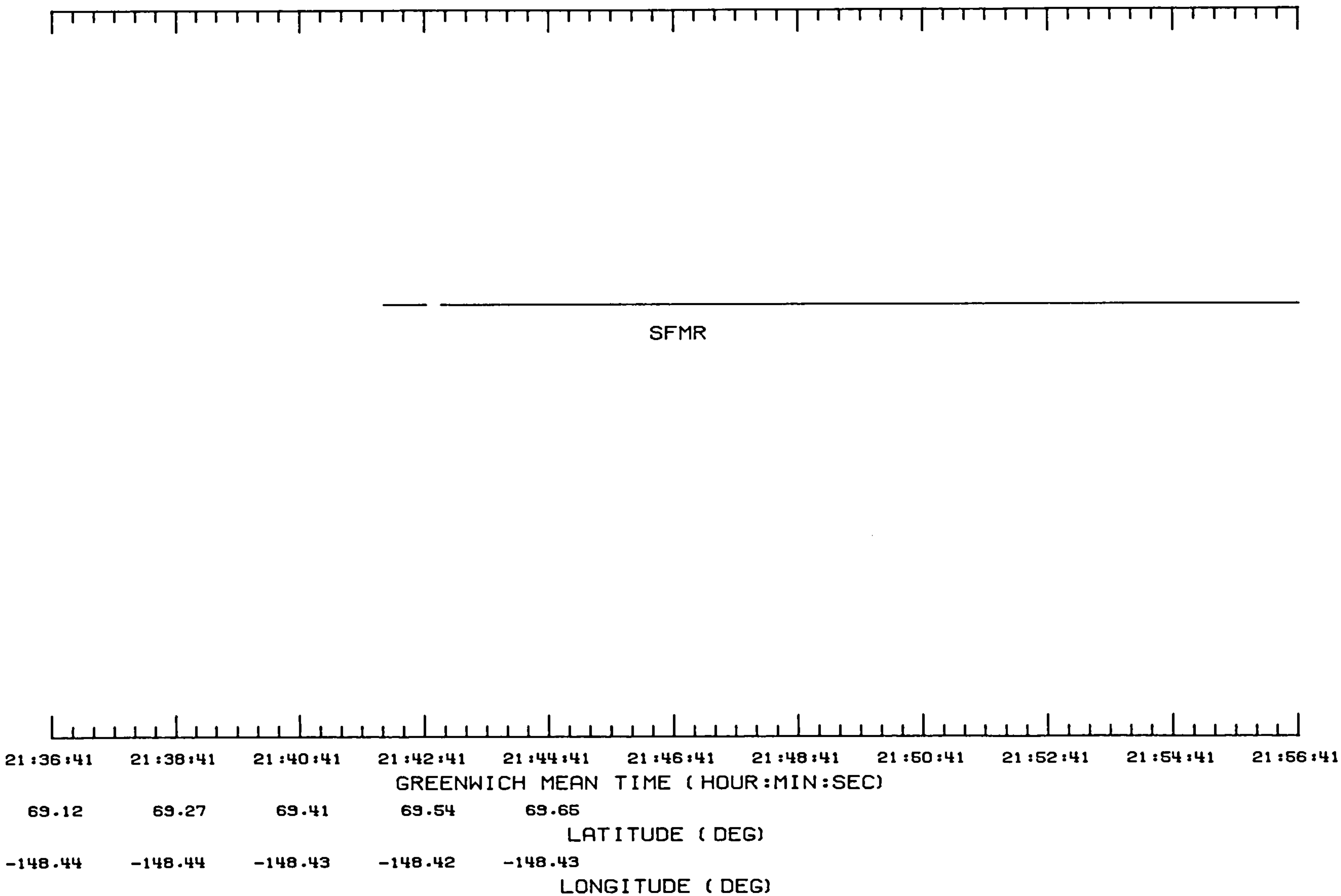

APPENDIX C

SIRE DATA SET SUMMARY
DAY 75

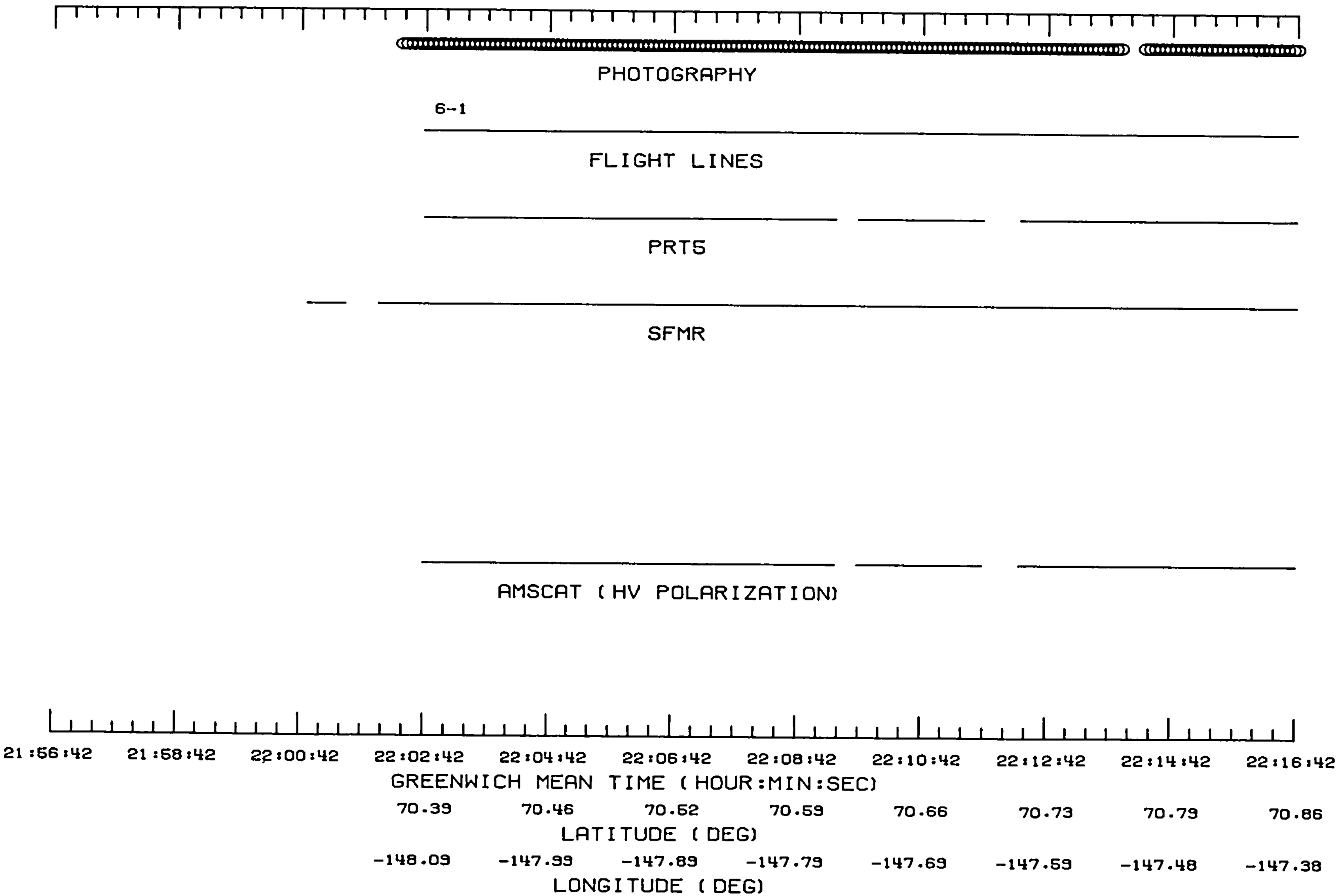

SIRE DATA SET SUMMARY
DAY 75

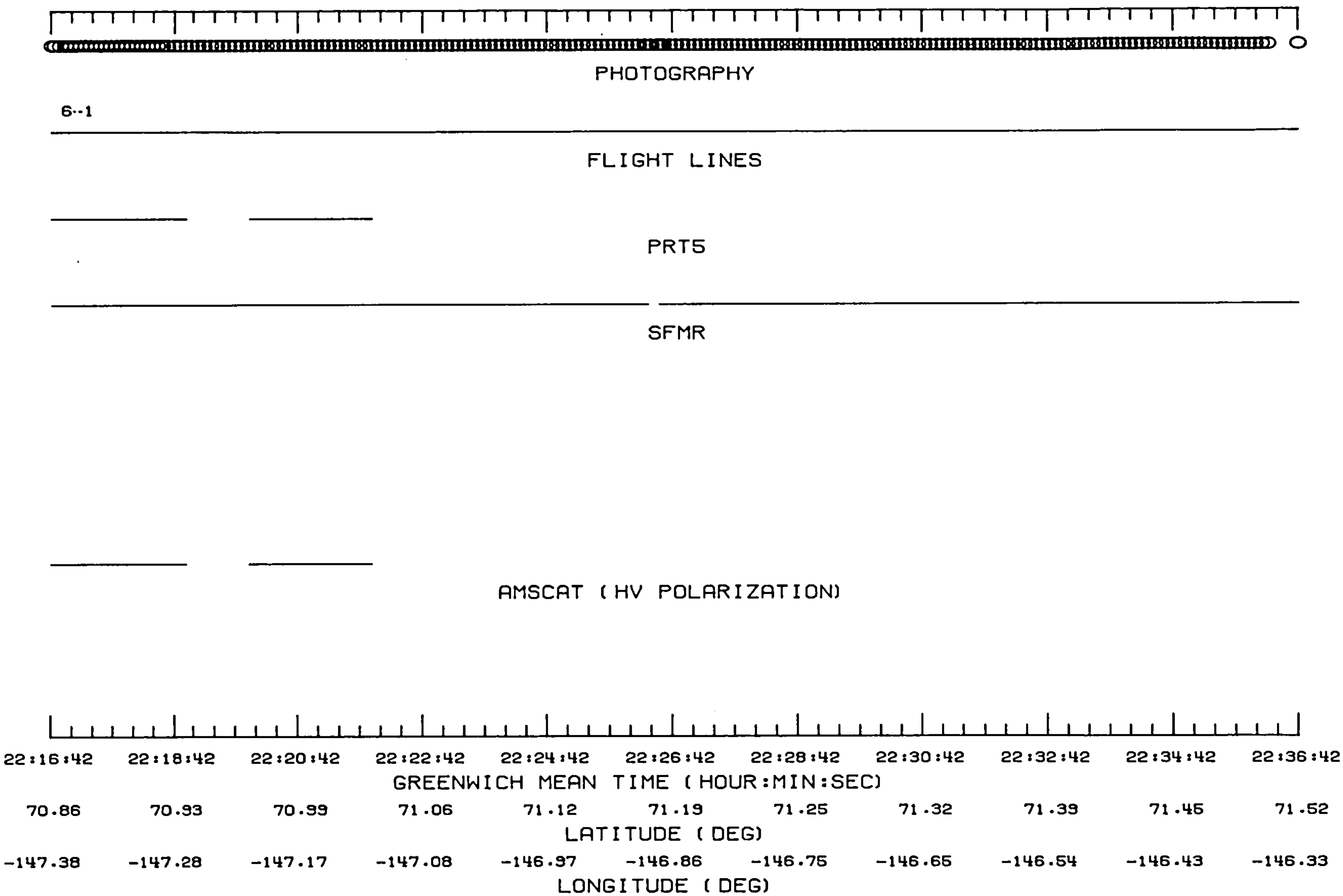

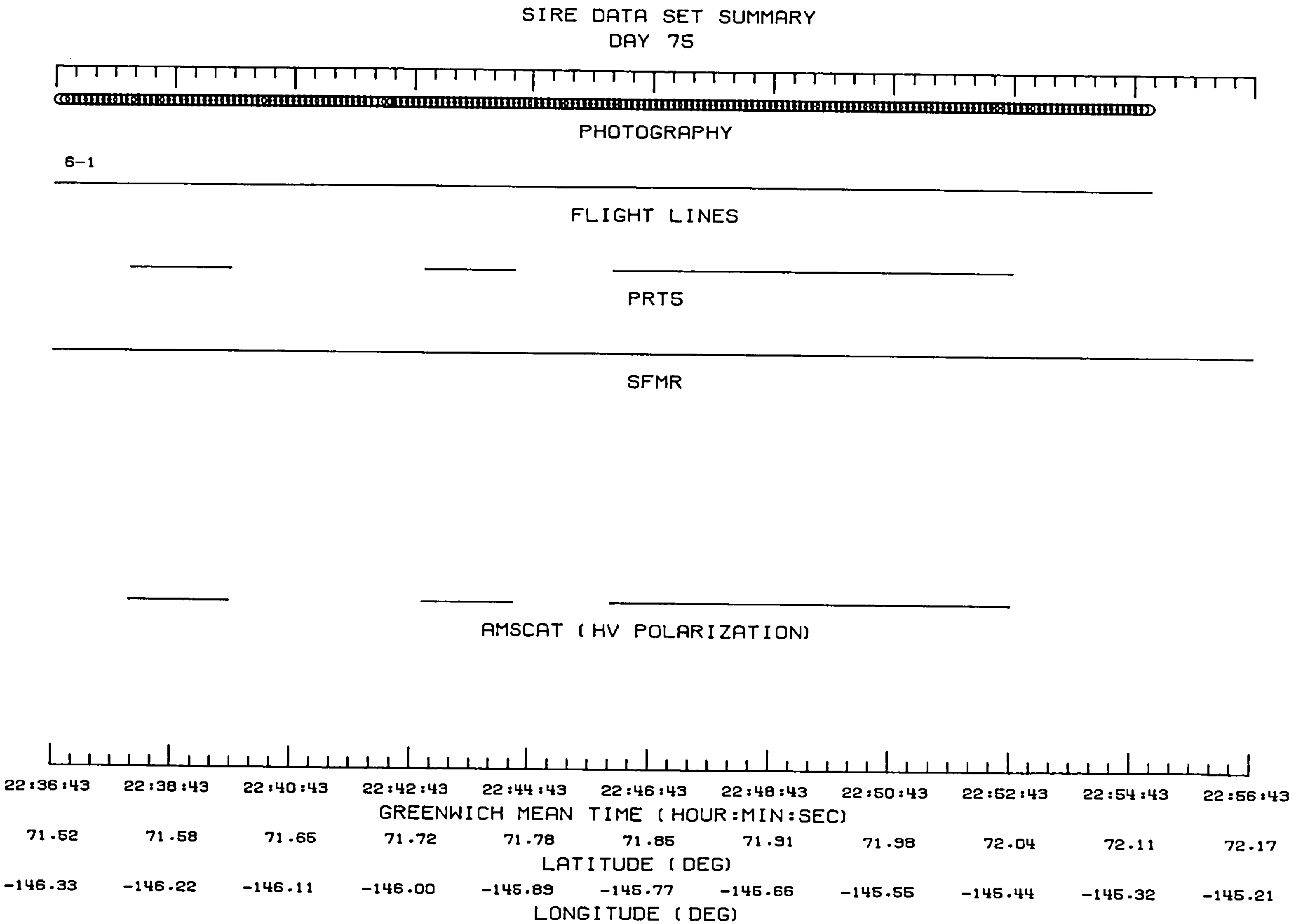
SIRE DATA SET SUMMARY
DAY 75
PHOTOGRAPHY
6-1
FLIGHT LINES
PRTS
SFMR
AMSCAT (HV POLARIZATION)
22:36:43
22:38:43
22:40:43
22:42:43
22:44:43
22:46:43
22:48:43
22:50:43
22:52:43
22:54:43
22:56:43
GREENWICH MEAN TIME (HOUR:MIN:SEC)
71.52
71.58
71.65
71.72
71.78
71.85
71.91
71.98
72.04
72.11
72.17
LATITUDE (DEG)
-146.33
-146.22
-146.11
-146.00
-145.89
-145.77
-145.66
-145.55
-145.44
-145.32
-145.21
LONGITUDE (DEG)

SIRE DATA SET SUMMARY
DAY 76

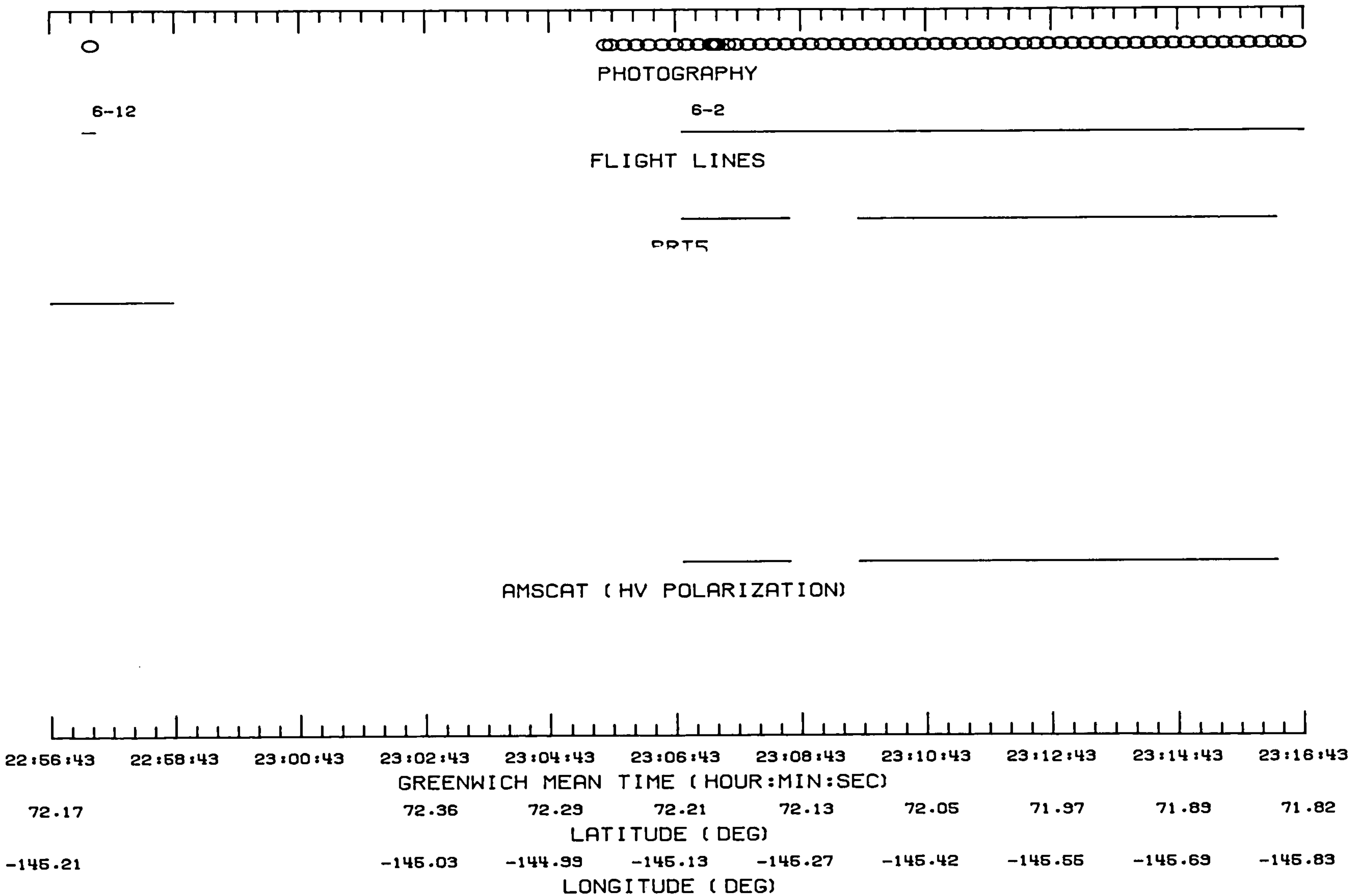

SIRE DATA SET SUMMARY
DAY 76

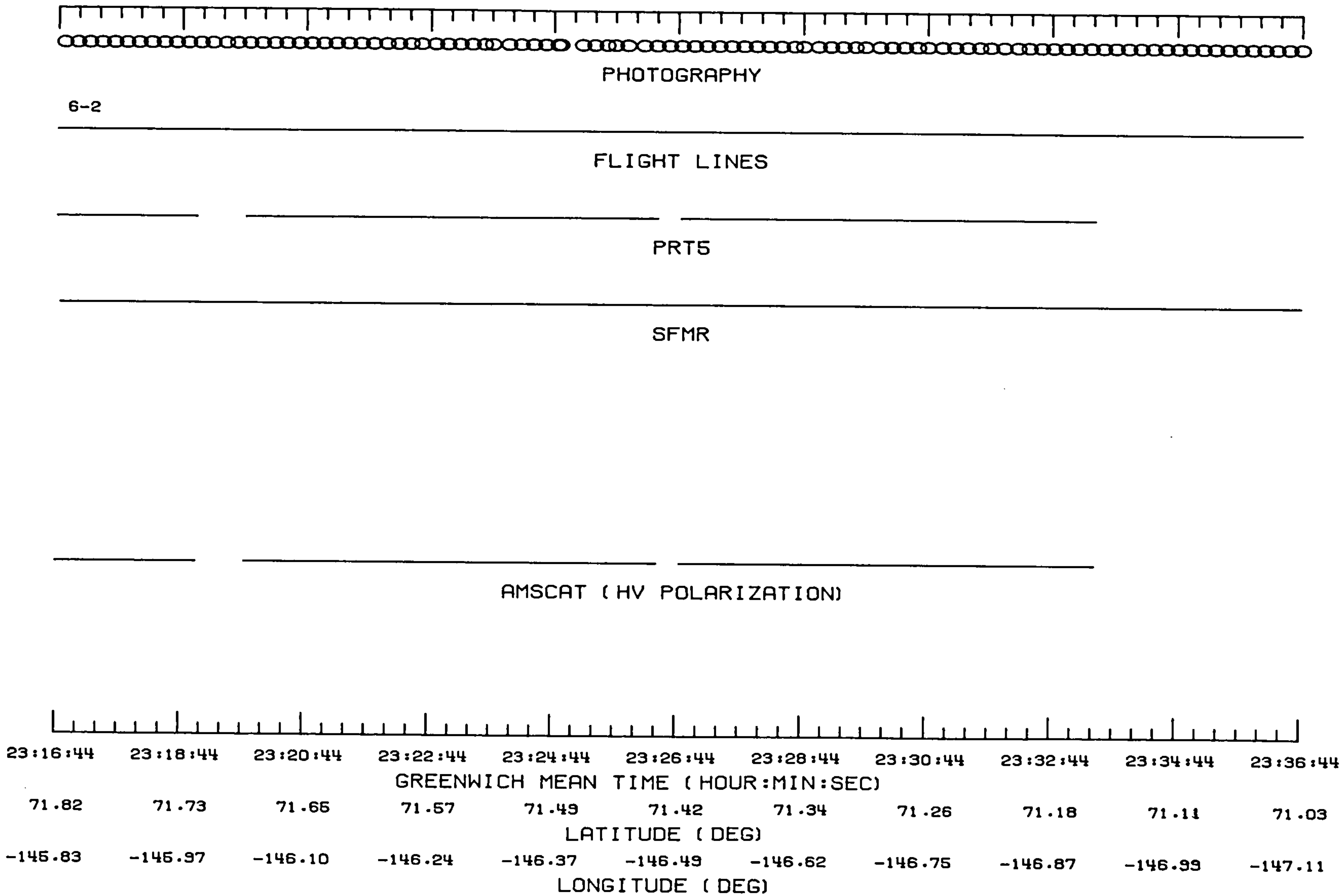

SIRE DATA SET SUMMARY
DAY 76

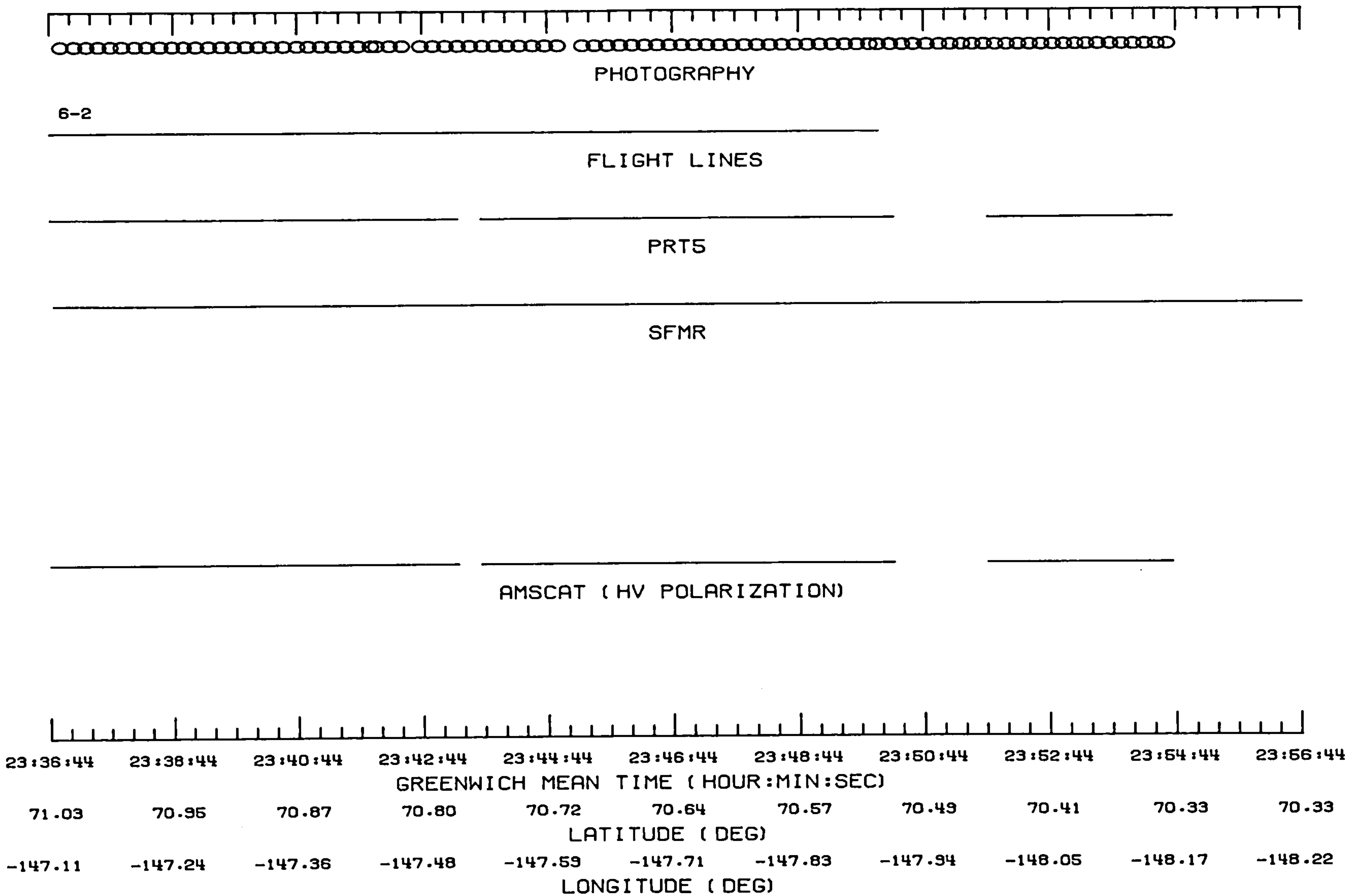

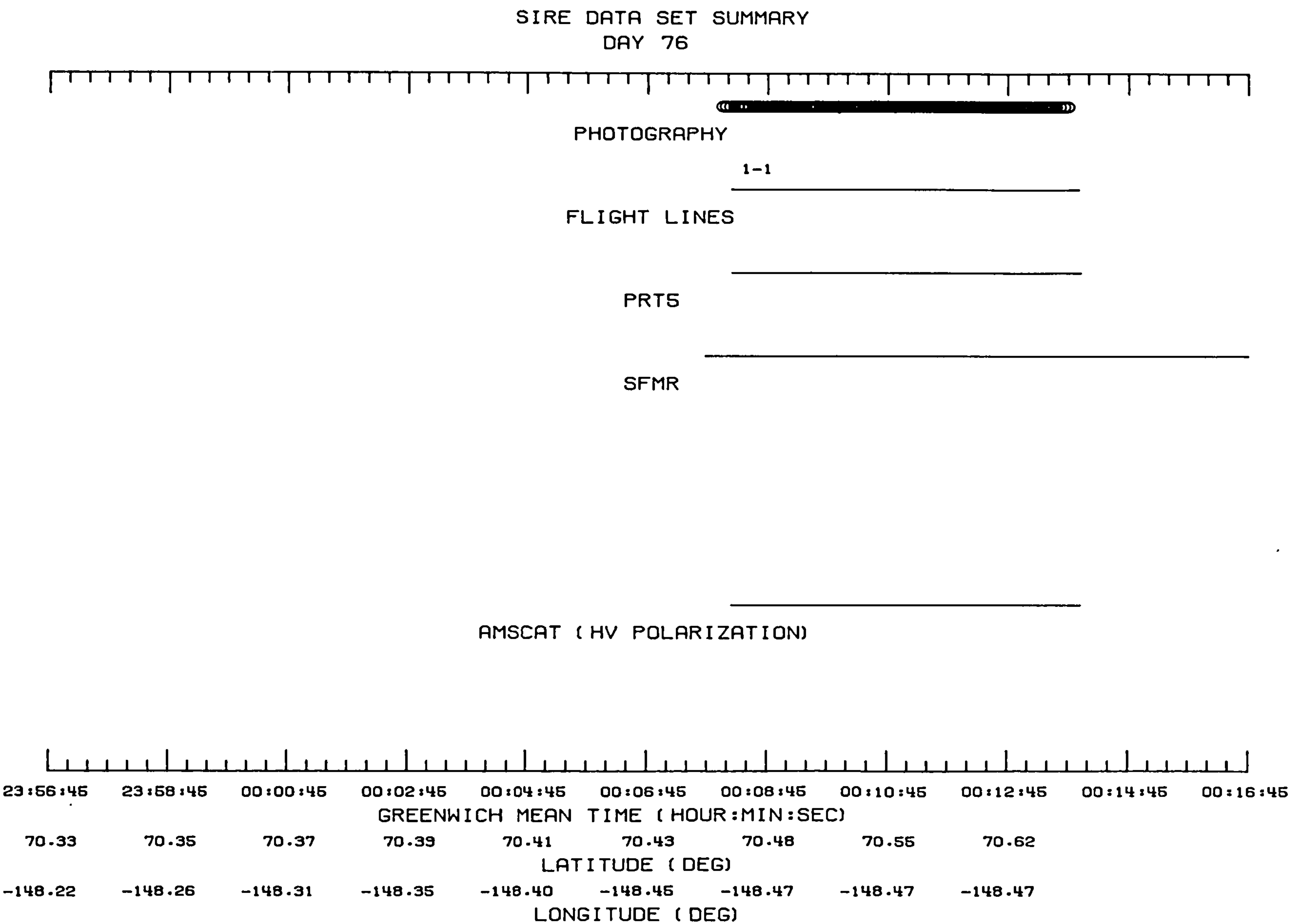
SIRE DATA SET SUMMARY
DAY 76
PHOTOGRAPHY
1-1
FLIGHT LINES
PRTS
SFMR
AMSCAT (HV POLARIZATION)
23:56:45 23:58:45 00:00:45 00:02:45 00:04:45 00:06:45 00:08:45 00:10:45 00:12:45 00:14:45 00:16:45
GREENWICH MEAN TIME (HOUR:MIN:SEC)
70.33 70.35 70.37 70.39 70.41 70.43 70.48 70.55 70.62
LATITUDE (DEG)
-148.22 -148.26 -148.31 -148.35 -148.40 -148.46 -148.47 -148.47 -148.47
LONGITUDE (DEG)

SIRE DATA SET SUMMARY
DAY 76

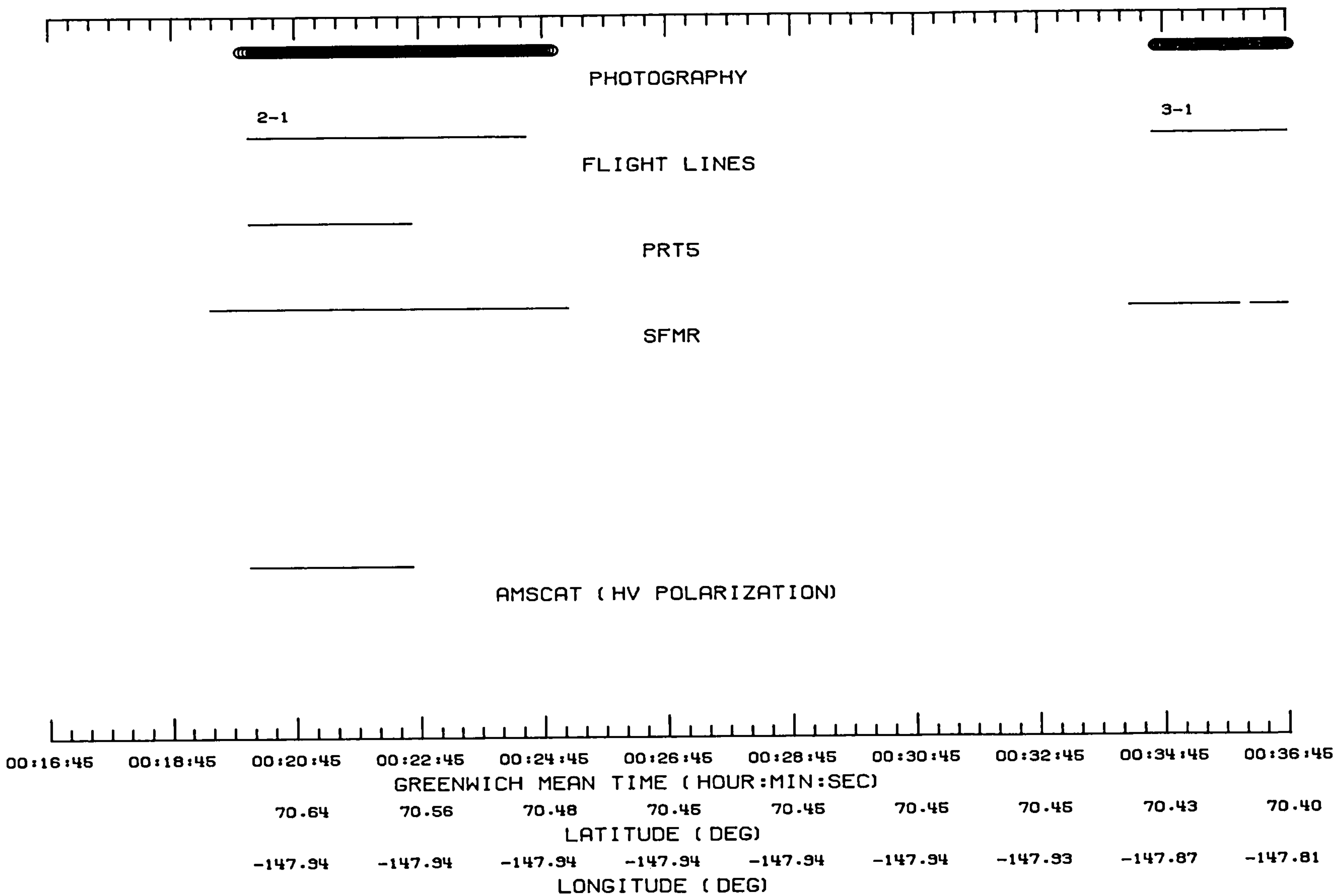

SIRE DATA SET SUMMARY
DAY 76

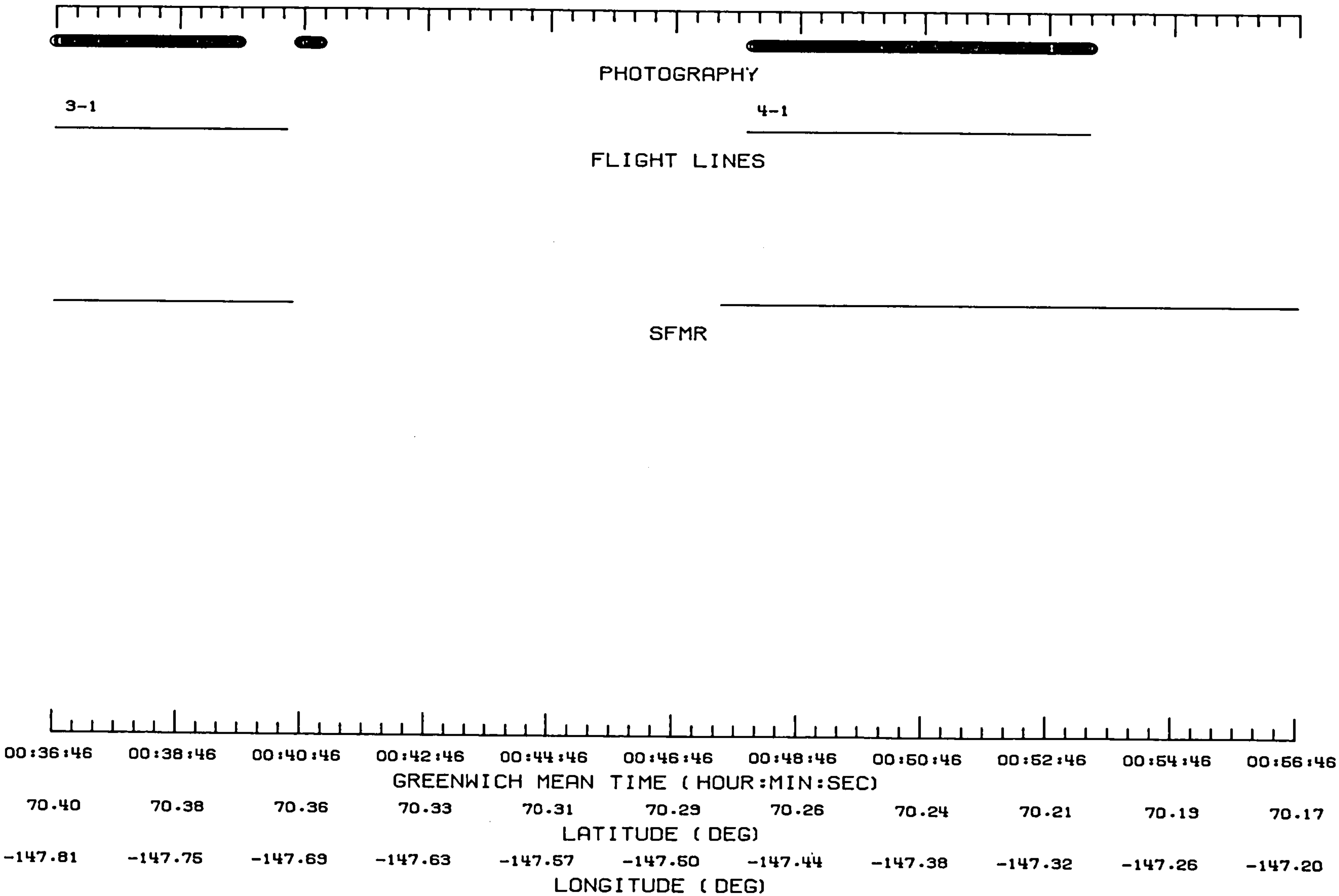

SIRE DATA SET SUMMARY
DAY 76

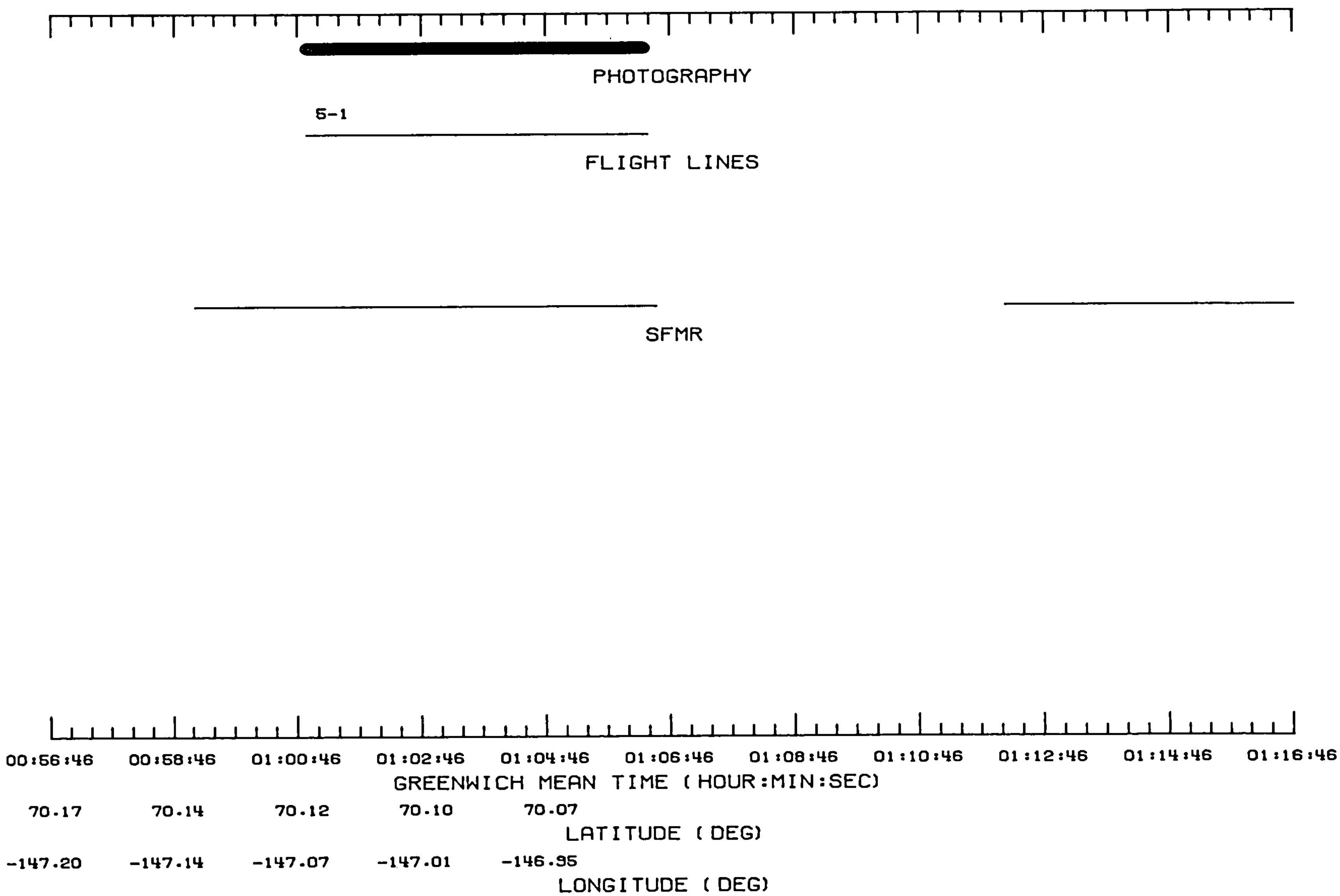

SIRE DATA SET SUMMARY
DAY 76

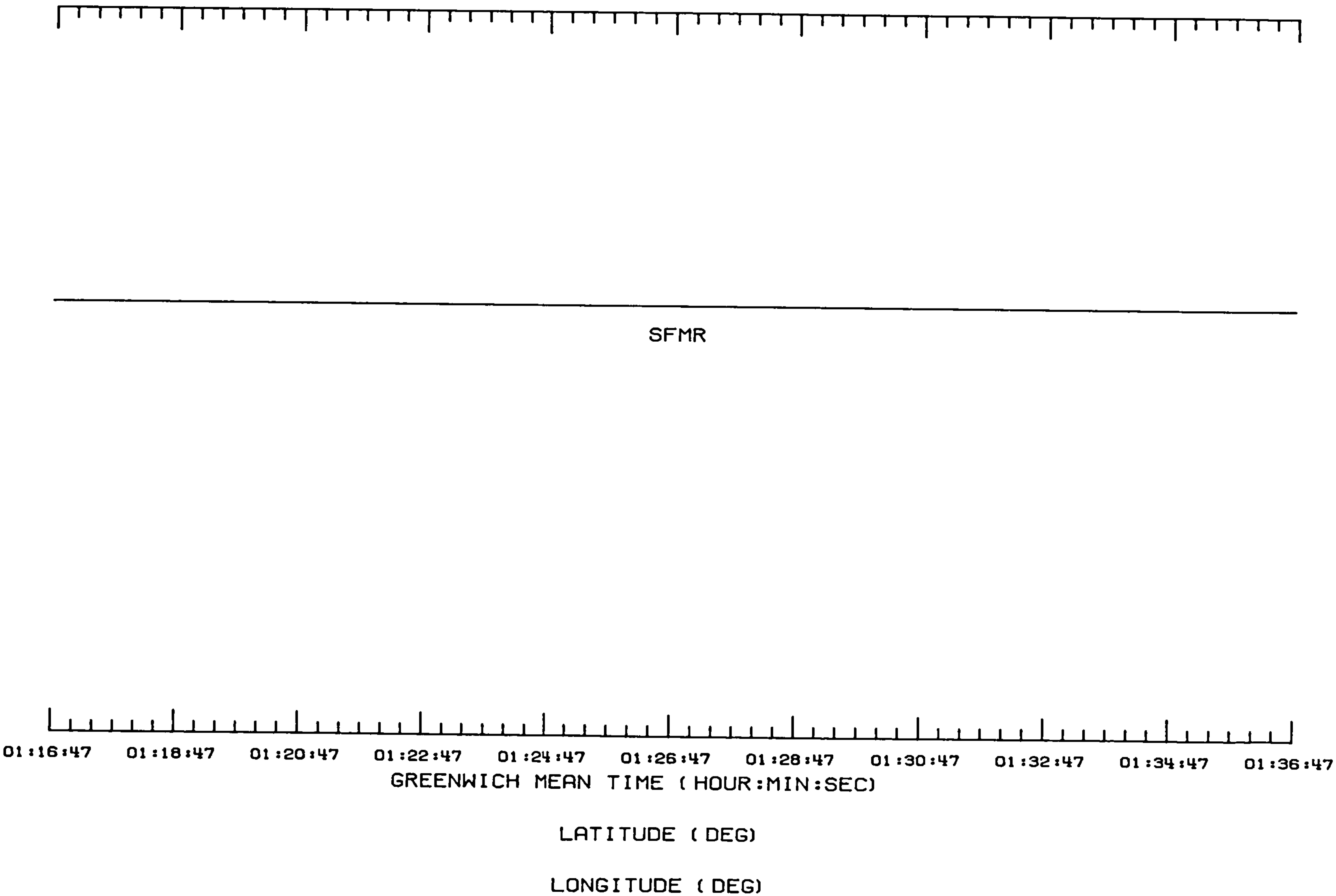

APPENDIX C

Day 77-78

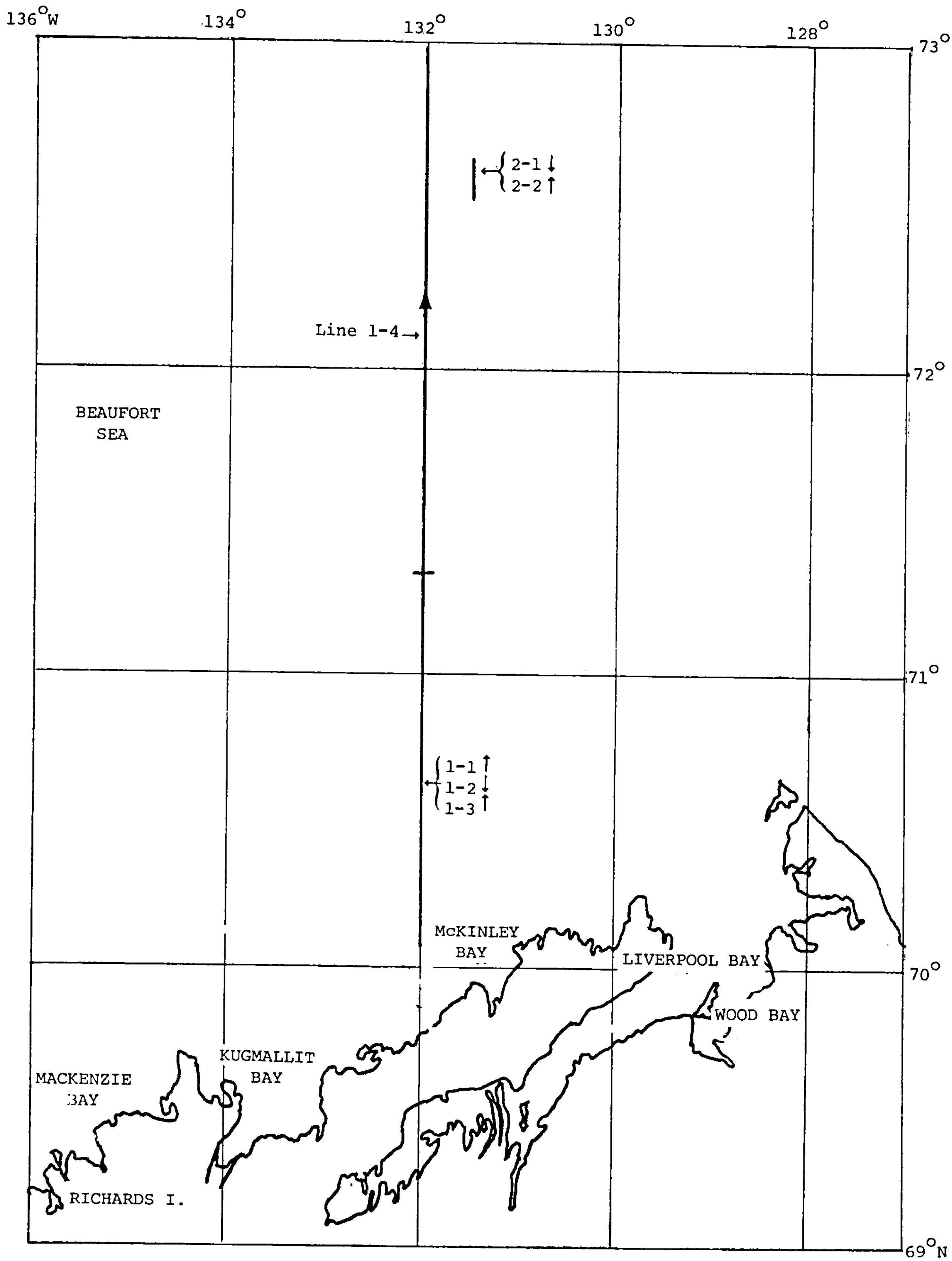

Flight lines for day 77-78

SIRE DATA SET SUMMARY
DAY 77

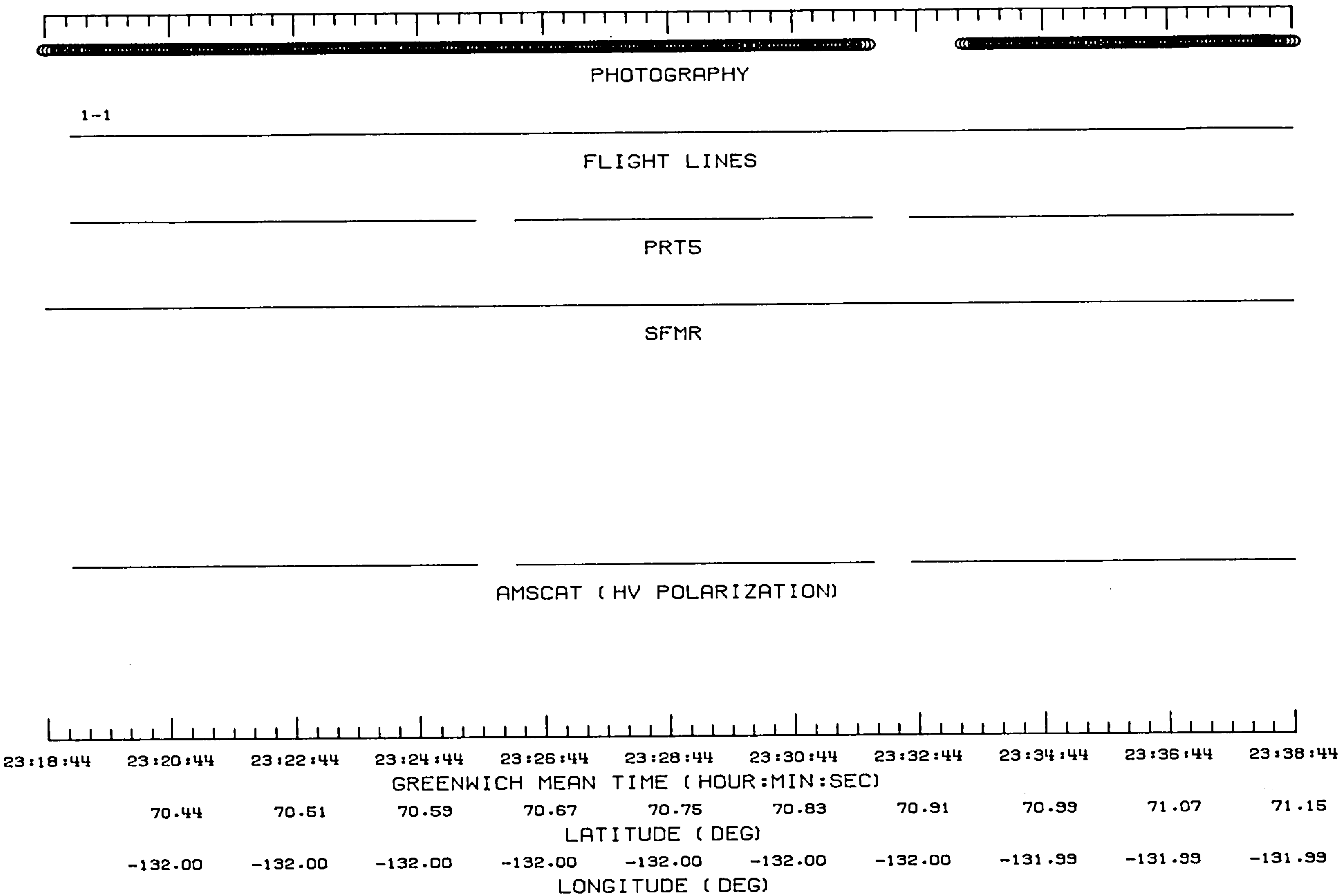

SIRE DATA SET SUMMARY
DAY 78

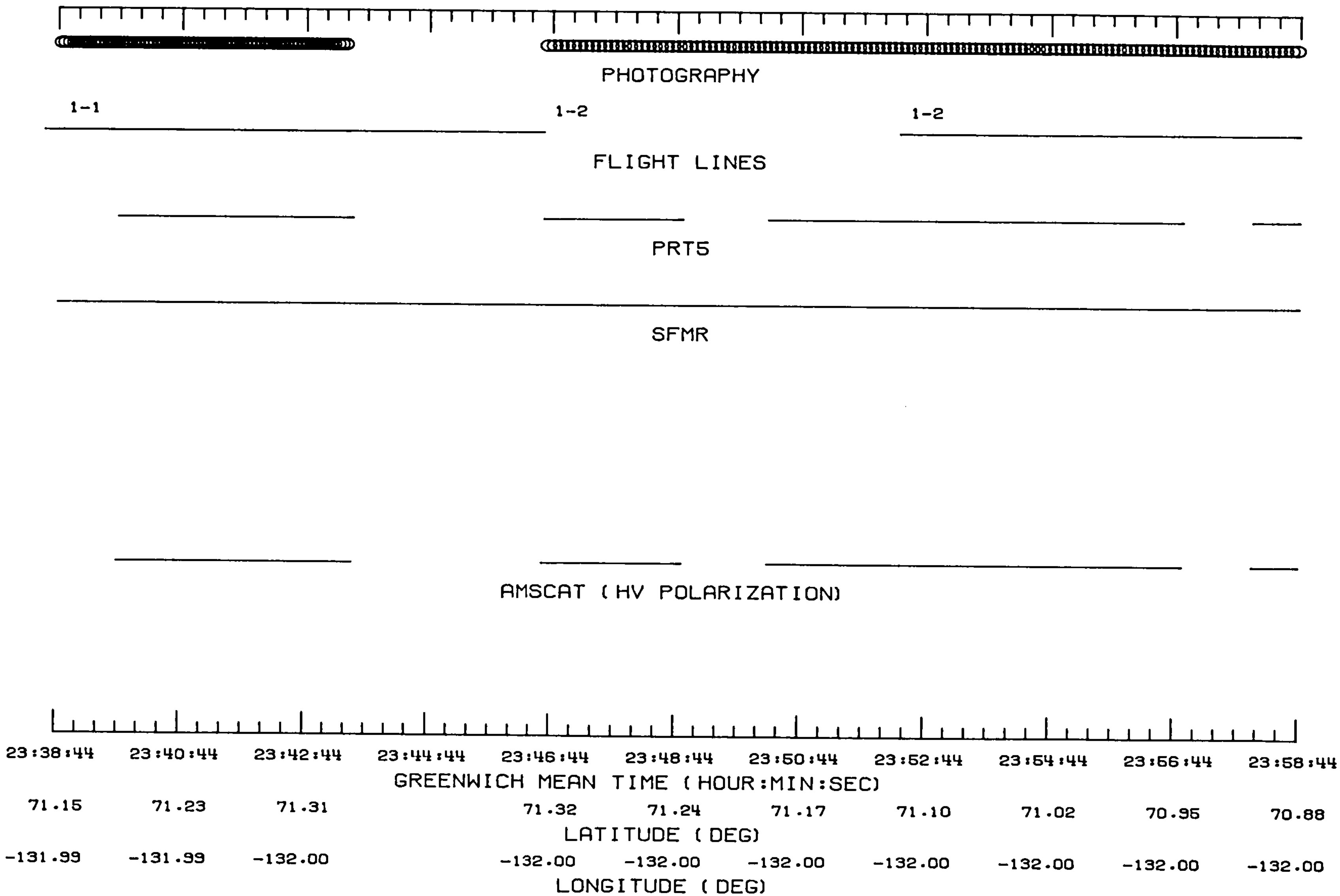

SIRE DATA SET SUMMARY
DAY 78

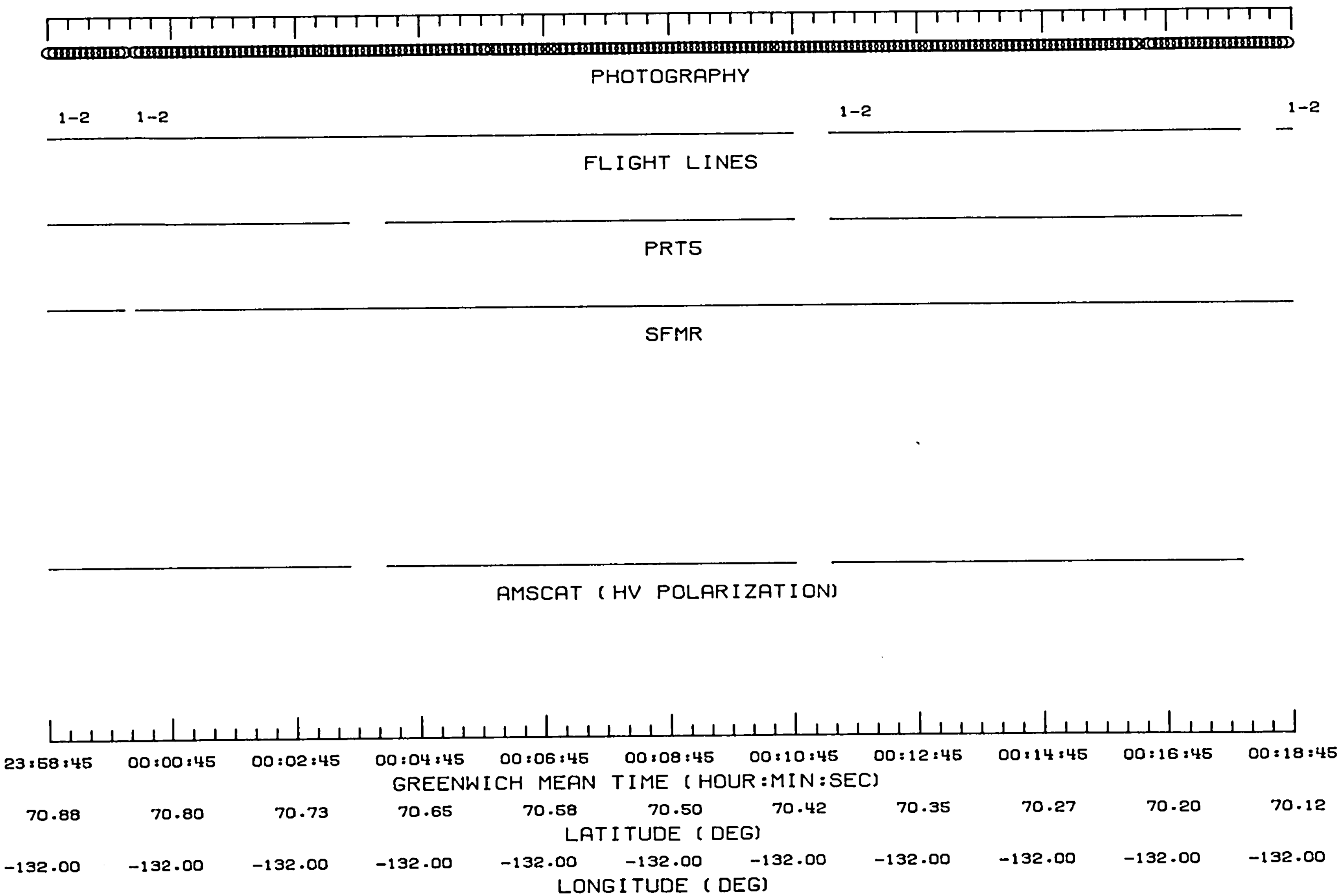

SIRE DATA SET SUMMARY
DAY 78

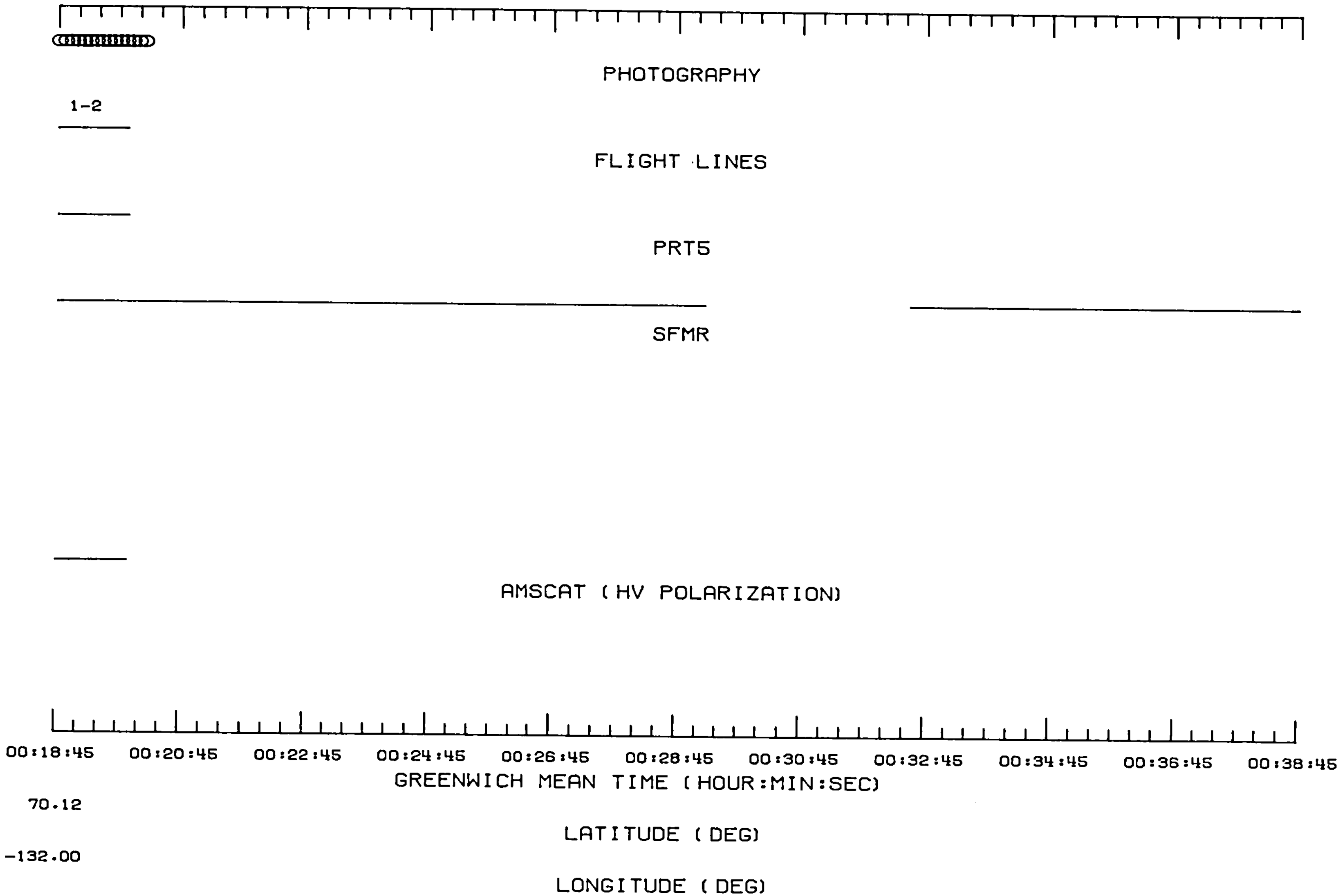

SIRE DATA SET SUMMARY
DAY 78

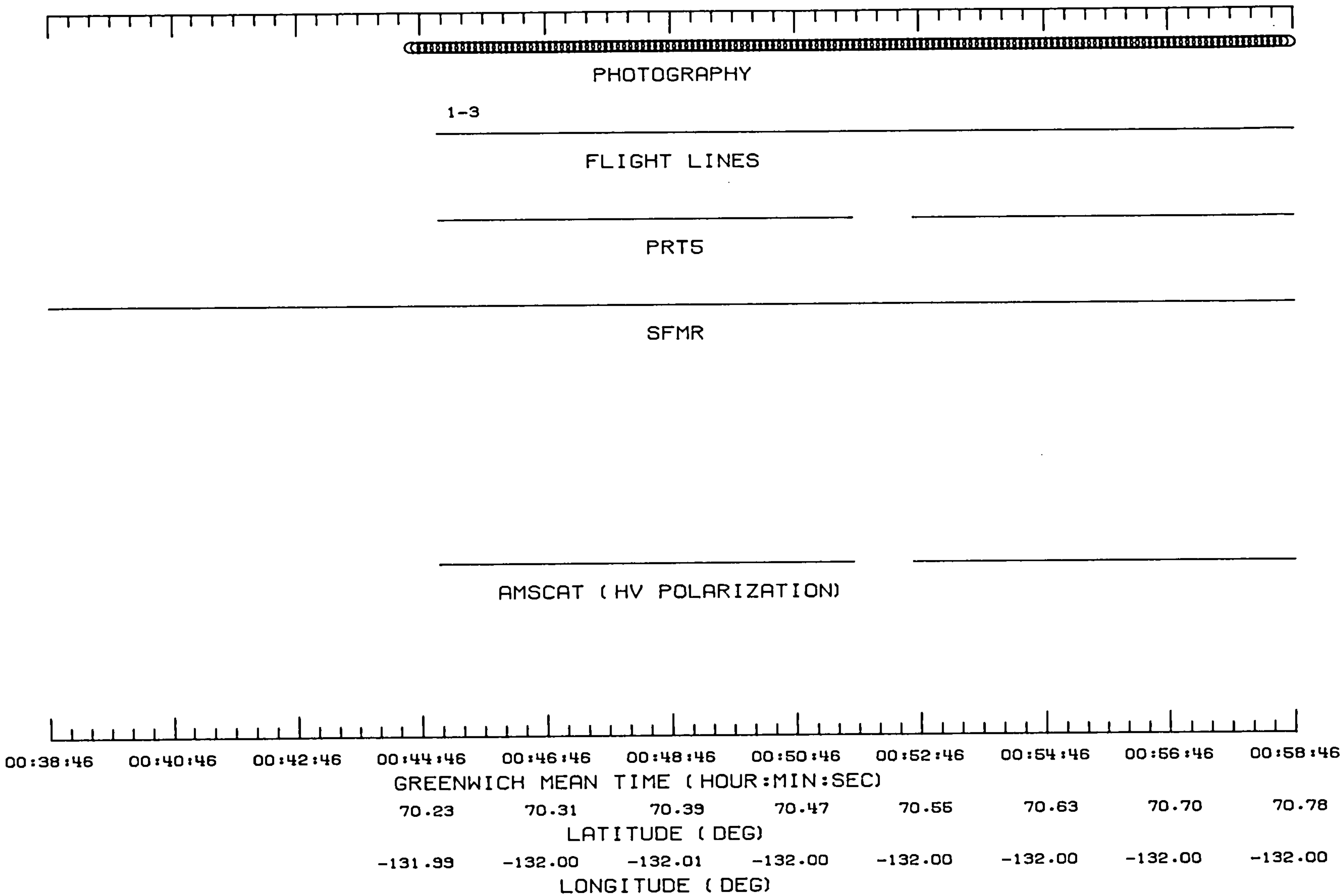

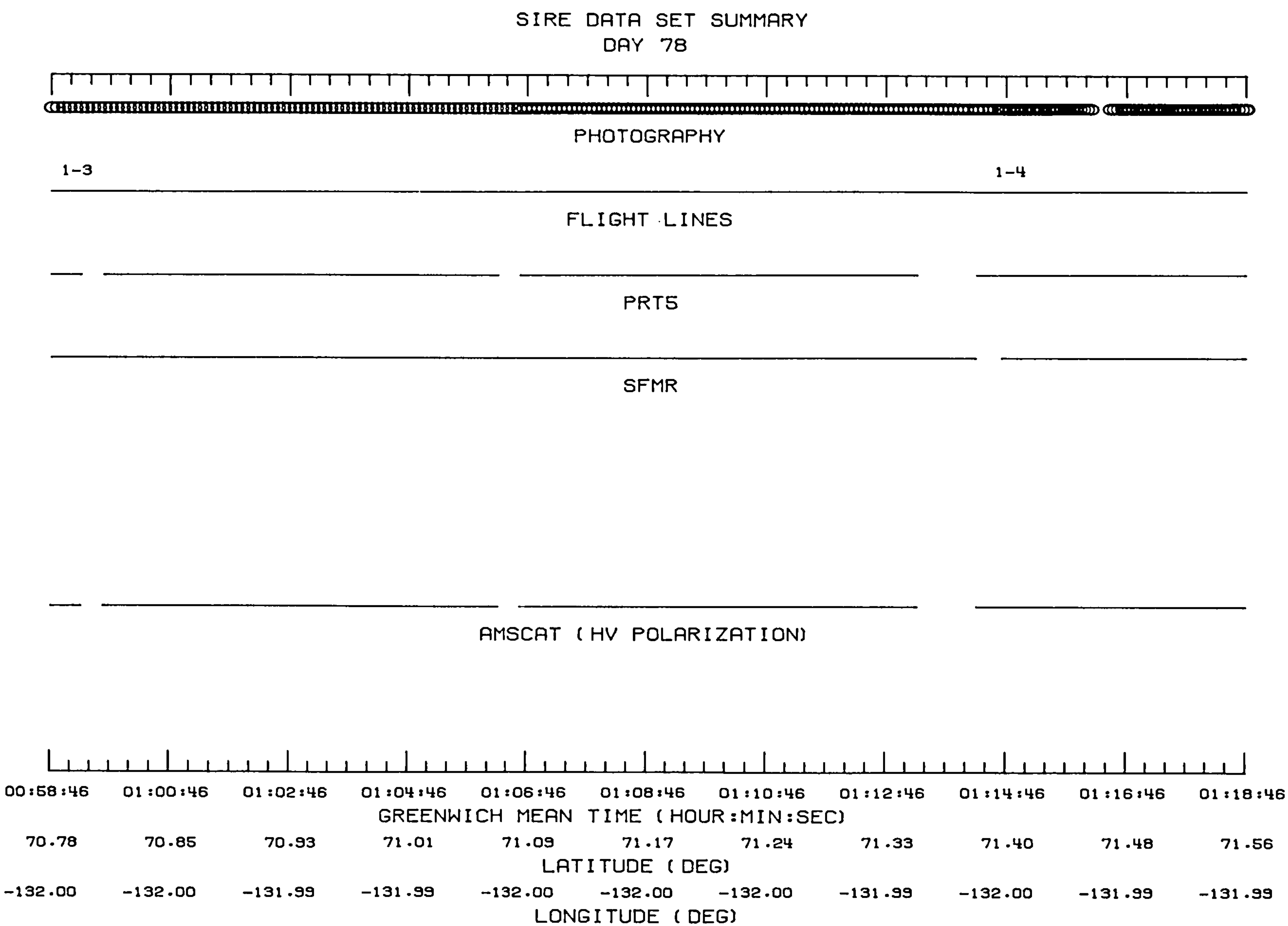
SIRE DATA SET SUMMARY
DAY 78
PHOTOGRAPHY
1-3
1-4
FLIGHT LINES
PRTS
SFMR
AMSCAT (HV POLARIZATION)
00:58:46 01:00:46 01:02:46 01:04:46 01:06:46 01:08:46 01:10:46 01:12:46 01:14:46 01:16:46 01:18:46
GREENWICH MEAN TIME (HOUR:MIN:SEC)
70.78 70.85 70.93 71.01 71.09 71.17 71.24 71.33 71.40 71.48 71.56
LATITUDE (DEG)
-132.00 -132.00 -131.99 -131.99 -132.00 -132.00 -132.00 -131.99 -132.00 -131.99 -131.99
LONGITUDE (DEG)

SIRE DATA SET SUMMARY
DAY 78

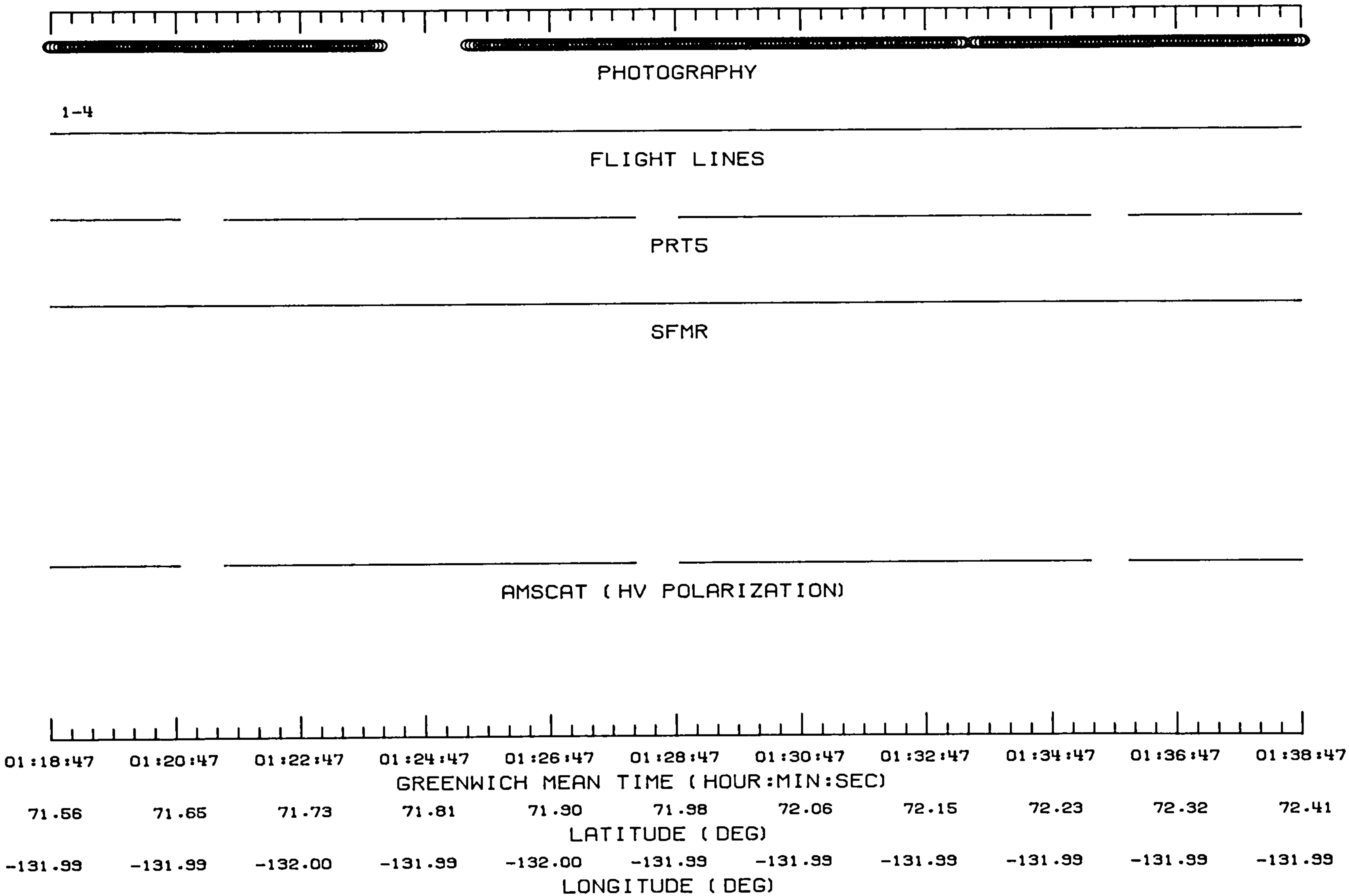

SIRE DATA SET SUMMARY
DAY 78

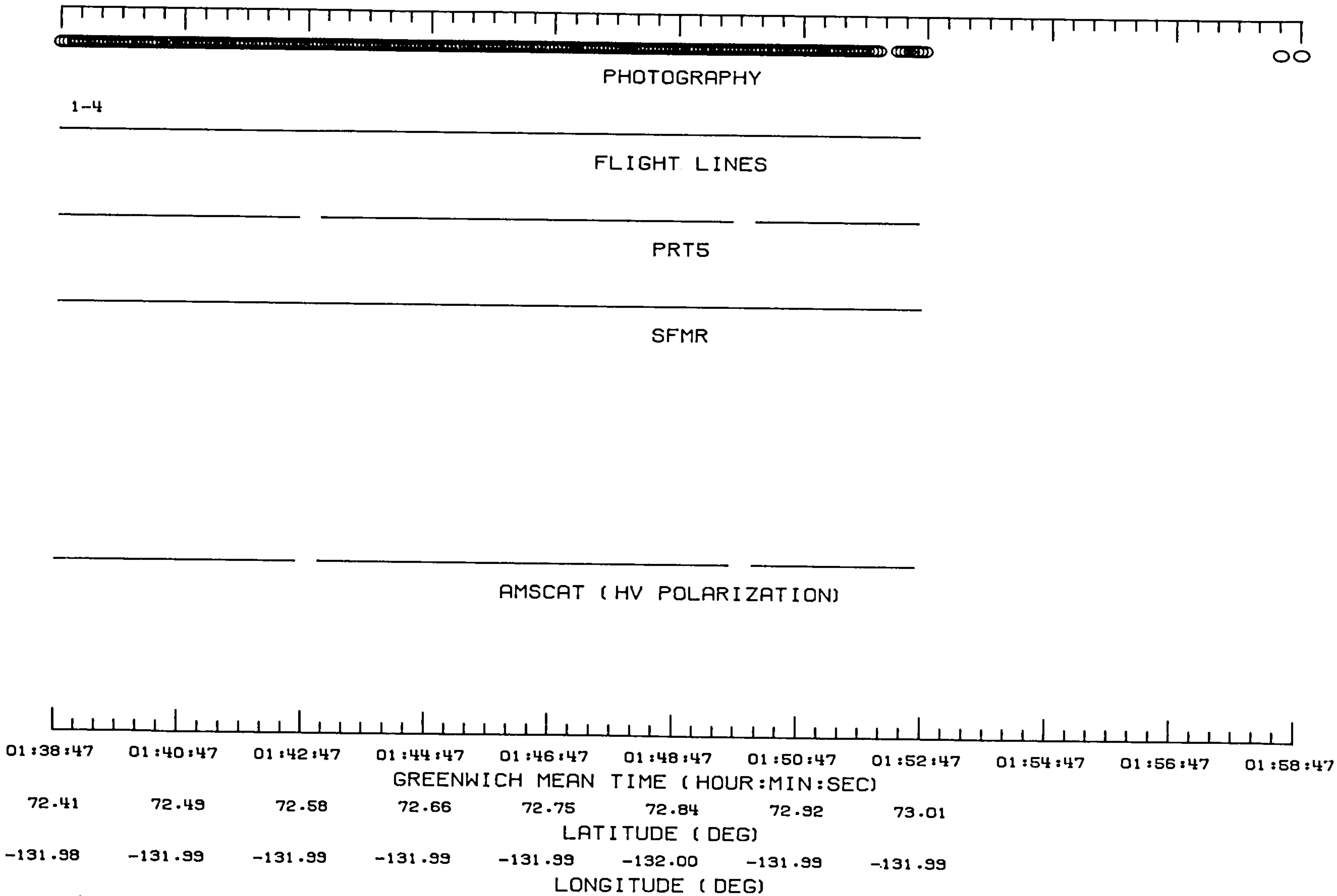

SIRE DATA SET SUMMARY
DAY 78

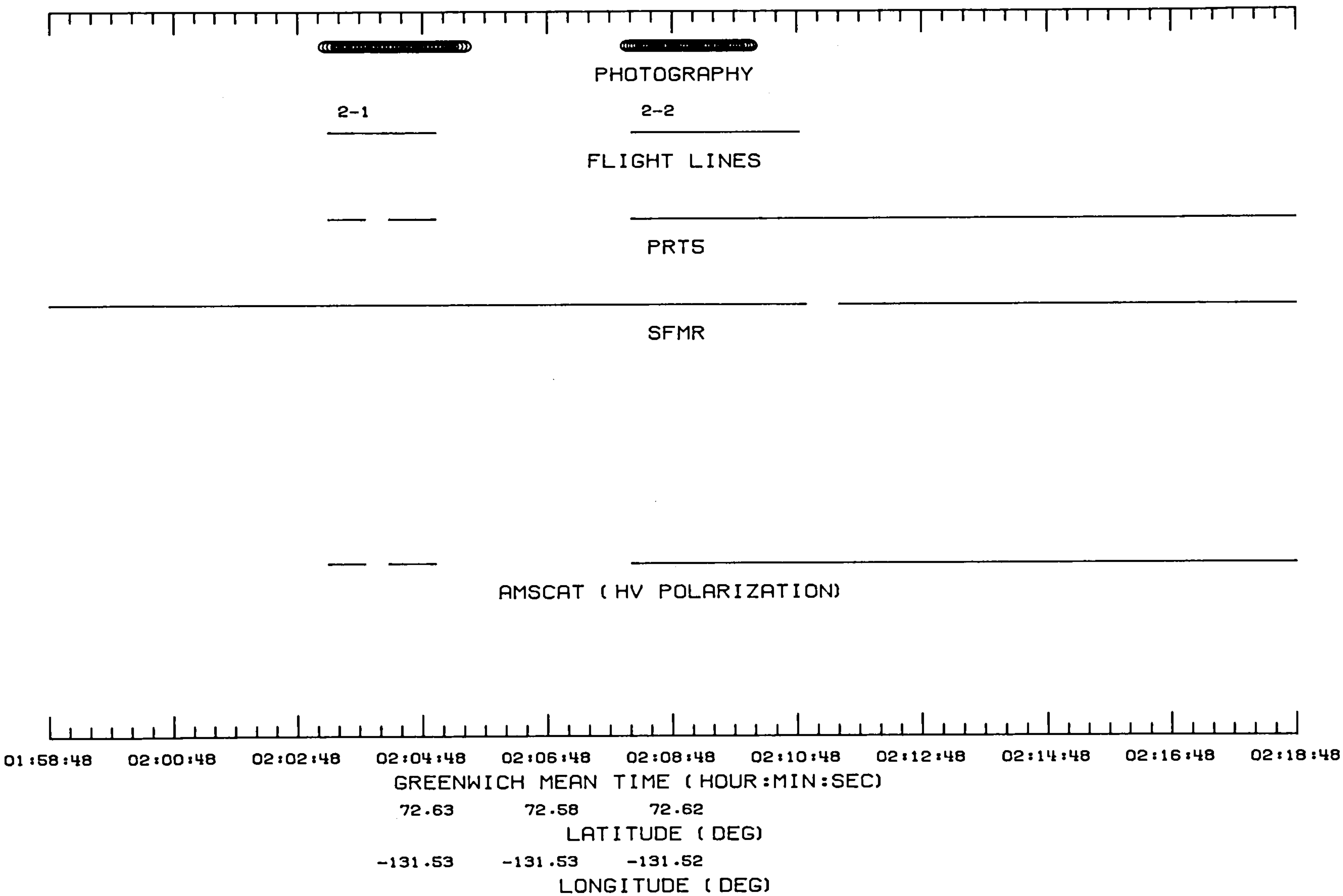

SIRE DATA SET SUMMARY
DAY 78

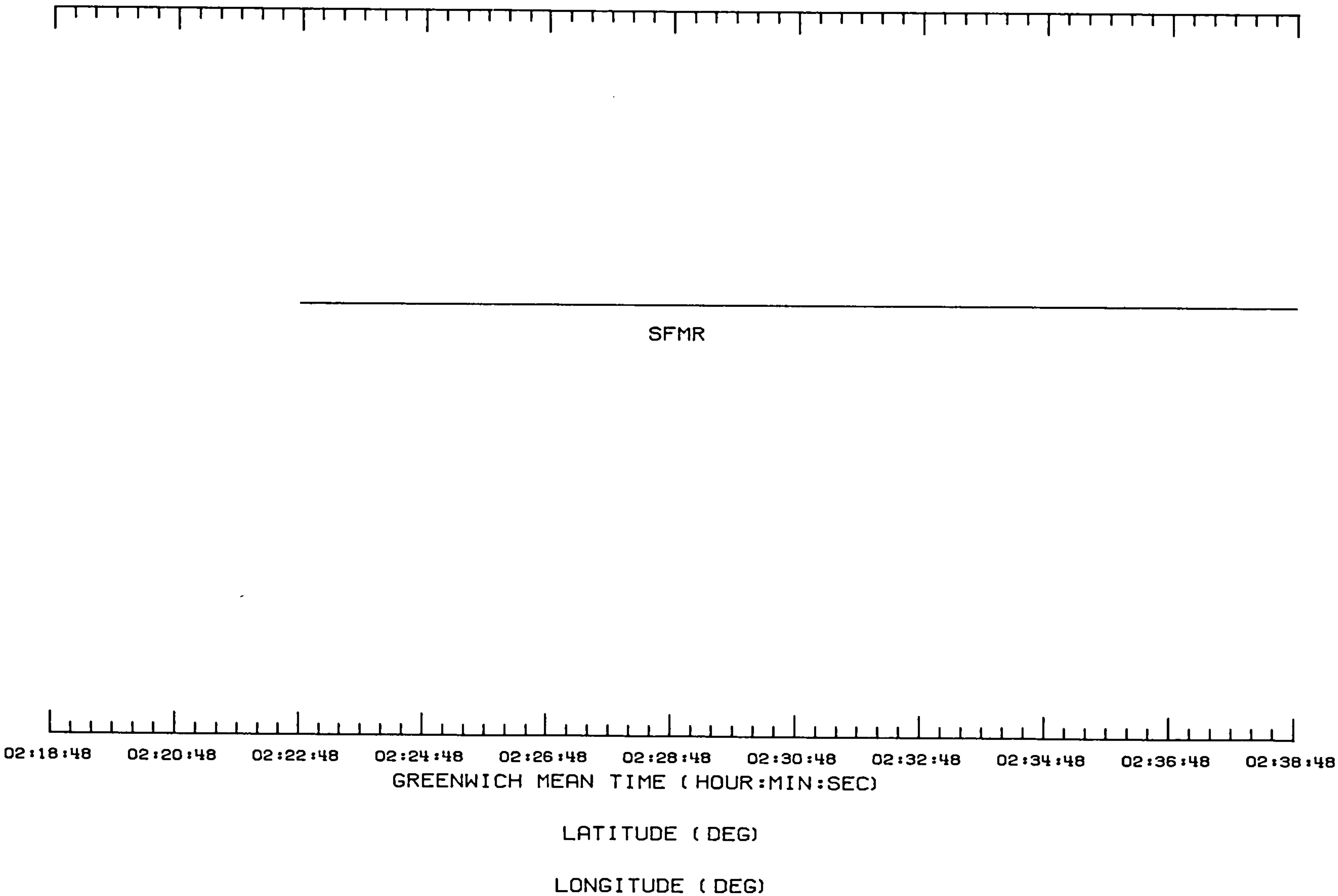

SIRE DATA SET SUMMARY
DAY 78

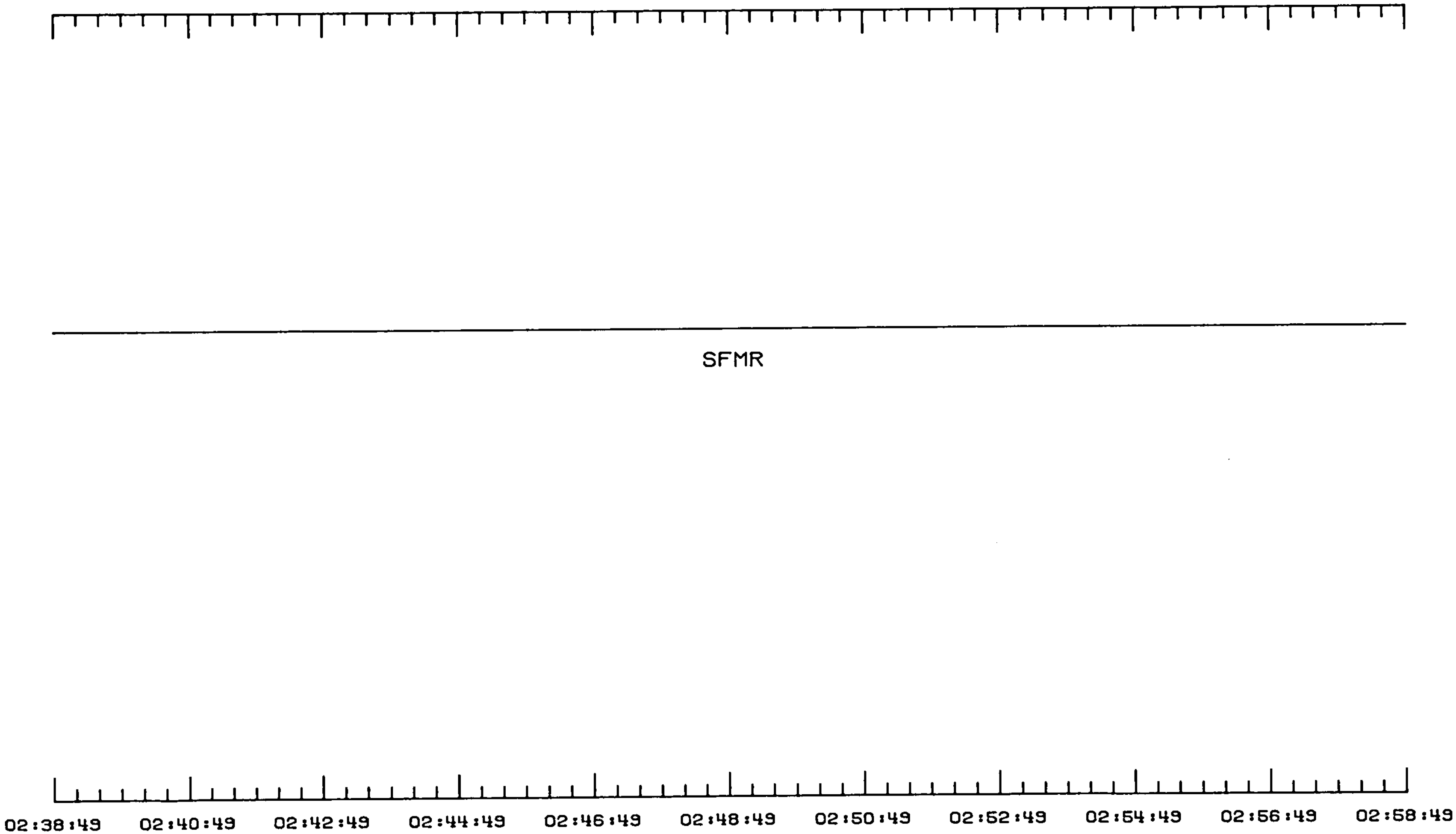

GREENWICH MEAN TIME (HOUR:MIN:SEC)

LATITUDE (DEG)

LONGITUDE (DEG)

SIRE DATA SET SUMMARY
DAY 78

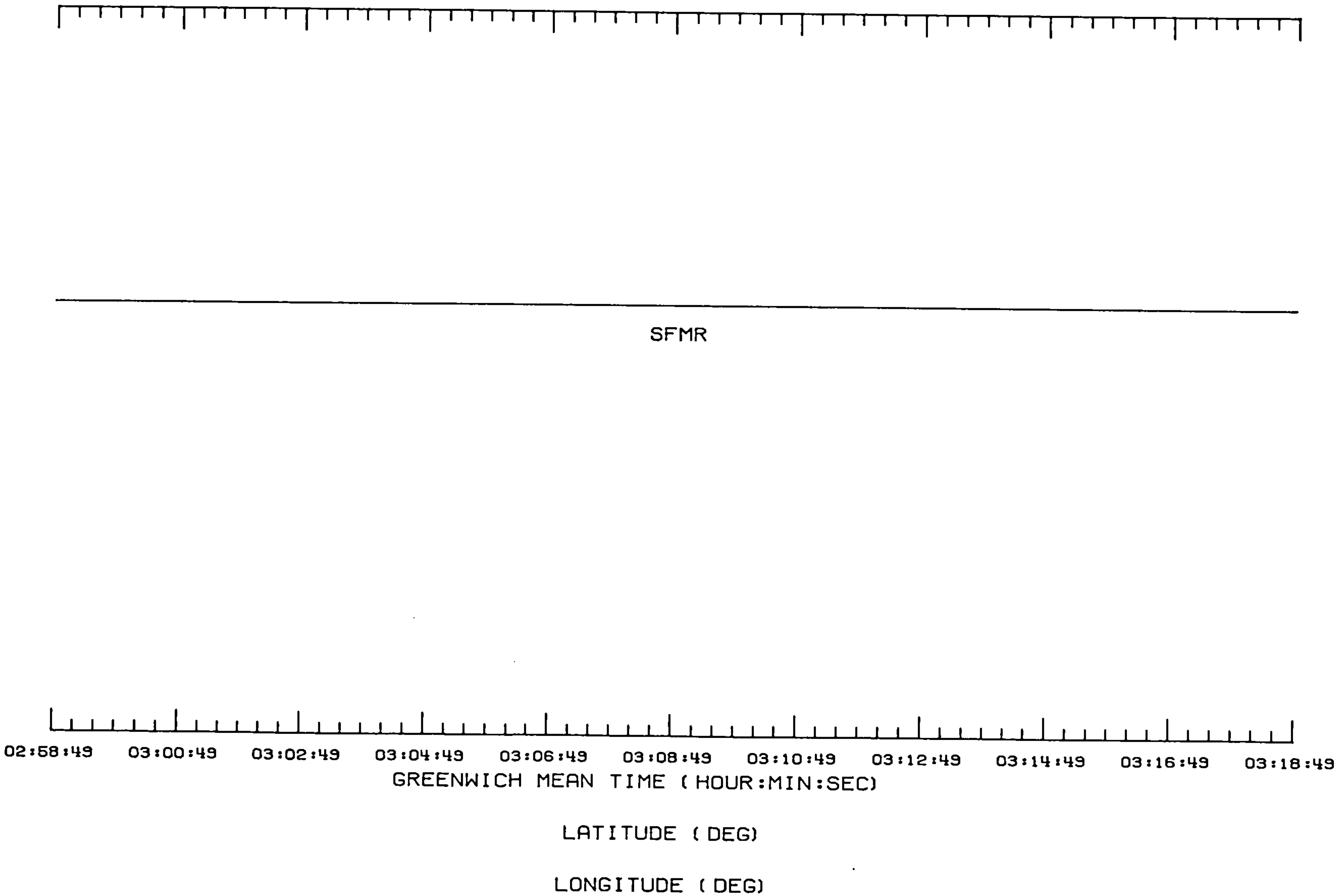

APPENDIX C

Day 79

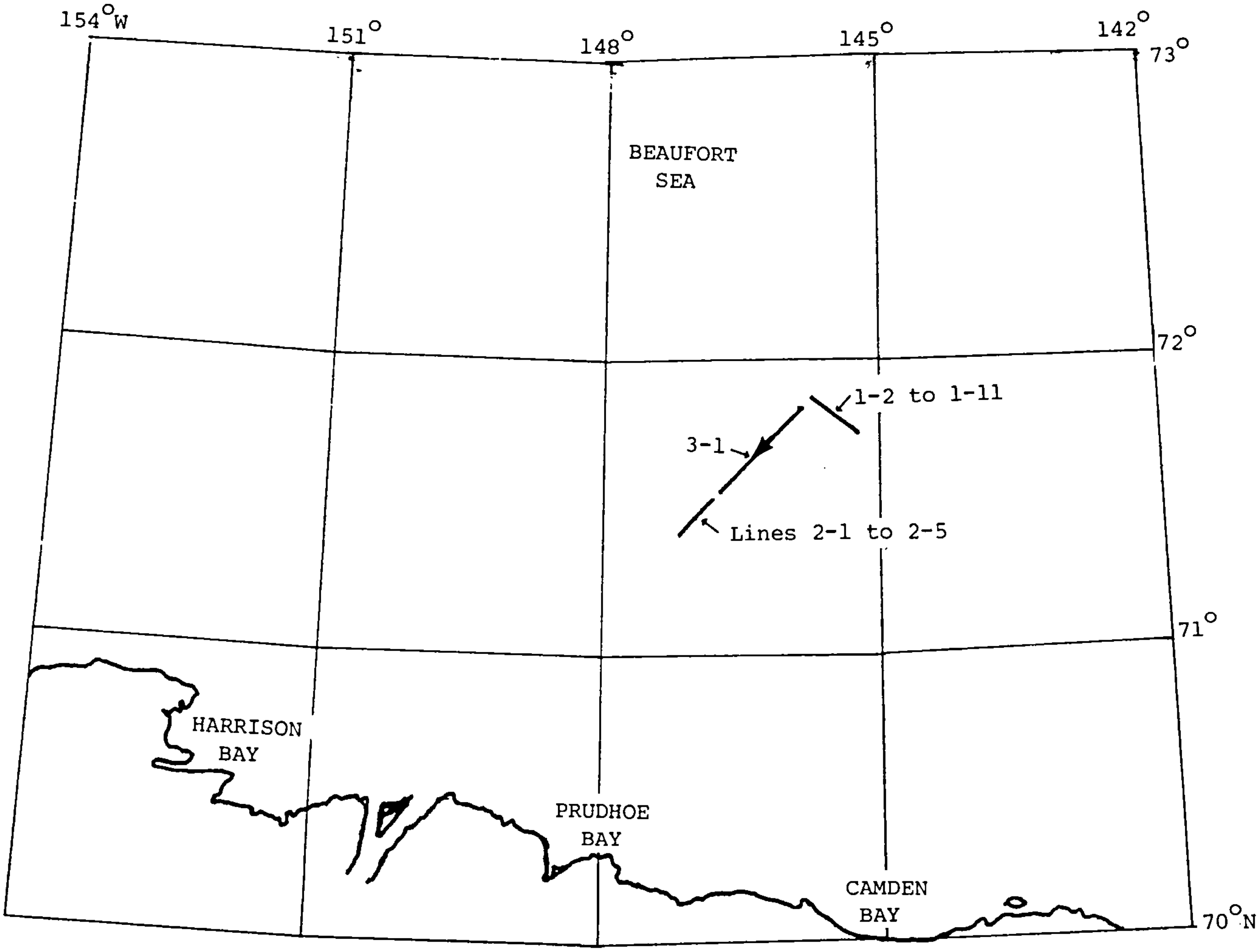

Flight lines for day 79

SIRE DATA SET SUMMARY
DAY 79

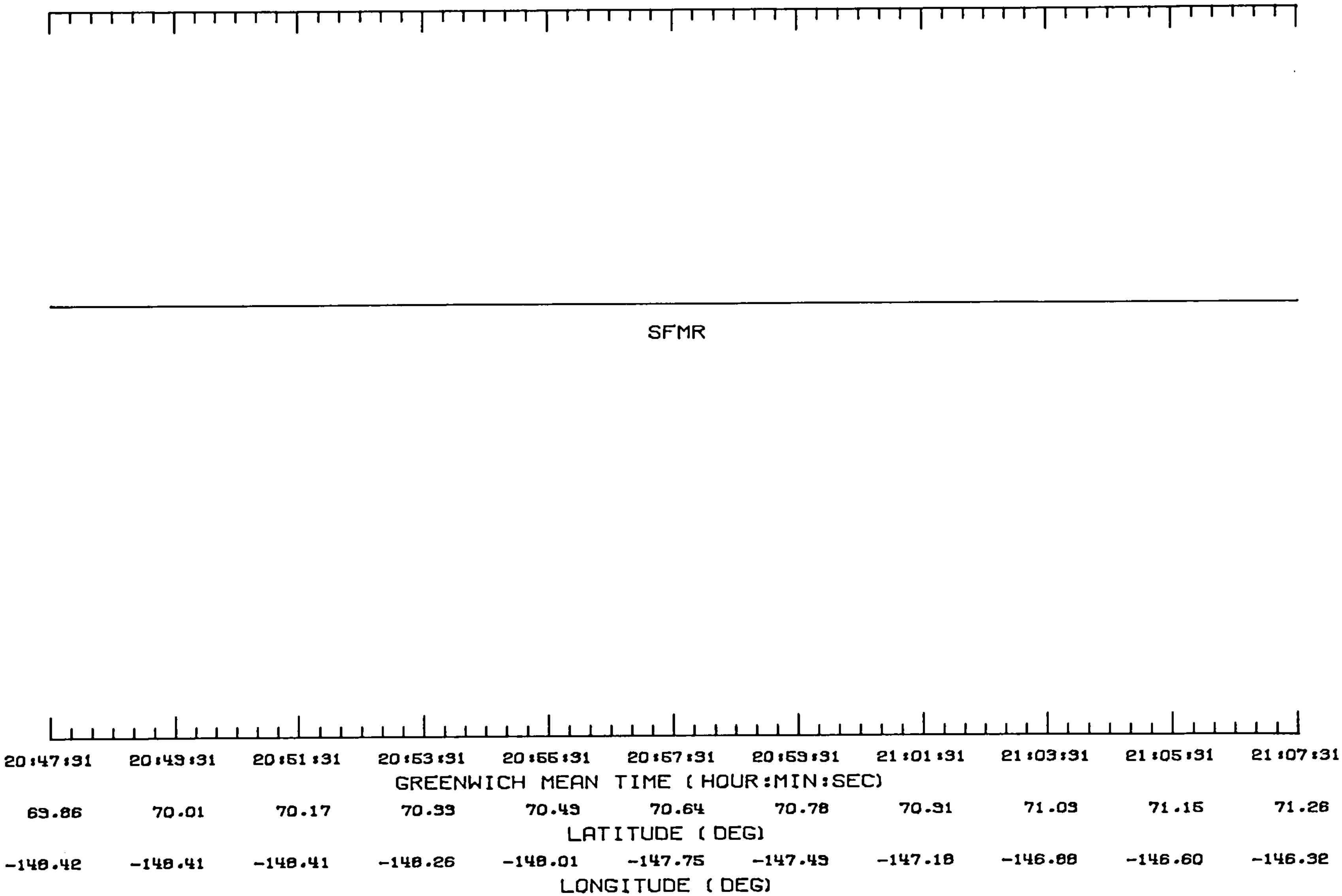

SIRE DATA SET SUMMARY
DAY 79

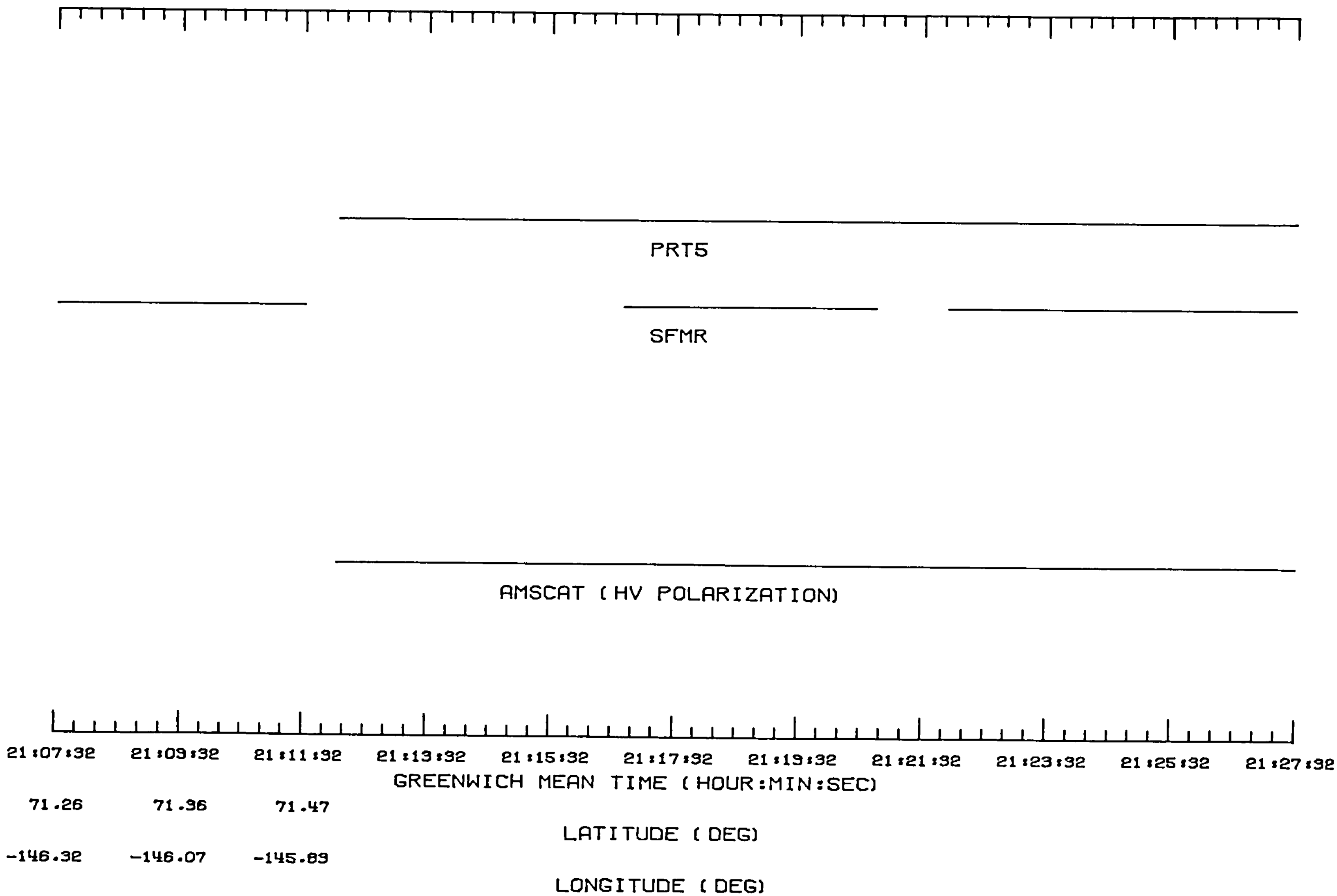

SIRE DATA SET SUMMARY
DAY 79

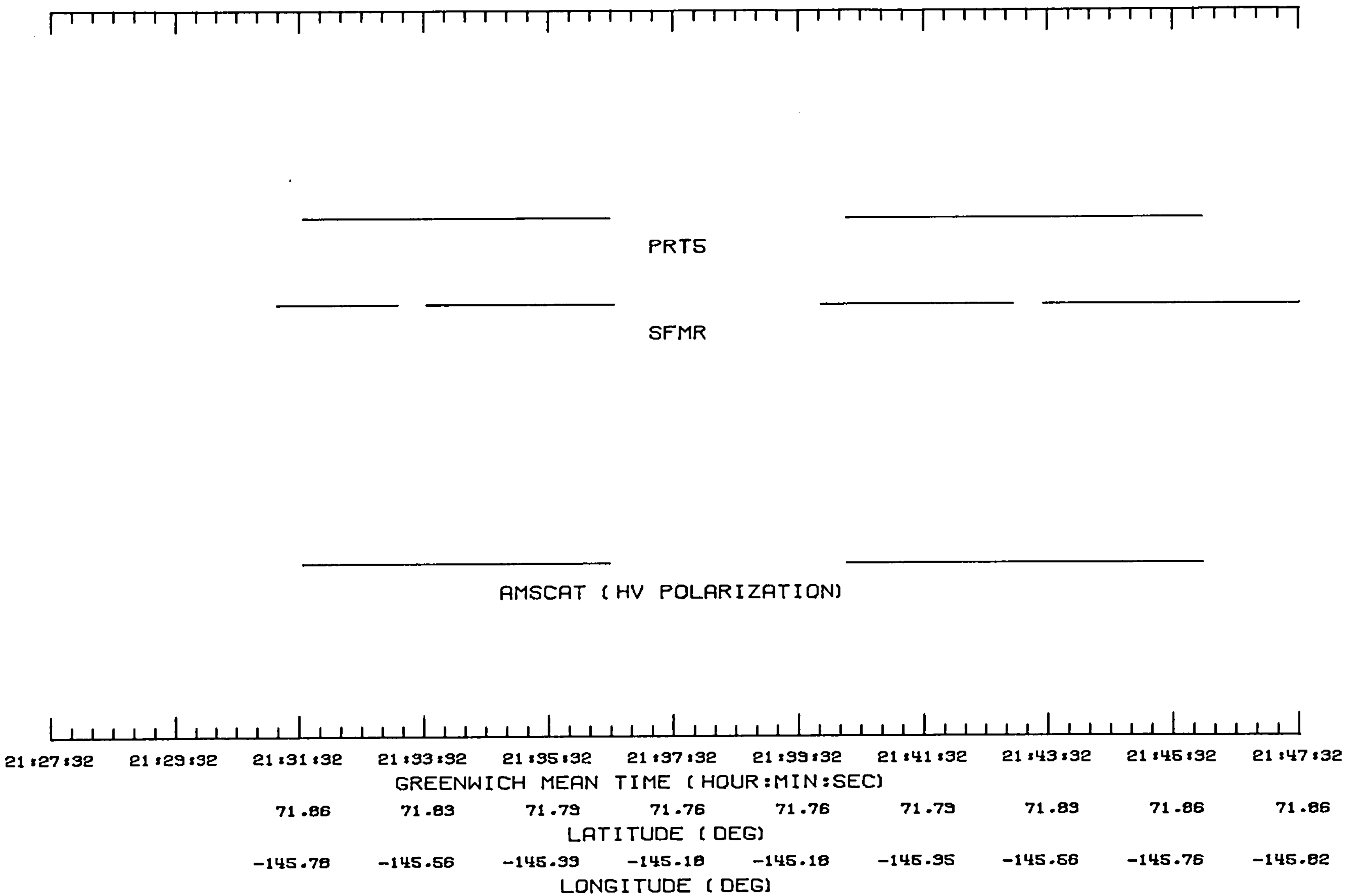

SIRE DATA SET SUMMARY
DAY 79

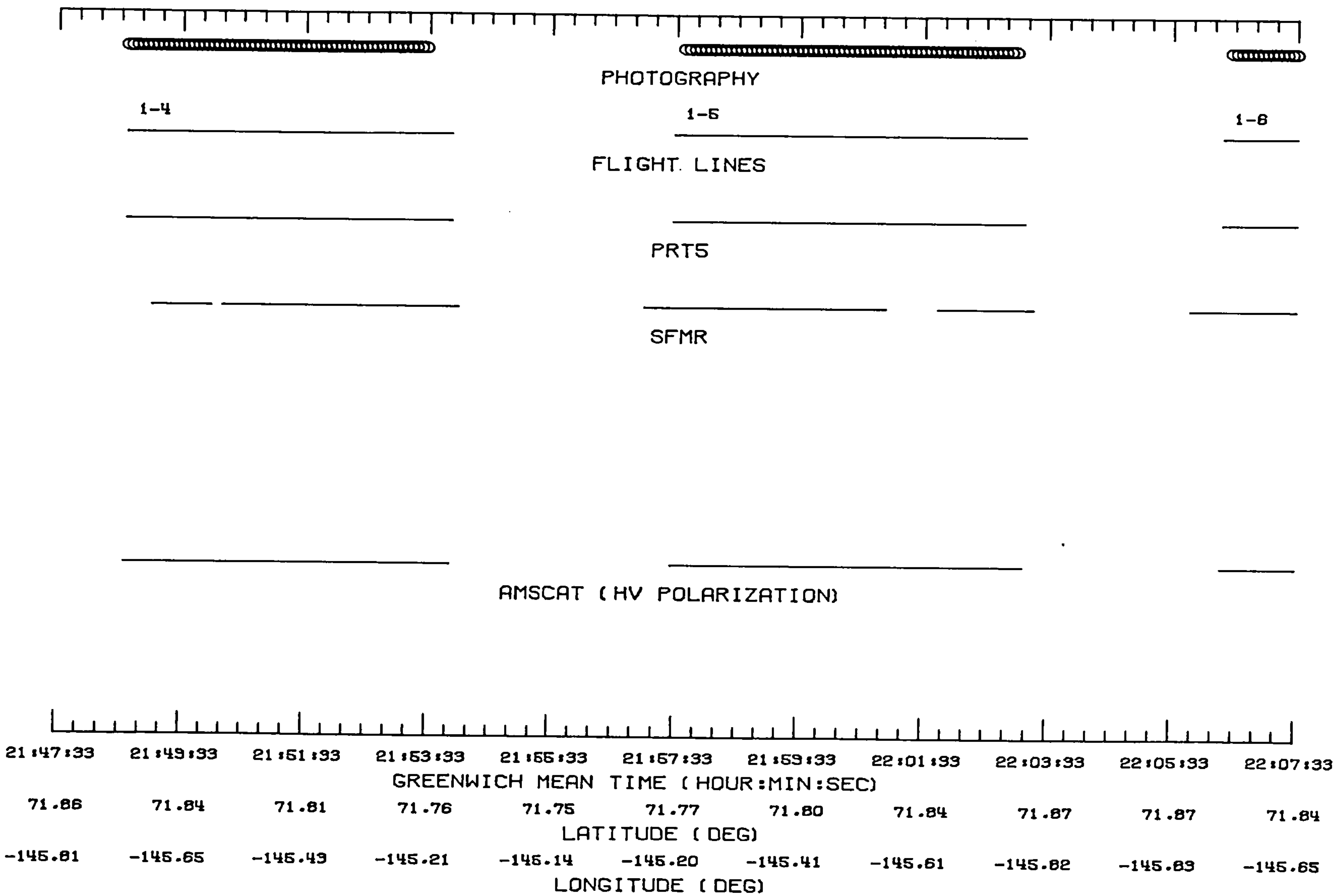

SIRE DATA SET SUMMARY
DAY 79

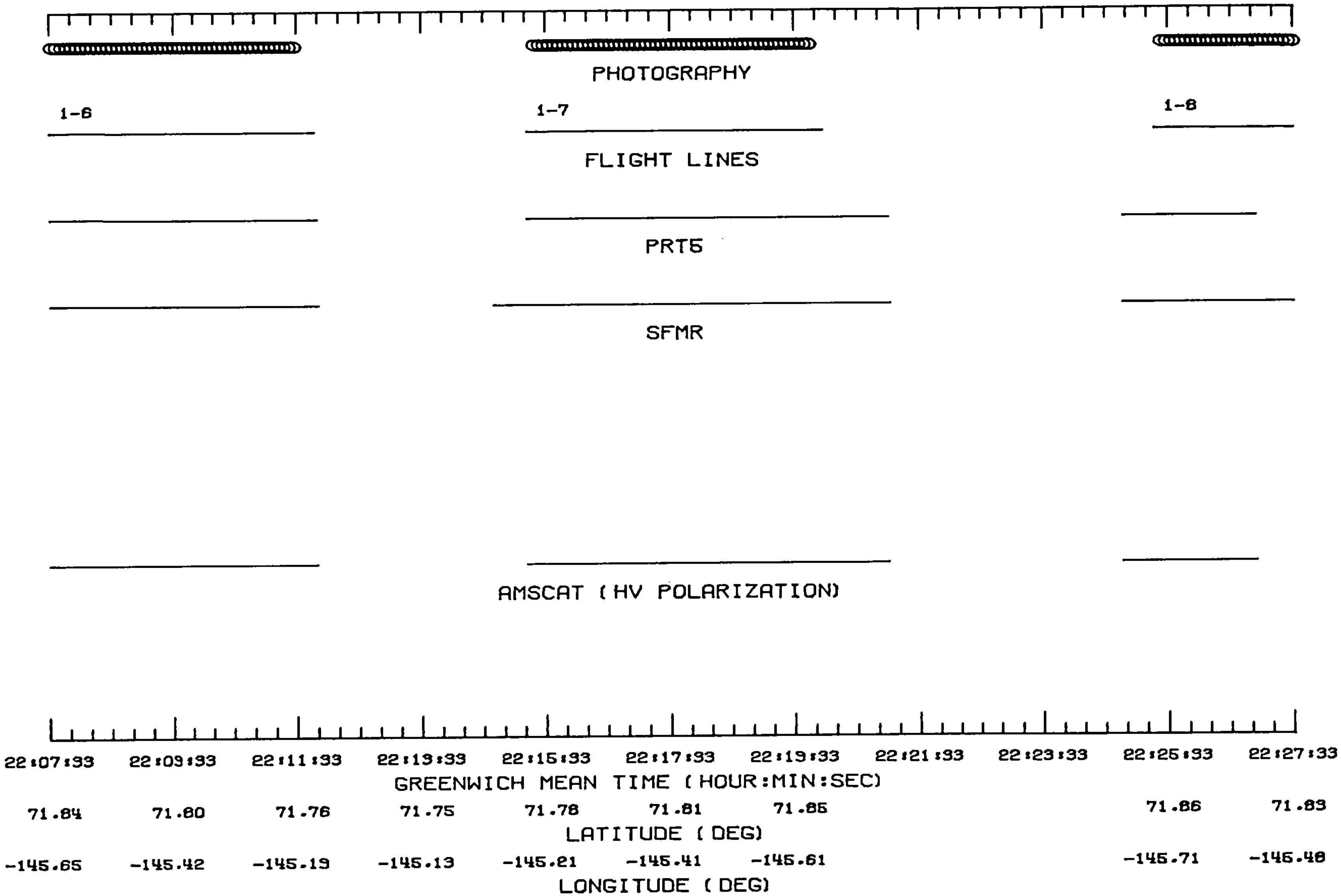

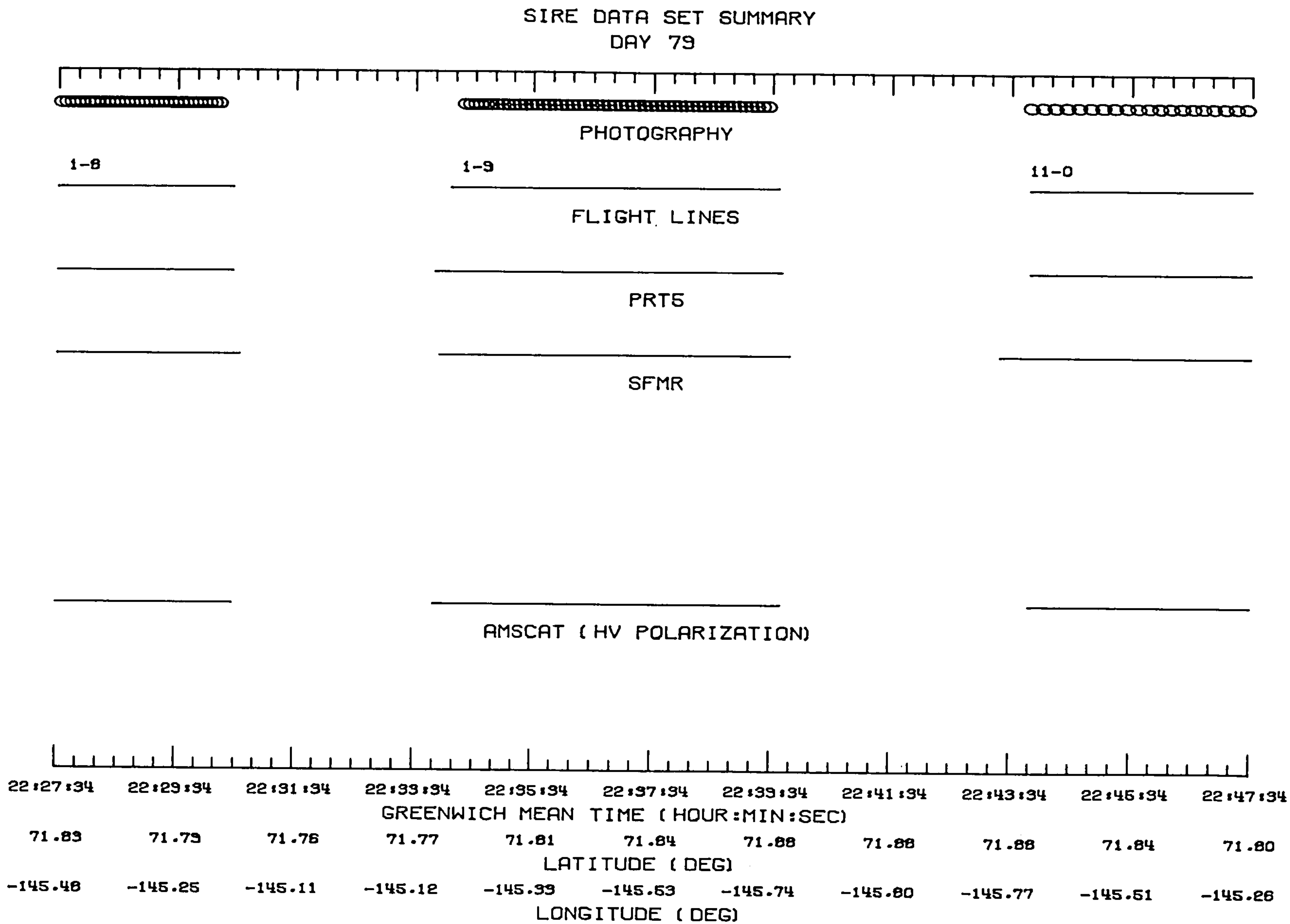
SIRE DATA SET SUMMARY
DAY 79
PHOTOGRAPHY
1-8
1-9
11-0
FLIGHT LINES
PRTS
SFMR
AMSCAT (HV POLARIZATION)
22:27:34
22:29:34
22:31:34
22:33:34
22:35:34
22:37:34
22:39:34
22:41:34
22:43:34
22:45:34
22:47:34
GREENWICH MEAN TIME (HOUR:MIN:SEC)
71.83
71.79
71.76
71.77
71.81
71.84
71.88
71.88
71.88
71.84
71.80
LATITUDE (DEG)
-145.48
-145.25
-145.11
-145.12
-145.39
-145.63
-145.74
-145.80
-145.77
-145.51
-145.26
LONGITUDE (DEG)

SIRE DATA SET SUMMARY
DAY 79

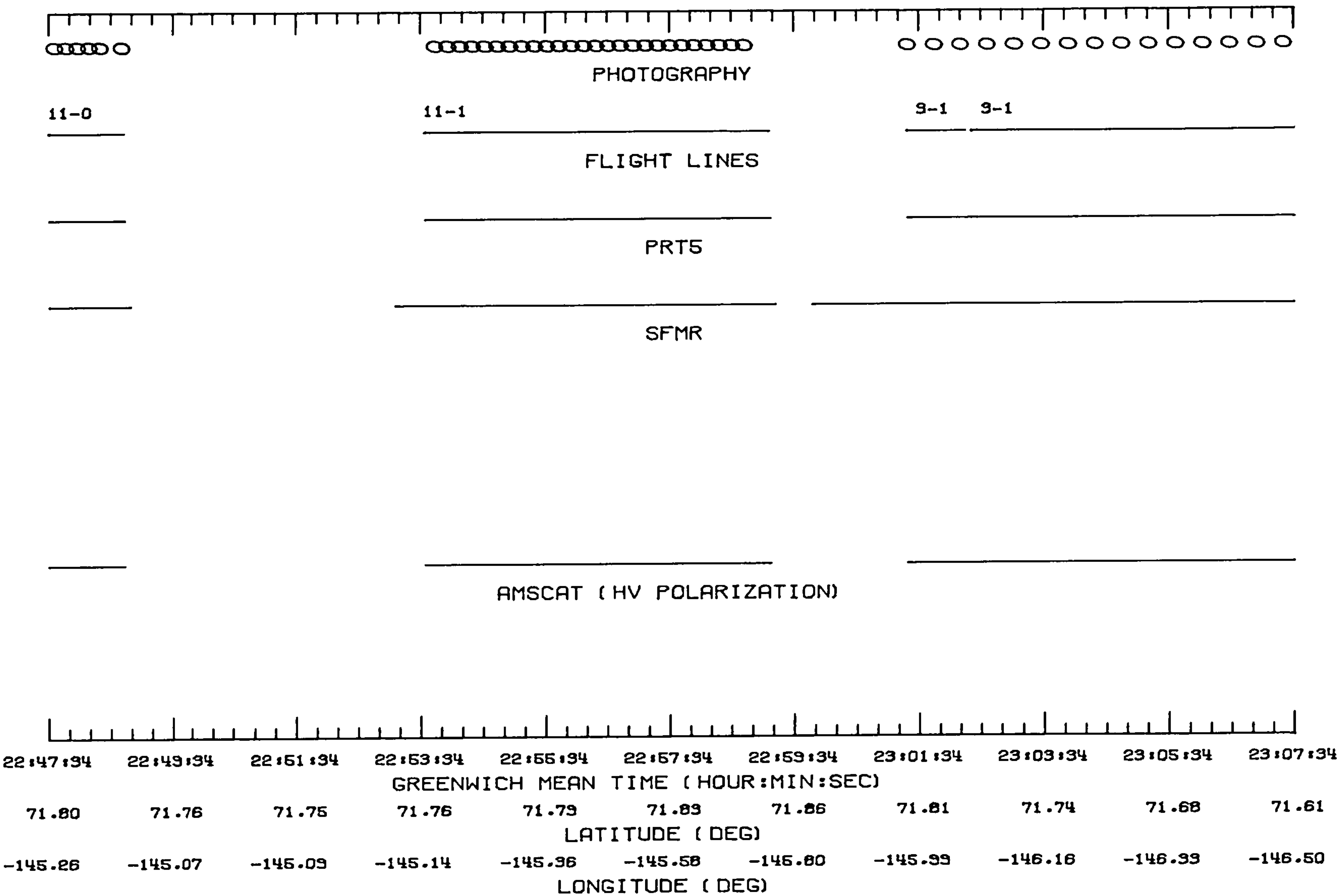

SIRE DATA SET SUMMARY
DAY 79

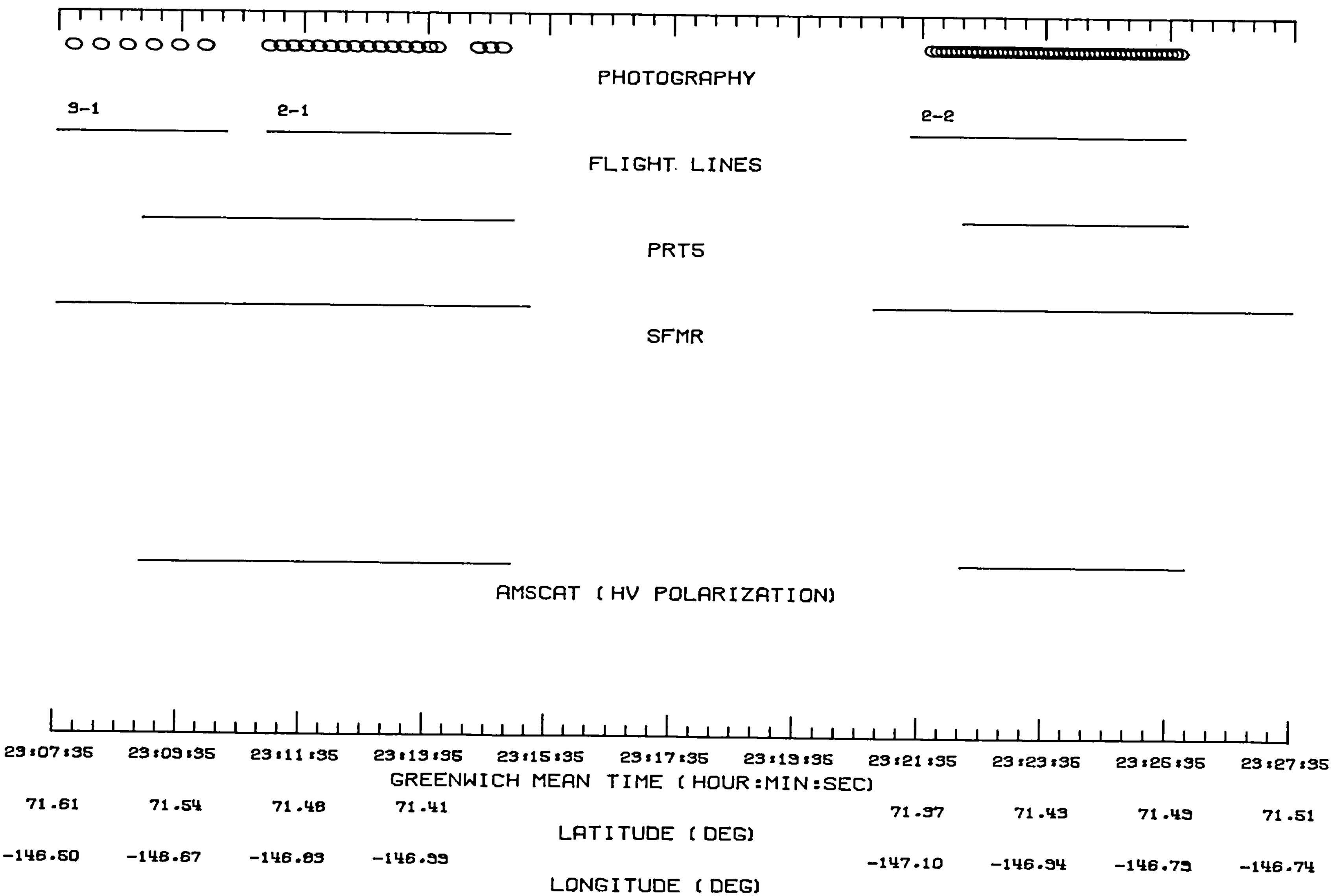

SIRE DATA SET SUMMARY
DAY 79

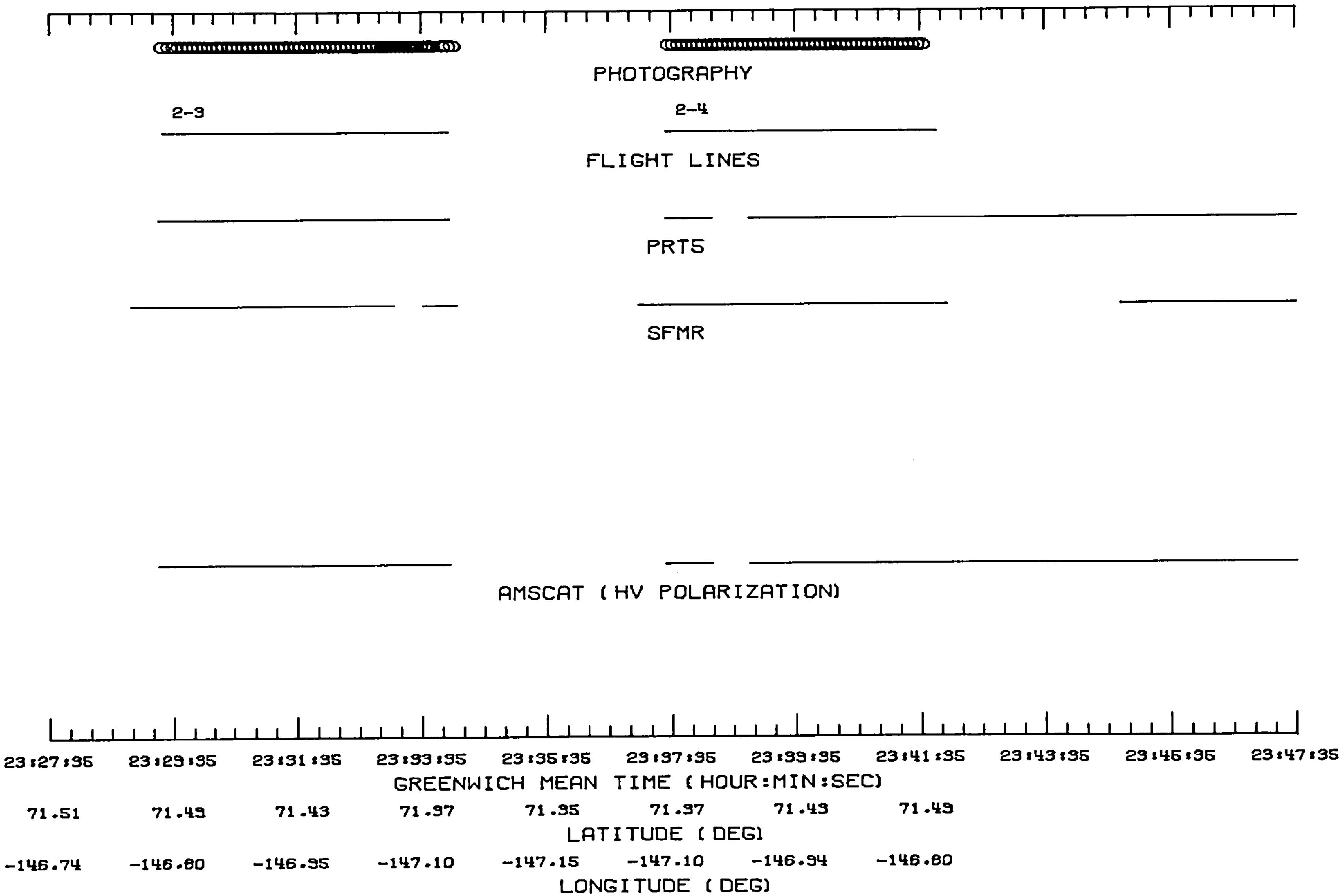

SIRE DATA SET SUMMARY
DAY 79

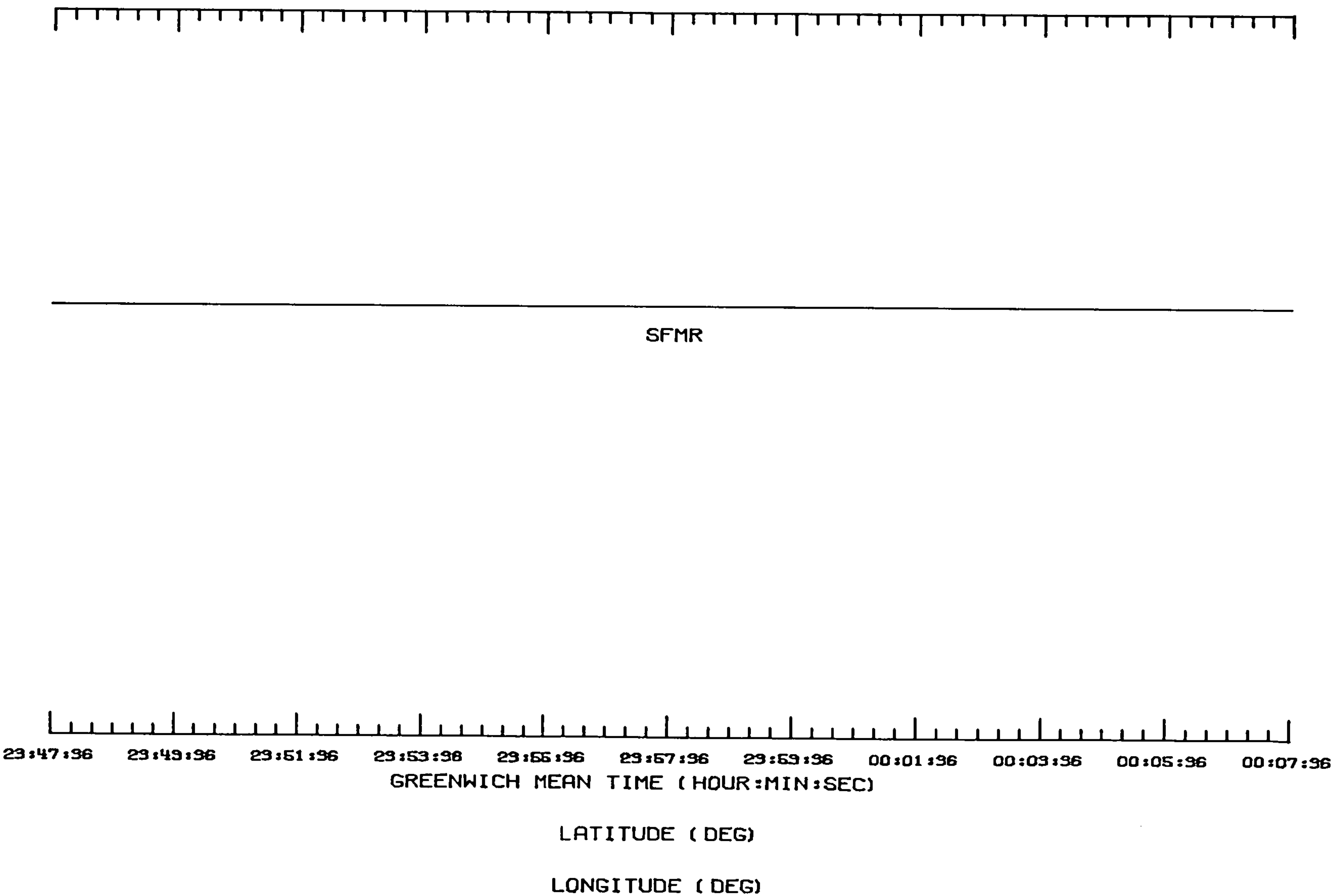

APPENDIX C

Day 82-83

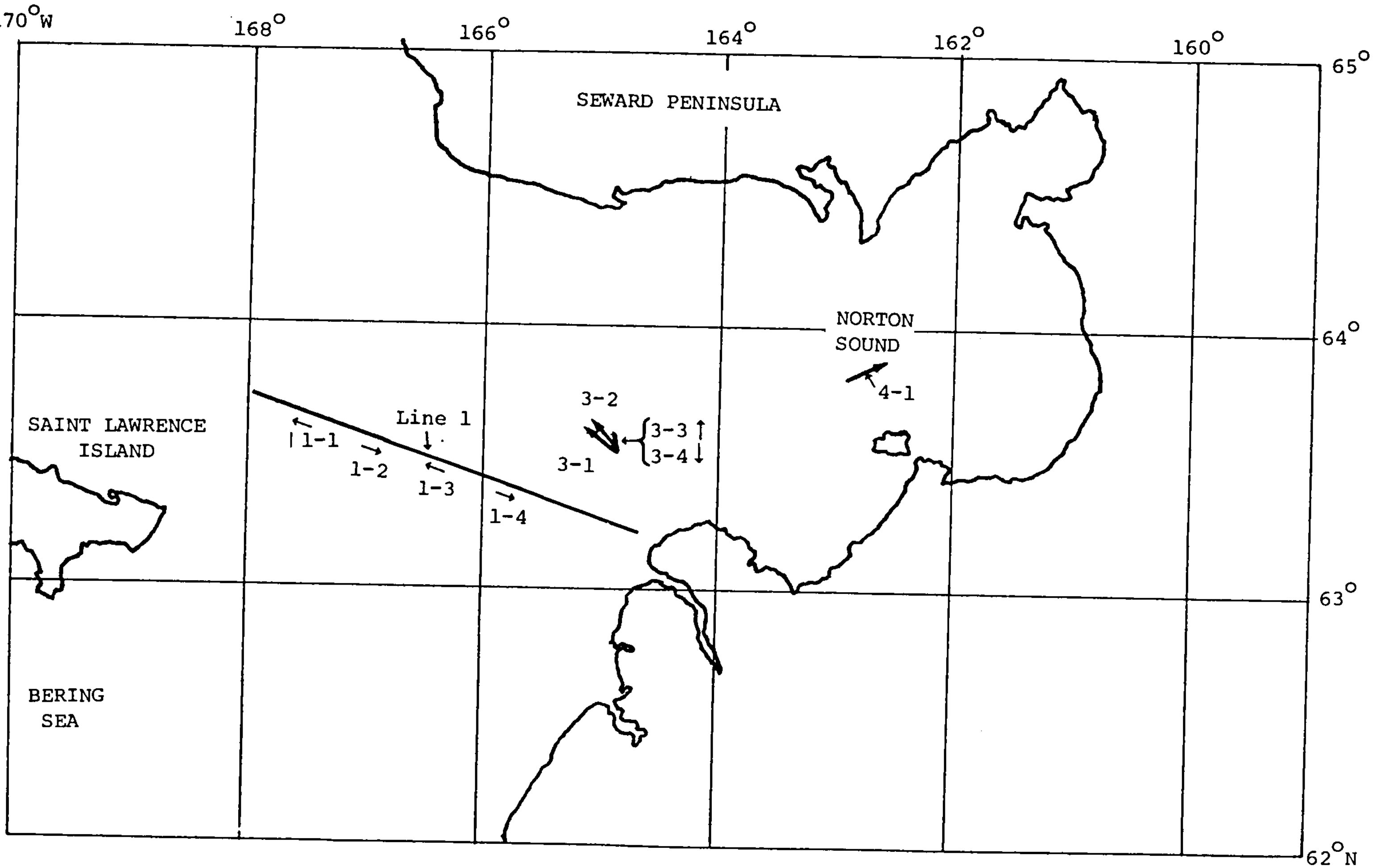

Flight lines for day 82-83

SIRE DATA SET SUMMARY
DAY 82

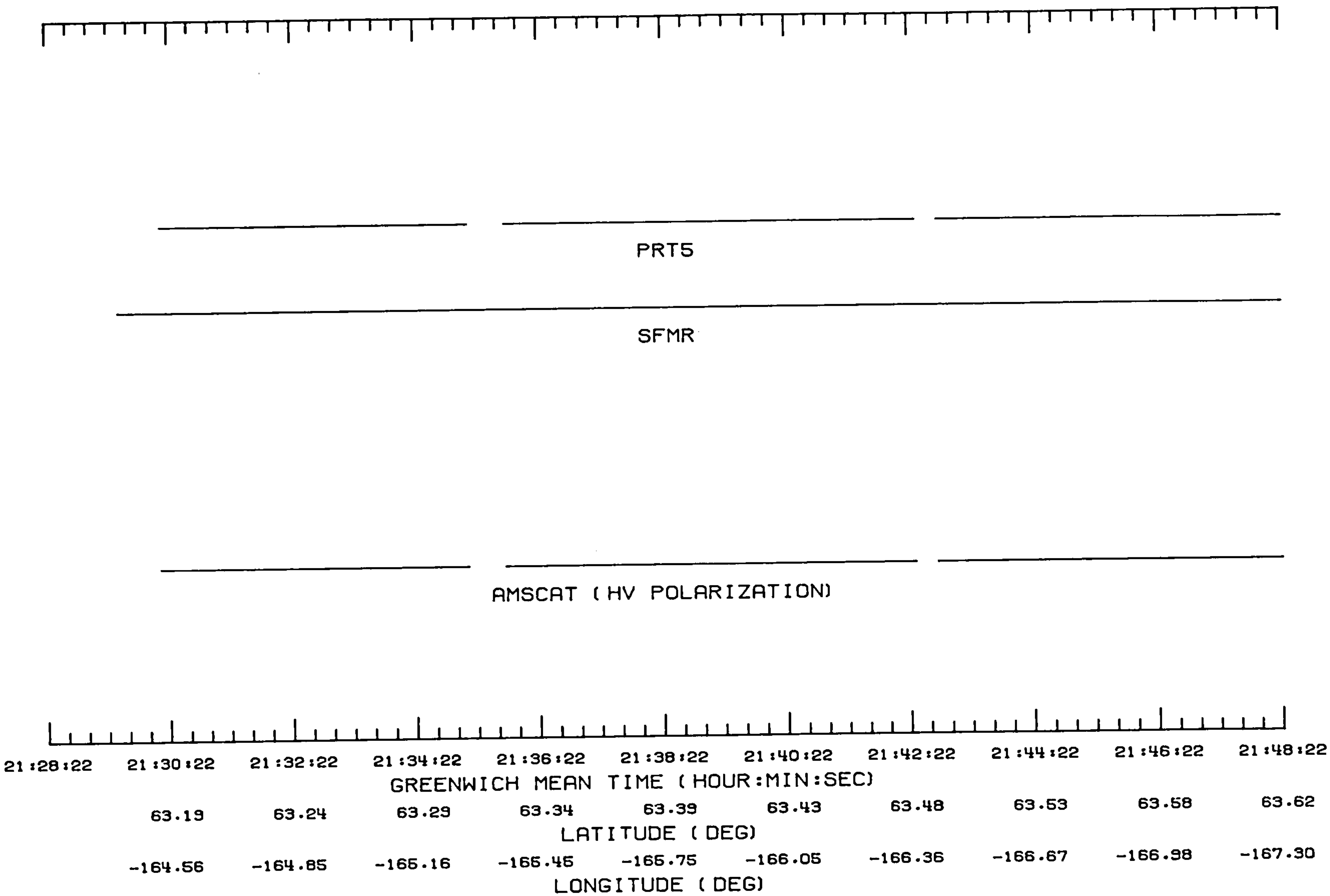

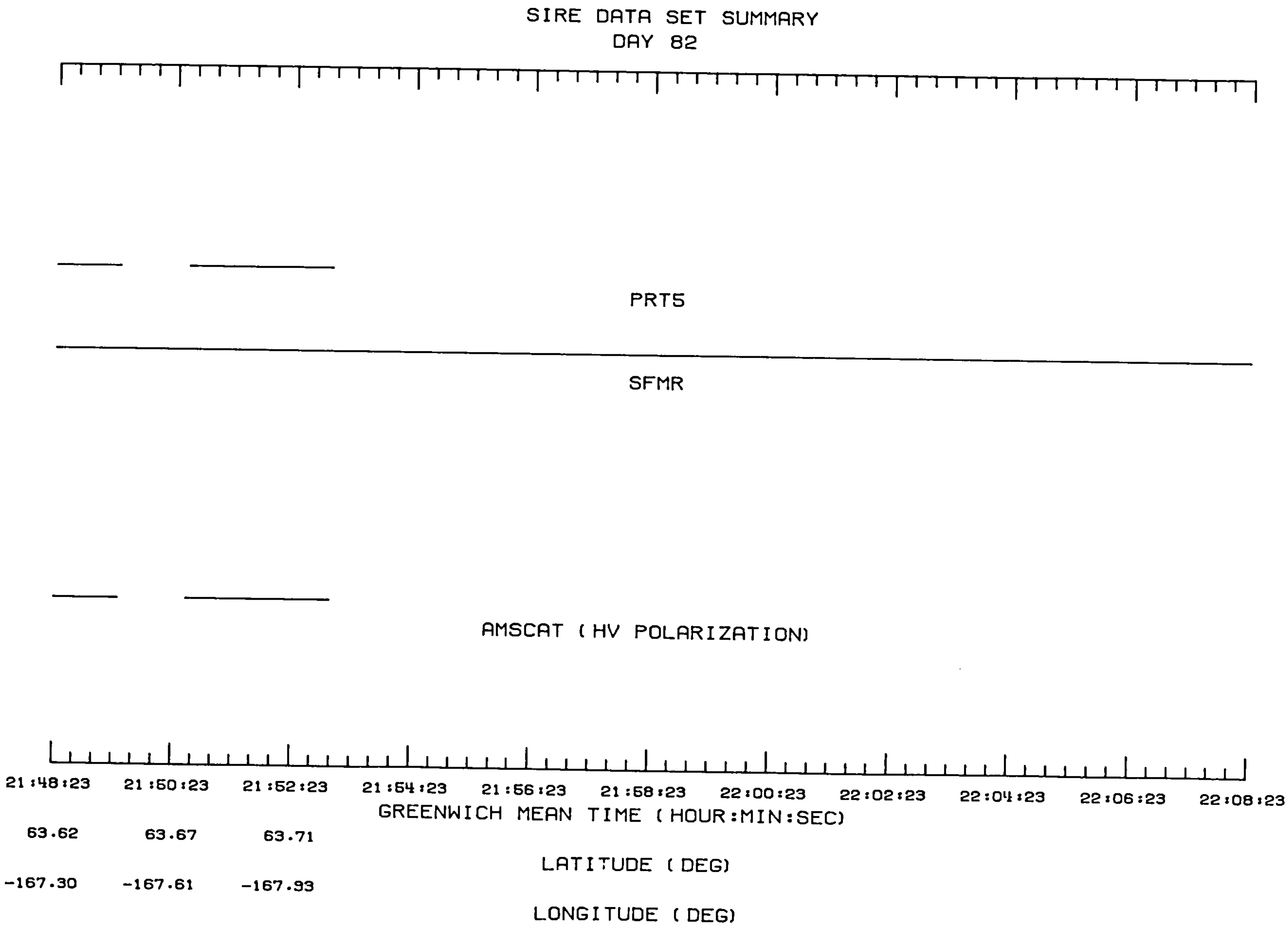
SIRE DATA SET SUMMARY
DAY 82
PRTS
SFMR
AMSCAT (HV POLARIZATION)
21:48:23
21:50:23
21:52:23
21:54:23
21:56:23
21:58:23
22:00:23
22:02:23
22:04:23
22:06:23
22:08:23
GREENWICH MEAN TIME (HOUR:MIN:SEC)
63.62
63.67
63.71
LATITUDE (DEG)
-167.30
-167.61
-167.93
LONGITUDE (DEG)

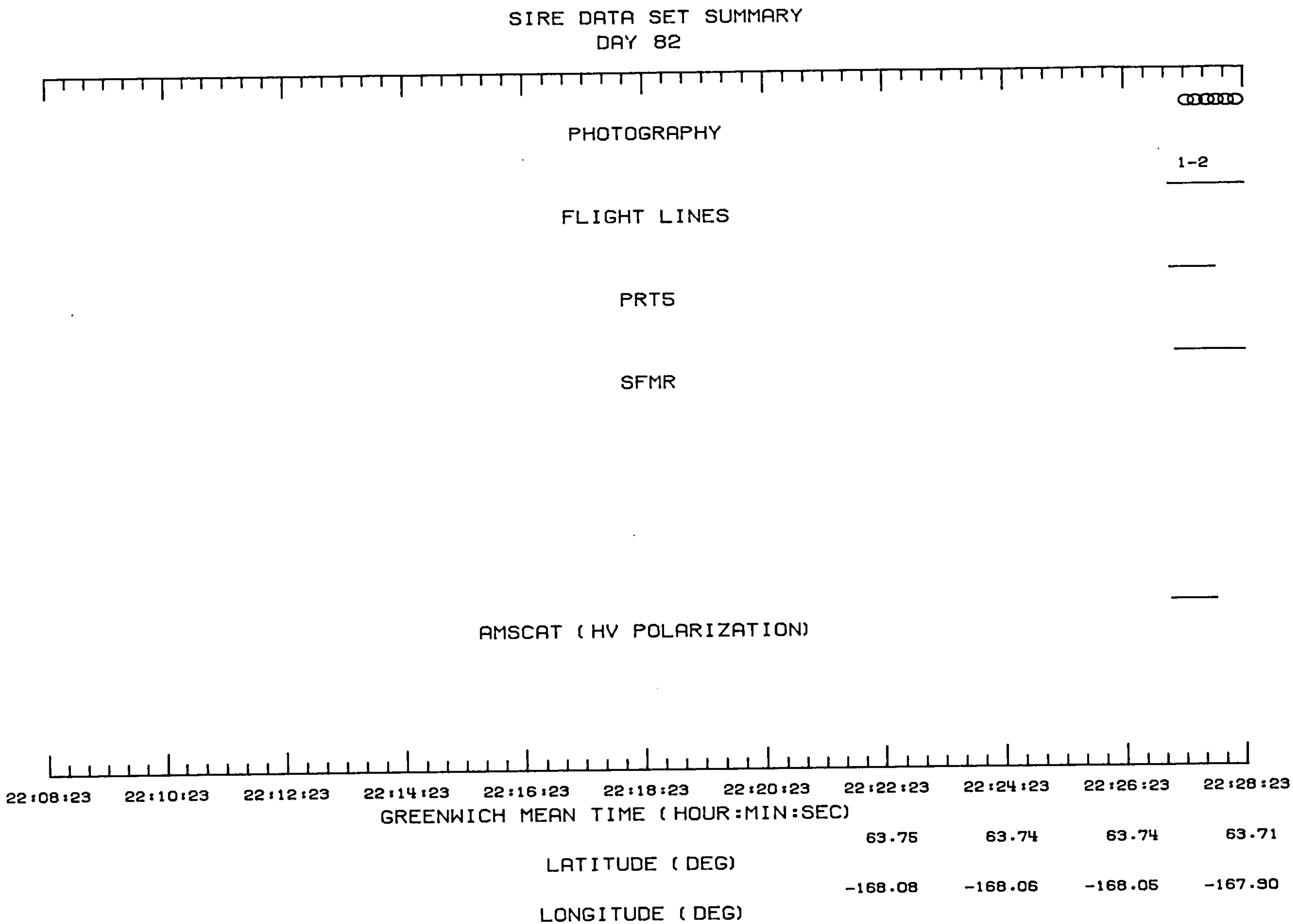
SIRE DATA SET SUMMARY
DAY 82
PHOTOGRAPHY
1-2
FLIGHT LINES
PRT5
SFMR
AMSCAT (HV POLARIZATION)
22:08:23
22:10:23
22:12:23
22:14:23
22:16:23
22:18:23
22:20:23
22:22:23
22:24:23
22:26:23
22:28:23
GREENWICH MEAN TIME (HOUR:MIN:SEC)
63.75
63.74
63.74
63.71
LATITUDE (DEG)
-168.08
-168.06
-168.05
-167.90
LONGITUDE (DEG)

SIRE DATA SET SUMMARY
DAY 82

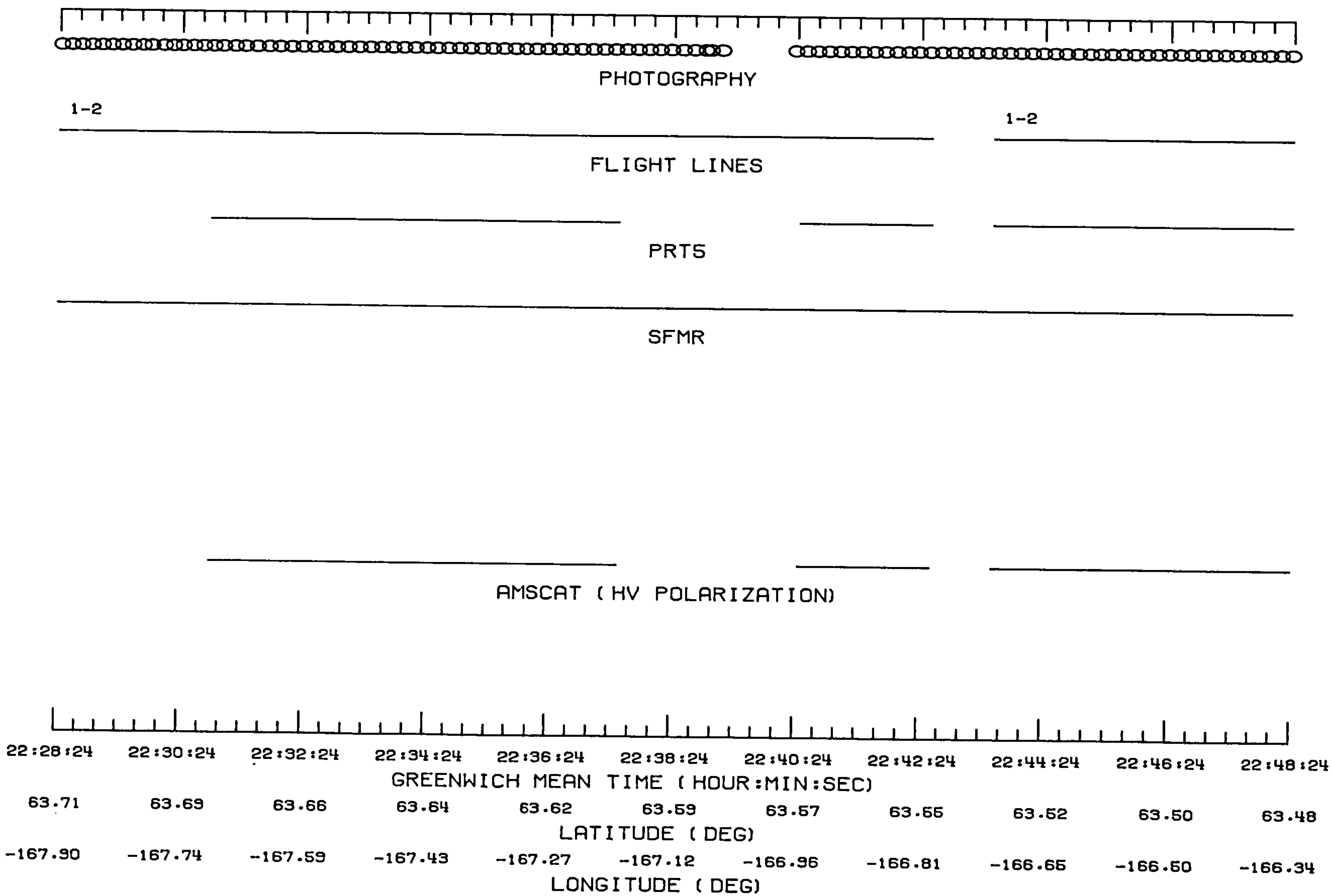

SIRE DATA SET SUMMARY
DAY 82

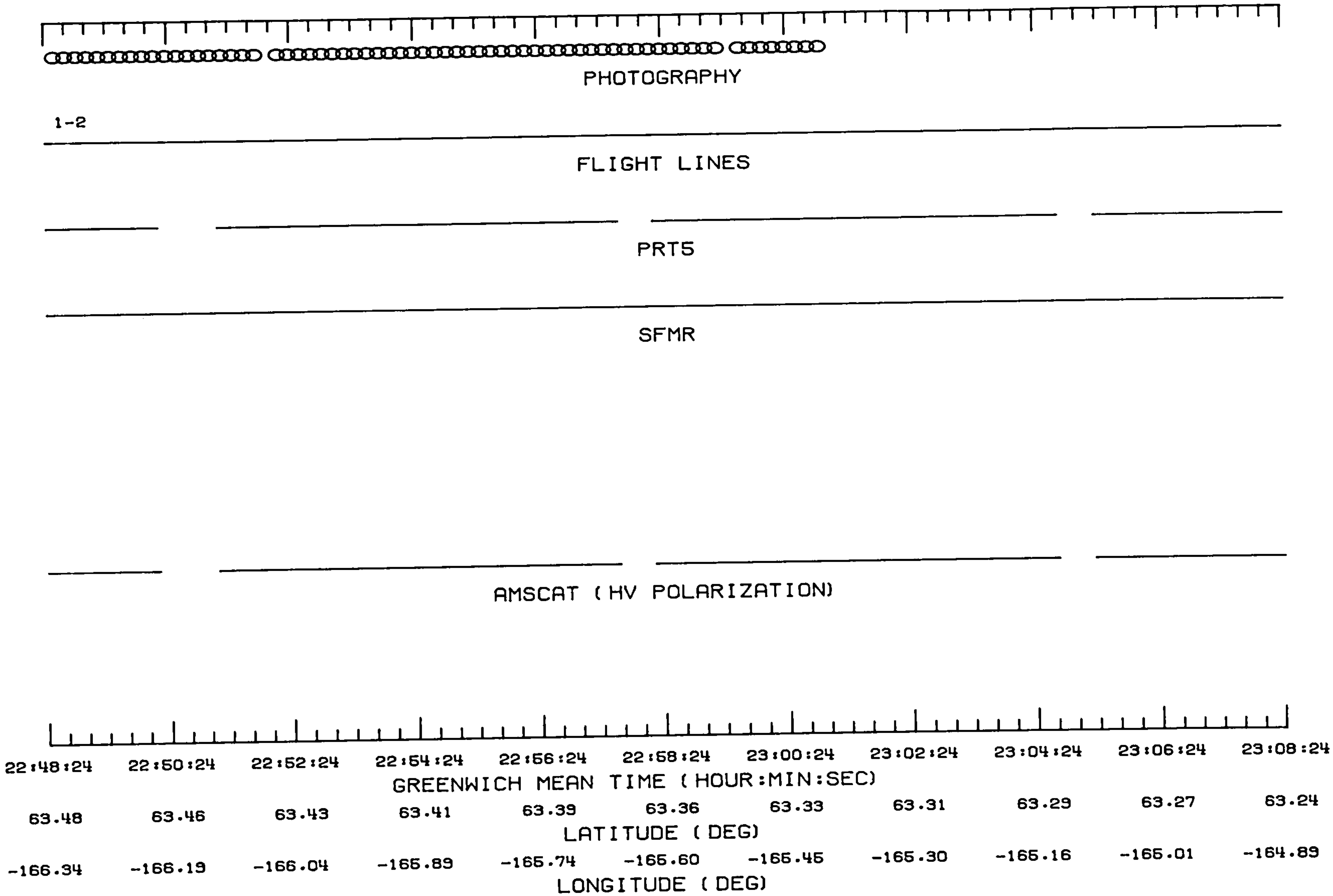

SIRE DATA SET SUMMARY
DAY 82

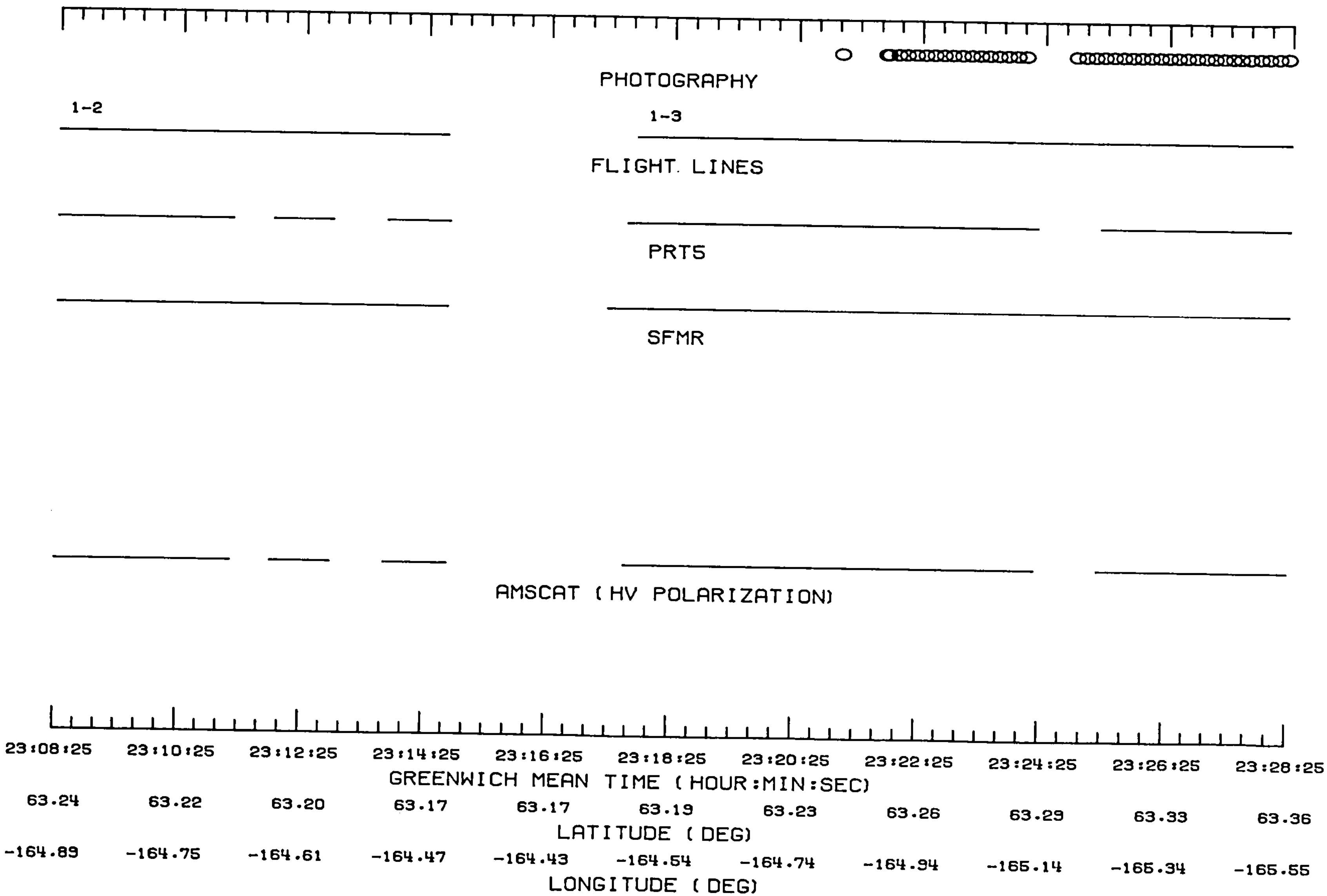

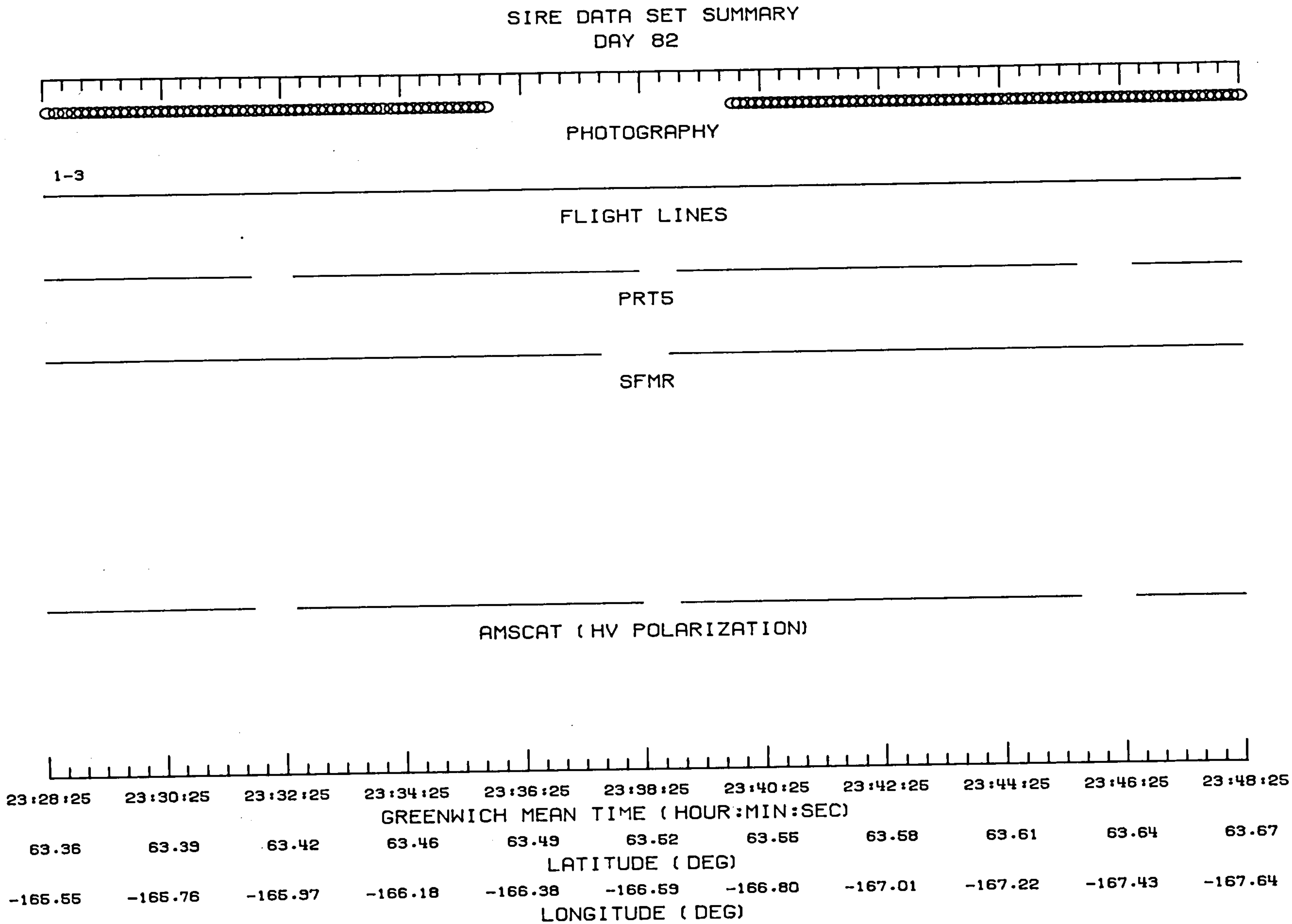
SIRE DATA SET SUMMARY
DAY 82
PHOTOGRAPHY
1-3
FLIGHT LINES
PRT5
SFMR
AMSCAT (HV POLARIZATION)
23:28:25
23:30:25
23:32:25
23:34:25
23:36:25
23:38:25
23:40:25
23:42:25
23:44:25
23:46:25
23:48:25
GREENWICH MEAN TIME (HOUR:MIN:SEC)
63.36
63.39
63.42
63.46
63.49
63.52
63.55
63.58
63.61
63.64
63.67
LATITUDE (DEG)
-165.55
-165.76
-165.97
-166.18
-166.38
-166.59
-166.80
-167.01
-167.22
-167.43
-167.64
LONGITUDE (DEG)

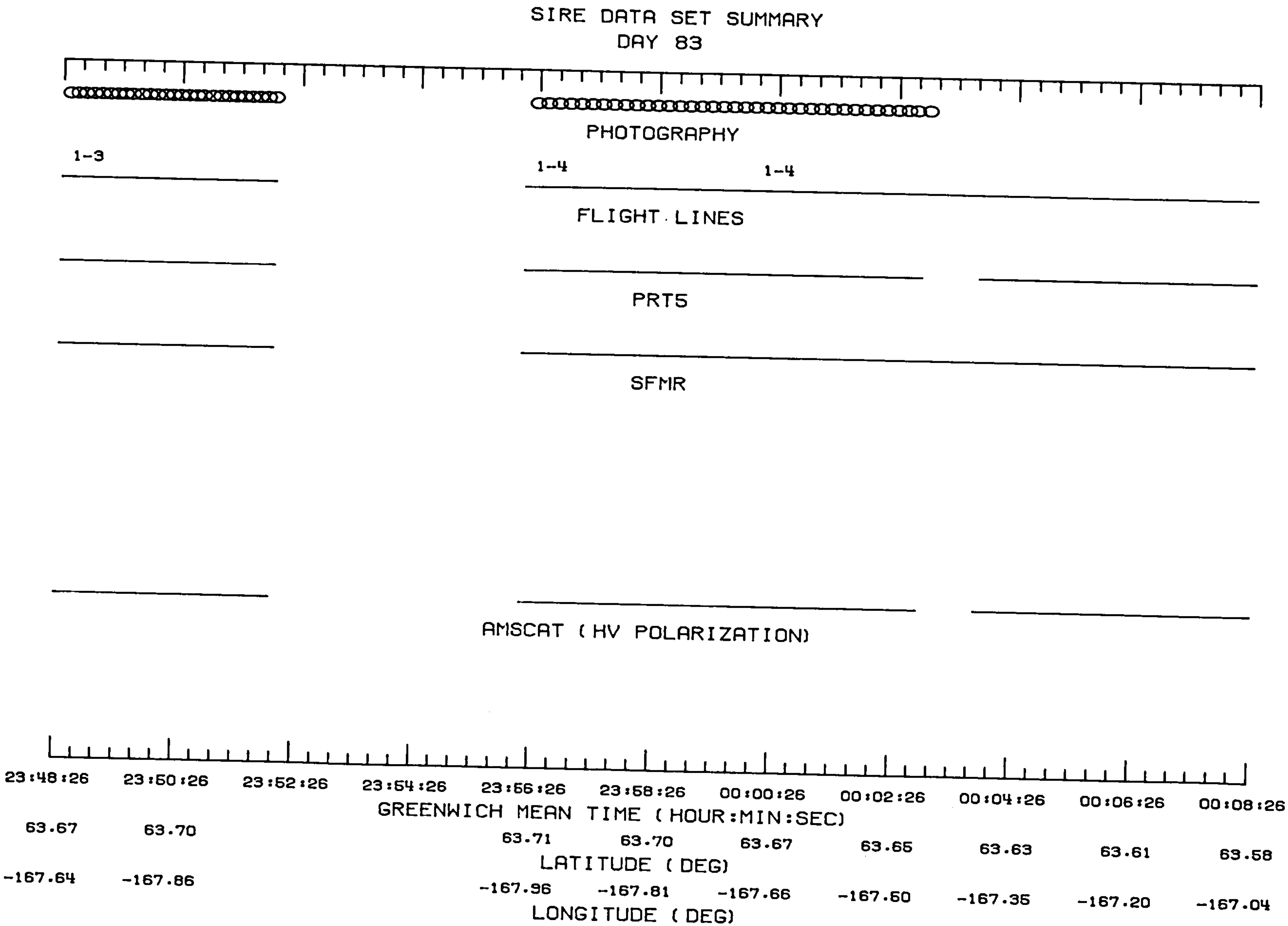
SIRE DATA SET SUMMARY
DAY 83
PHOTOGRAPHY
1-3
1-4
1-4
FLIGHT LINES
PRT5
SFMR
AMSCAT (HV POLARIZATION)
23:48:26
23:50:26
23:52:26
23:54:26
23:56:26
23:58:26
00:00:26
00:02:26
00:04:26
00:06:26
00:08:26
GREENWICH MEAN TIME (HOUR:MIN:SEC)
63.67
63.70
63.71
63.70
63.67
63.65
63.63
63.61
63.58
LATITUDE (DEG)
-167.64
-167.86
-167.96
-167.81
-167.66
-167.50
-167.35
-167.20
-167.04
LONGITUDE (DEG)

SIRE DATA SET SUMMARY
DAY 83

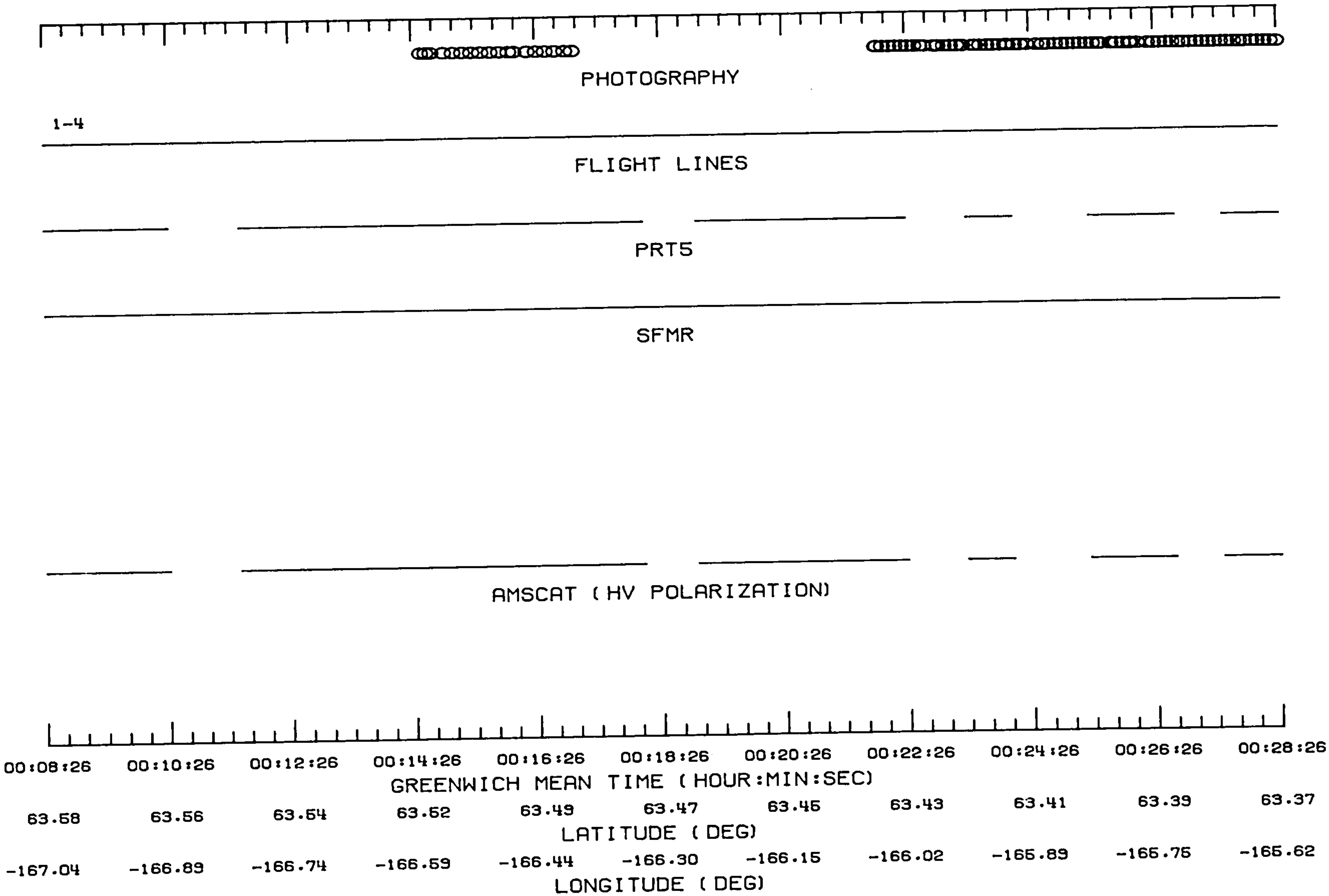

SIRE DATA SET SUMMARY
DAY 83

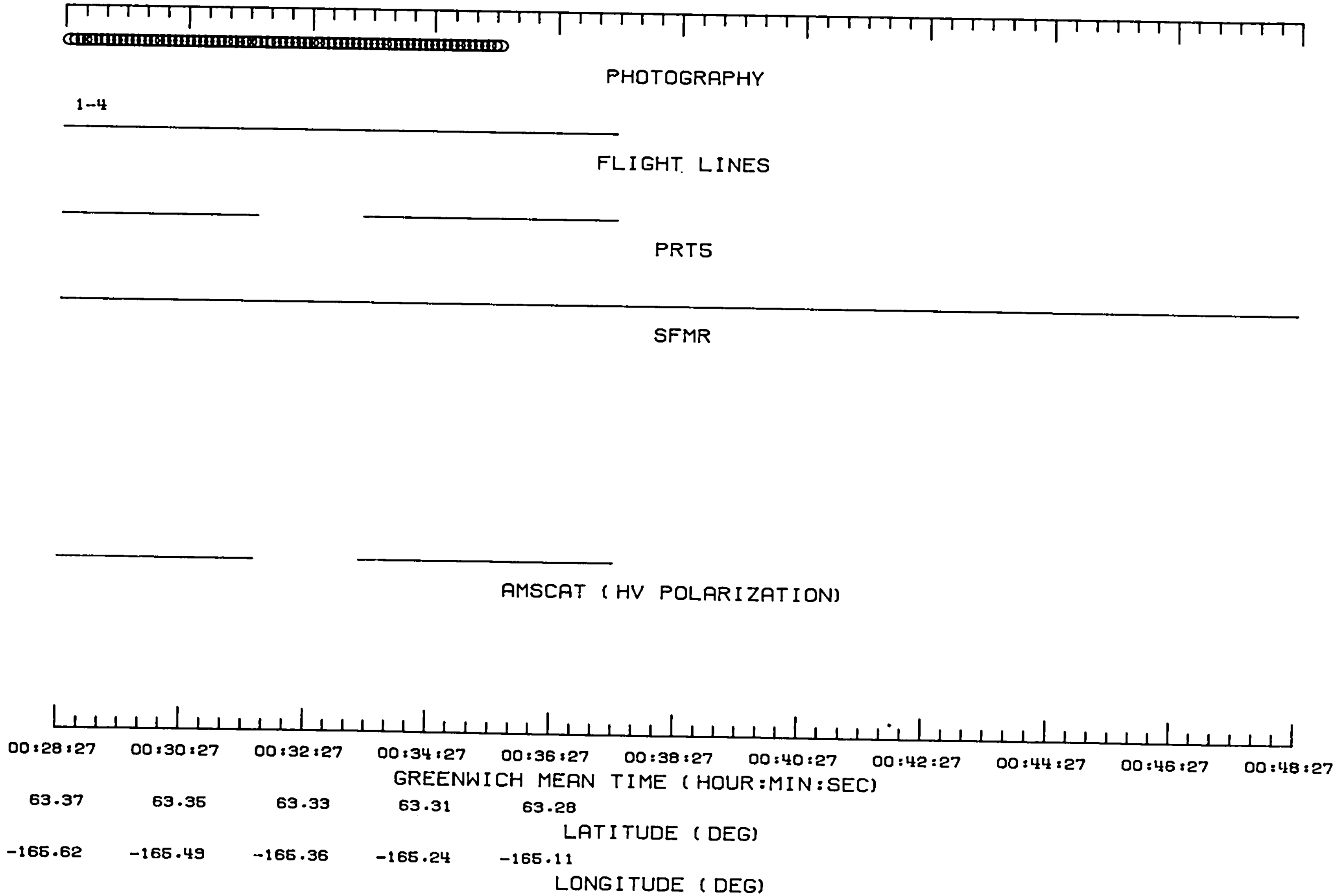

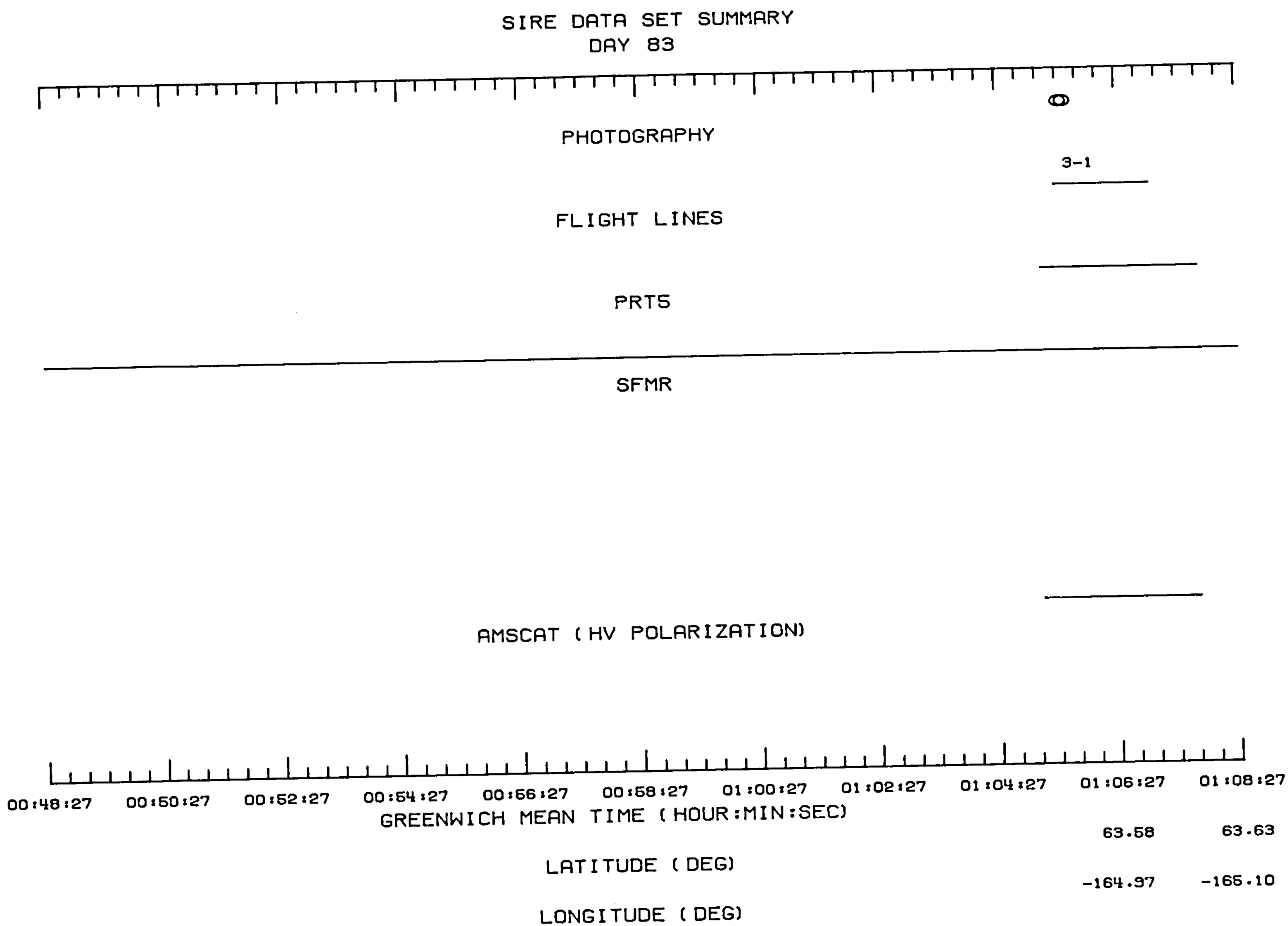
SIRE DATA SET SUMMARY
DAY 83
PHOTOGRAPHY
3-1
FLIGHT LINES
PRTS
SFMR
AMSCAT (HV POLARIZATION)
00:48:27
00:50:27
00:52:27
00:54:27
00:56:27
00:58:27
01:00:27
01:02:27
01:04:27
01:06:27
01:08:27
GREENWICH MEAN TIME (HOUR:MIN:SEC)
63.58
63.63
LATITUDE (DEG)
-164.97
-165.10
LONGITUDE (DEG)

SIRE DATA SET SUMMARY
DAY 83

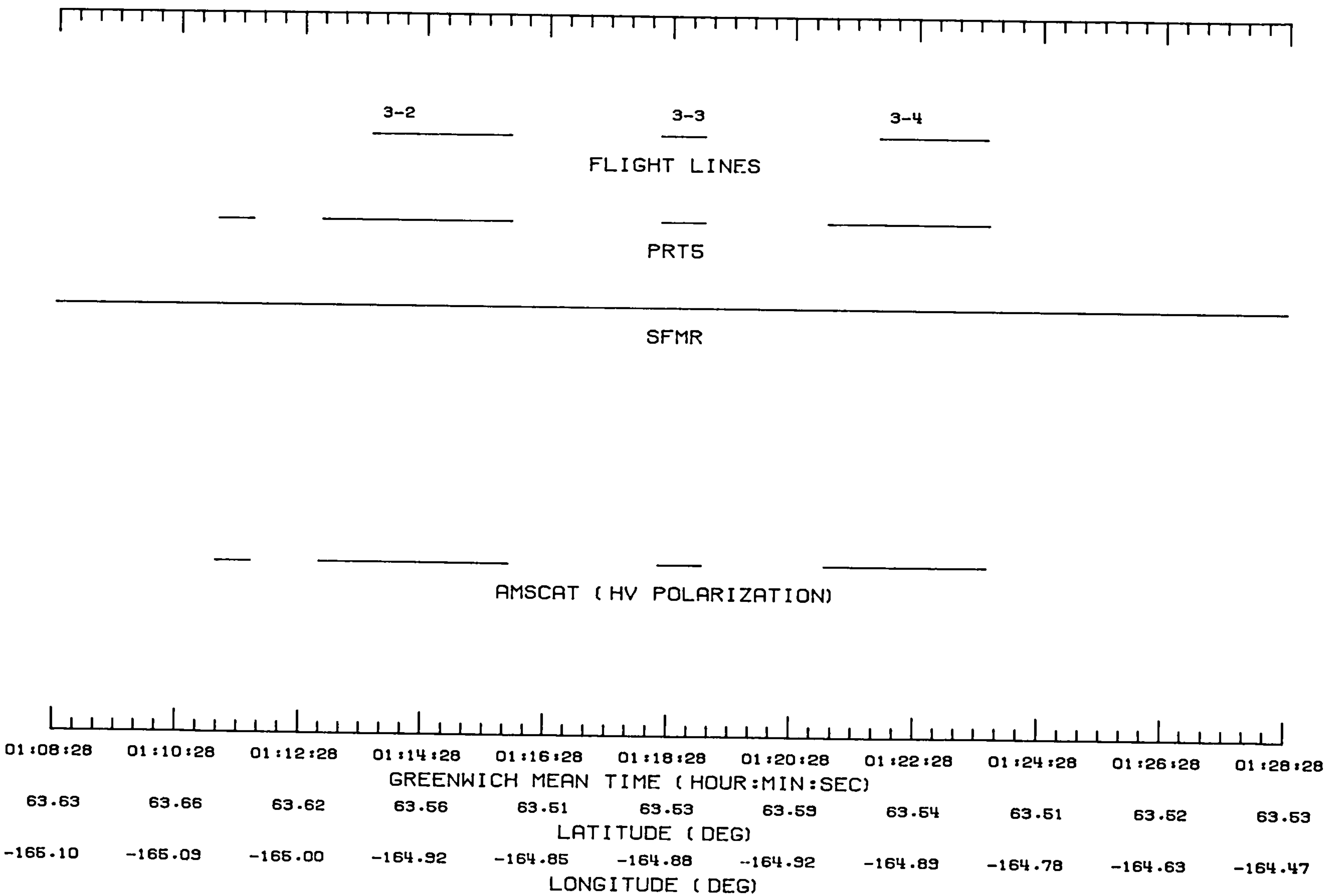

SIRE DATA SET SUMMARY
DAY 83

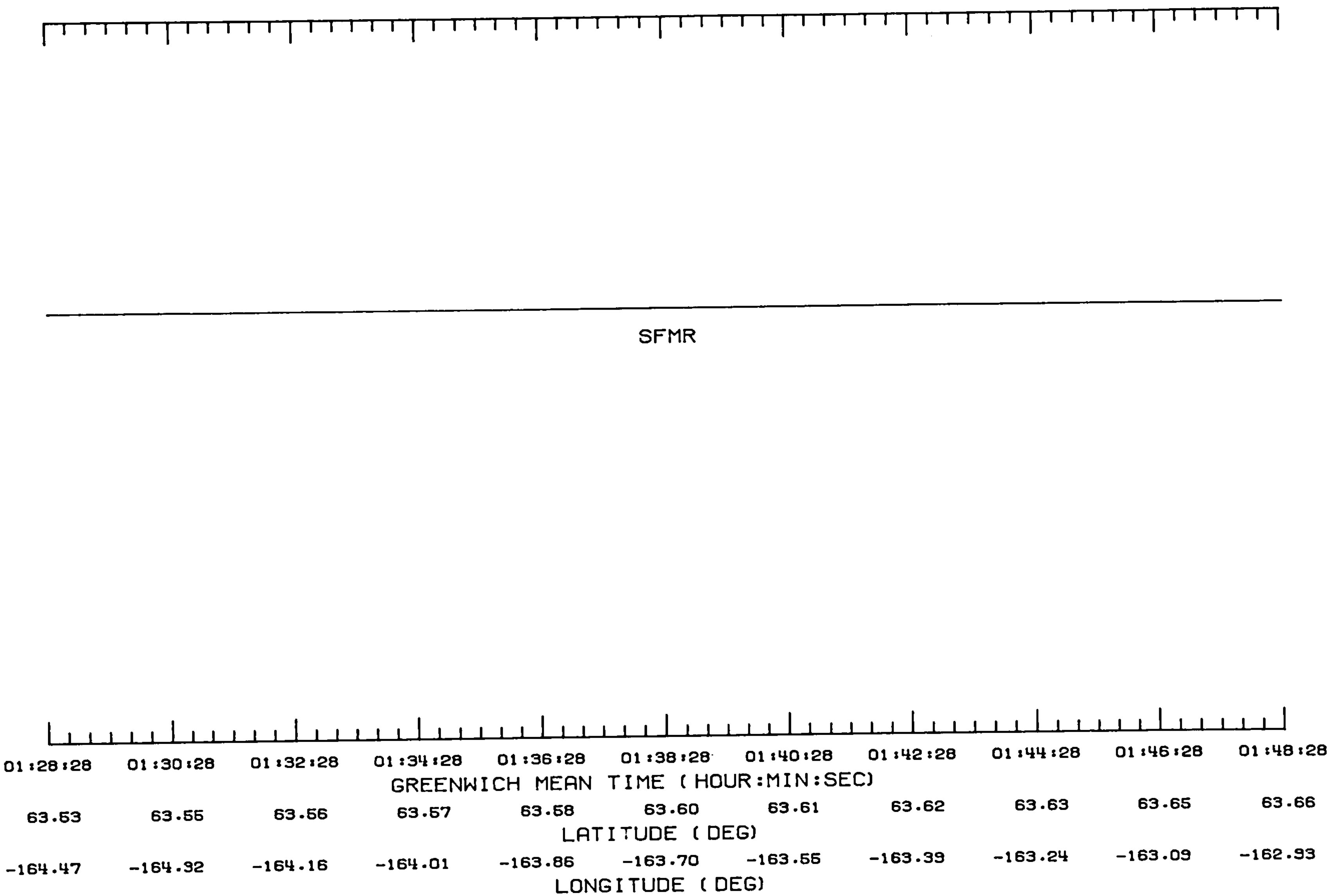

SIRE DATA SET SUMMARY
DAY 83

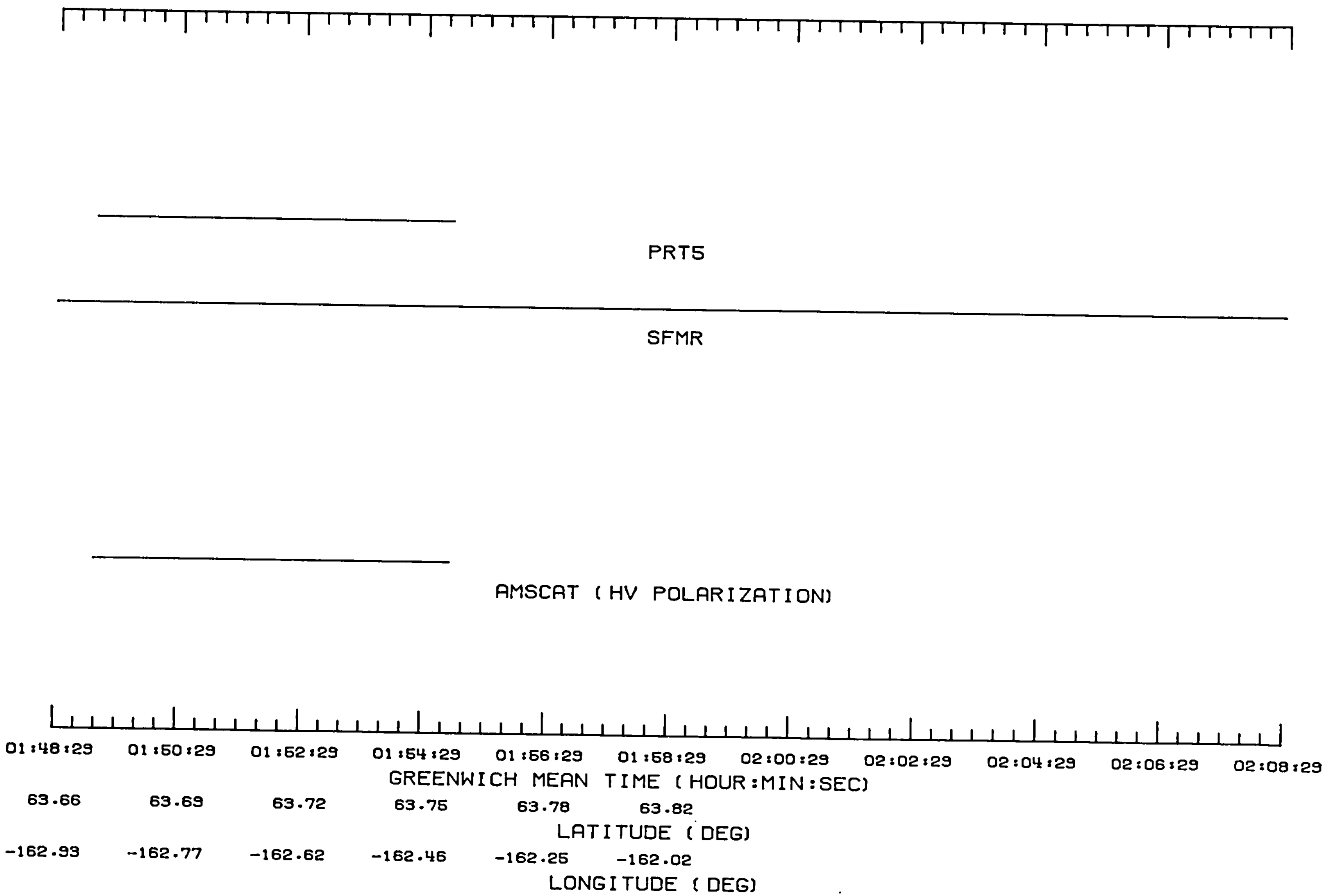

REFERENCES

1. Schroeder, Lyle C.; Jones, W. L., Jr.; and Mitchell, John L.: Laboratory Calibration of AAFE Radiometer/Scatterometer (RADSCAT). NASA TM X-73900, 1976.

2. Harrington, Richard F.: The Development of a Stepped Frequency Microwave Radiometer and Its Application to Remote Sensing of the Earth. NASA TM-81847, 1980.

3. Instruction Manual for Precision Radiation Thermometer Model PRT-5. Barnes Eng. Co.

BIBLIOGRAPHY

General

Campbell, W. J.; Weeks, W. F.; Ramseier, R. O.; and Gloersen, P.: Geophysical Studies of Floating Ice by Remote Sensing. J. Glaciology, vol. 15, no. 73, 1975, pp. 305-328.

Campbell, W. J.; Gloersen, P.; Webster, W. J.; and Wilheit, T. T.: Beaufort Sea Ice Zones as Delineated by Microwave Imagery. J. Geophys. Res., vol. 81, no. 6, Feb. 20, 1976, pp. 1103-1110.

Campbell, W. J.; Ramseier, R. O.; Zwally, H. J.; and Gloersen, P.: Arctic Sea-Ice Variations From Time-Lapse Passive Microwave Imagery. Boundary-Layer Meteorol., vol. 18, no. 1, Feb. 1980, pp. 99-106.

Campbell, W. J.; Gloersen, P.; Zwally, H. J.; Ramseier, R. O.; and Elachi, C.: Simultaneous Passive and Active Microwave Observations of Near-Shore Beaufort Sea Ice. J. Pet. Technol., vol. 32, no. 6, June 1980, pp. 1105-1112.

Gloersen, P.; Nordberg, W.; Schmugge, T. J.; Wilheit, T. T.; and Campbell, W. J.: Microwave Signatures of First-Year and Multiyear Sea Ice. NASA TM X-66006, 1972.

Gloersen, Per; and Barath, Frank T.: A Scanning Multichannel Microwave Radiometer for Nimbus-G and SeaSat-A. IEEE J. Oceanic Eng., vol. OE-2, no. 2, Apr. 1977, pp. 172-178.

Jackson, Betty L.; Jones, W. Linwood, Jr.; and Stanley, William D.: Measure of Arctic Sea Ice Characteristics Using Microwave Scatterometry. Proceedings of SOUTHEASTCON '79, IEEE, c.1979, pp. 278-280.

Onstott, Robert G.; Moore, Richard K.; and Weeks, W. F.: Surface-Based Scatterometer Results of Arctic Sea Ice. IEEE Trans. Geosci. Electron., vol. GE-17, no. 3, July 1979, pp. 78-85.

Parashar, S. K.; Haralick, Robert M.; Moore, R. K.; and Biggs, A. W.: Radar Scatterometer Discrimination of Sea-Ice Types. IEEE Trans. Geosci. Electron., vol. GE-15, no. 2, Apr. 1977, pp. 83-87.

Rouse, John W.: Arctic Ice Type Identification by Radar. Proc. IEEE, vol. 57, no. 4, Apr. 1969, pp. 605-611.

Swift, C. T.; Jones, W. L., Jr.; Harrington, R. F.; Fedors, J. C.; Couch, R. H.; and Jackson, B. L.: Microwave Radar and Radiometric Remote Sensing Measurements of Lake Ice. Geophys. Res. Lett., vol. 7, no. 4, Apr. 1980, pp. 243-246.

Wadhams, Peter: The Ice Cover in the Greenland and Norwegian Seas. Rev. Geophys. & Space Phys., vol. 19, no. 3, Aug. 1981, pp. 345-393.

Walsh, John E.; and Johnson, Claudia M.: Interannual Atmospheric Variability and Associated Fluctuations in Arctic Sea Ice Extent. J. Geophys. Res., vol. 84, no. C11, Nov. 20, 1979, pp. 6915-6928.

Weeks, W. F.: Sea Ice: The Potential of Remote Sensing. Oceanus, vol. 24, no. 3, Fall 1981, pp. 39-48.

Wilheit, T.; Blinn, J.; Campbell, W.; Edgerton, A.; and Nordberg, W.: Aircraft Measurements of Microwave Emission From Arctic Sea Ice. NASA TM X-65742, 1971.

Instrumentation

Instruction Manual for Precision Radiation Thermometer Model PRT-5. Barnes Eng. Co.

Harrington, Richard F.: The Development of a Stepped Frequency Microwave Radiometer and Its Application to Remote Sensing of the Earth. NASA TM-81847, 1980.

Philco-Ford Corp.: Earth Resources Data Format Control Book. Revision A. 1977.
Volume 1. NASA CR-160804.
Volume 2. NASA CR-160805.
Volume 3. NASA CR-160806.

Schroeder, Lyle C.; Jones, W. L., Jr.; and Mitchell, John L.: Laboratory Calibration of AAFE Radiometer/Scatterometer (RADSCAT). NASA TM X-73900, 1976.

SIRE

Gloersen, P.; Wilheit, T. T.; Chang, T. C.; Nordberg, W.; and Campbell, W. J.: Microwave Maps of the Polar Ice of the Earth. Bull. American Meteorol. Soc., vol. 55, no. 12, Dec. 1974, pp. 1442-1448.

Gedney, R. T.; Jirberg, R. J.; Schertler, R. J.; Mueller, R. A.; Chase, T. L.; Kramarchuk, I.; Nagy, L. A.; Hanlon, R. A.; and Mark, H.: All-Weather Ice Information System for Alaskan Arctic Coastal Shipping. NASA TM X-73619, [1977].

Gray, A. L.; Ramseier, R. O.; and Campbell, W. J.: Scatterometer and SLAR Results Obtained Over Arctic Sea-Ice and Their Relevance to the Problems of Arctic Ice Reconnaissance. 4th Canadian Symposium on Remote Sensing, Canadian Aeronaut. & Space Inst., May 1977, pp. 424-443.

Ramseier, R. O.; Gloersen, P.; and Campbell, W. J.: Variation in the Microwave Emissivity of Sea Ice in the Beaufort and Bering Sea. Proceedings of the URSI Commission II Specialist Meeting on Microwave Scattering and Emission From the Earth, I. Schanda, ed., Inst. Appl. Phys., Univ. of Berne, 1974, pp. 87-93.

Schertler, R. J.; Mueller, R. A.; Jirberg, R. J.; Cooper, D. W.; Chase, T.; Heighway, J. E.; Holmes, A. D.; Gedney, R. T.; and Mark, H.: Great Lakes All-Weather Ice Information System. NASA TM X-71815, [1975].

TABLE I.- DATA FLIGHT DAYS

Julian Day	Calendar day	Location
73-74	3/14-15/79	Bering Sea
75-76	3/16-17/79	Prudhoe Bay
77-78	3/18-19/79	East Beaufort Sea
79	3/20/79	Prudhoe Bay
82-83	3/23-24/79	Norton Sound

TABLE II.- AMSCAT OPERATING CHARACTERISTICS

Selectable characteristics:	
Polarization	HH,* HV, VV, VH
Incidence angle, deg	0 to 54
Azimuth angle (relative to heading), deg	15 to 345
Nonselectable characteristics:	
Frequency, GHz	14.6
σ^o sampling rate, sec^{-1}	2
Absolute σ^o accuracy, dB	±1.0
σ^o precision, dB	±0.1
Antenna beam width, deg	3.5
Total σ^o range, dB	-30 to 15

*Transmit horizontal/receive horizontal. With transmit and receive each either horizontal or vertical, there are four possible combinations. When transmit and receive are of like polarization, the system is said to be in dominant polarization, and when opposed, in cross-polarization.

TABLE III.- SCATTEROMETER PROCESSOR STATISTICS

Flight	Polarization	Number of data points (0.5-s integrations)	Percent of time signal in SCAT-2	Percent of time signal in SCAT-1	Percent of time signal in SCAT-2 and SCAT-1	Difference in σ^o between two channels when both on-scale and SCAT-1 near saturation, dB	
						Mean	Standard deviation
Beaufort Sea flights (days 75-76, 77-78, and 79)	HH	17 136	31	33	25	0.42	0.97
	VV	5 194	34	41	21	-.03	.95
Bering Sea flights (days 73-74 and 82-83)	HH	3 942	2	82	13	-0.26	0.17
	VV	3 971	5	72	20	-.29	.42

TABLE IV.- PRT-5 OPERATING CHARACTERISTICS

Temperature measurement range, ^oC	-20 to +75
Accuracy, ^oC	0.5
Sensitivity (at 25^oC), ^oC	0.1
Filter band, μm	8 to 14
Field of view, deg	2

L-82-12,487

Figure 1.- NASA C-130 aircraft (NASA 929).

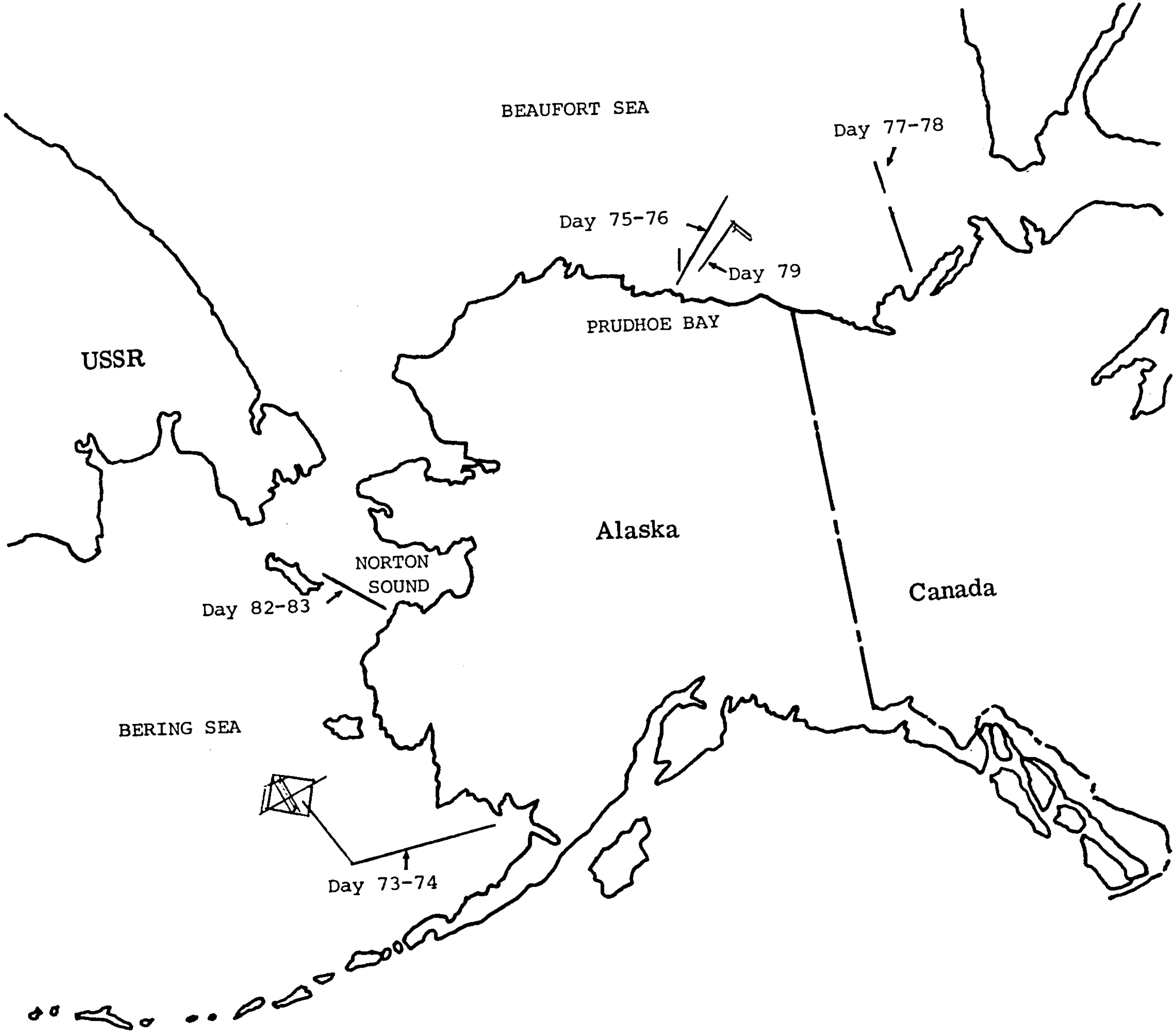

Figure 2.- Map of 1979 SIRE experiment area.

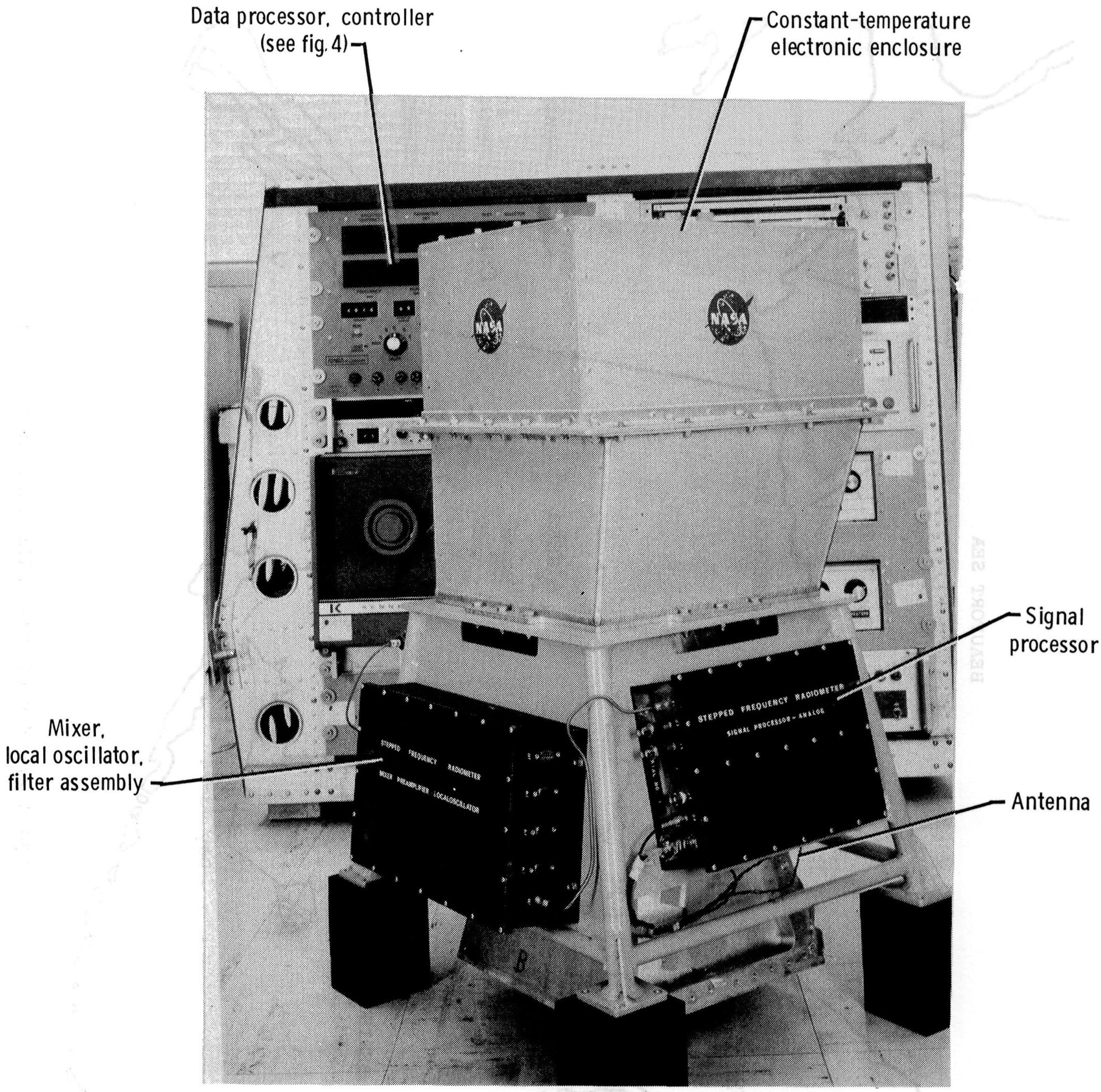

L-83-35

Figure 3.- Stepped frequency microwave radiometer.

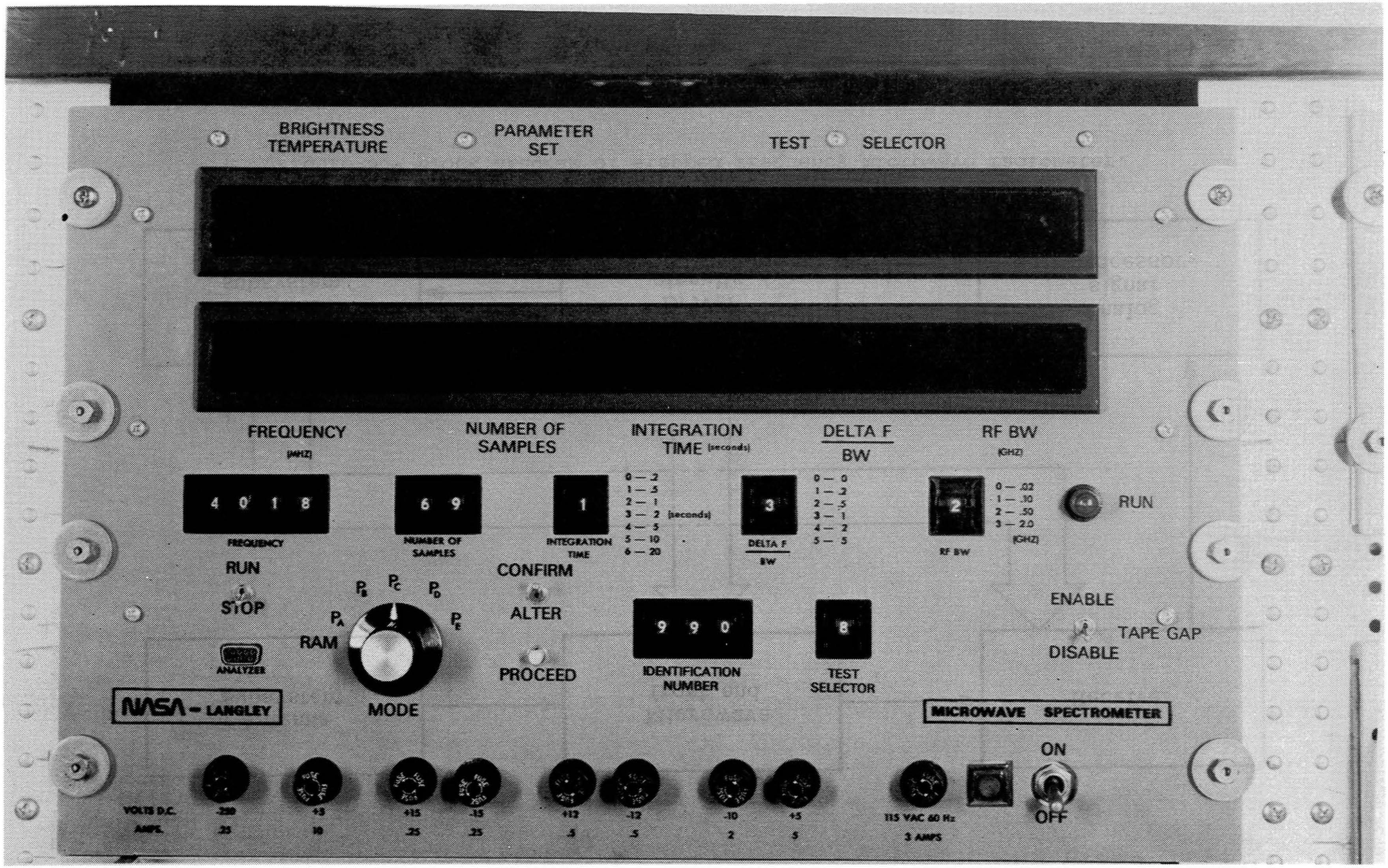

L-774488

Figure 4.- Front panel of digital controller for stepped frequency microwave radiometer.

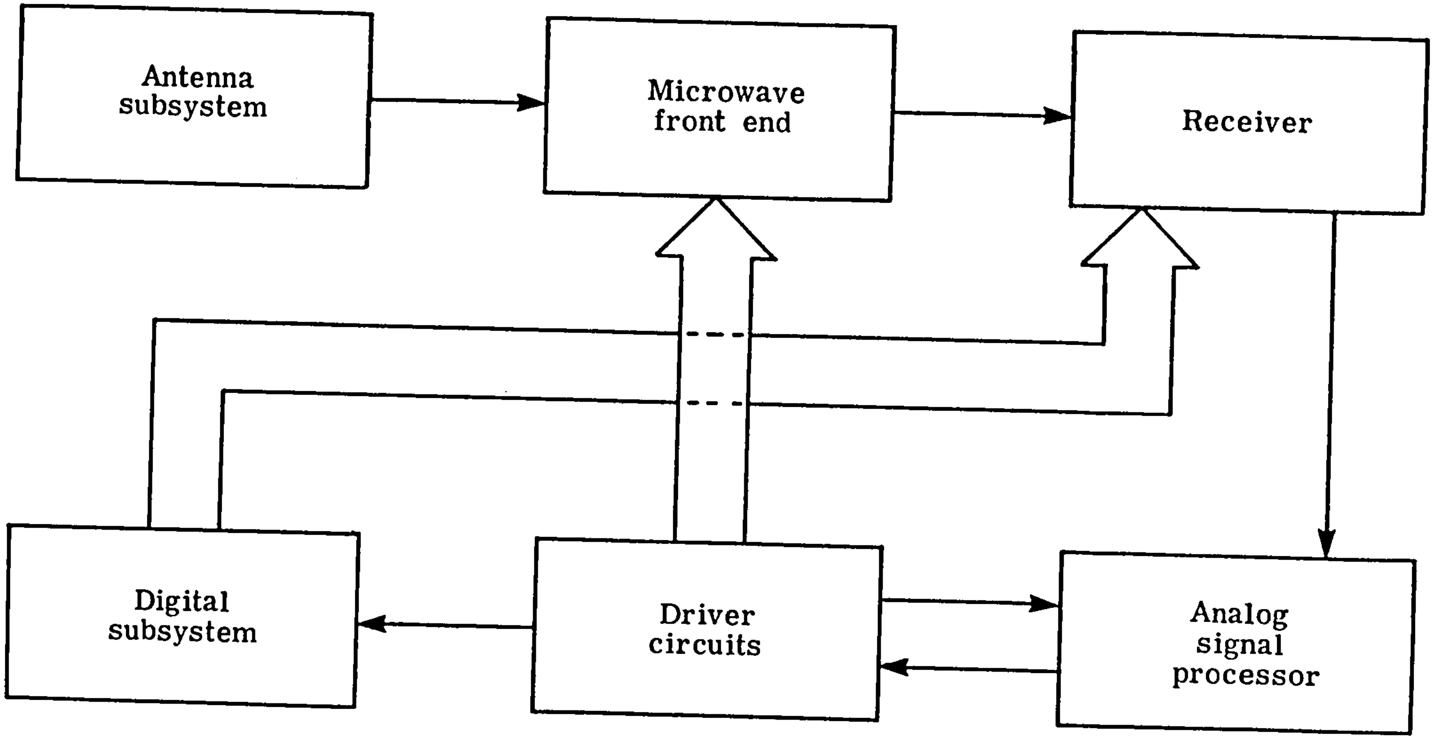

Figure 5.- Block diagram of stepped frequency microwave radiometer.

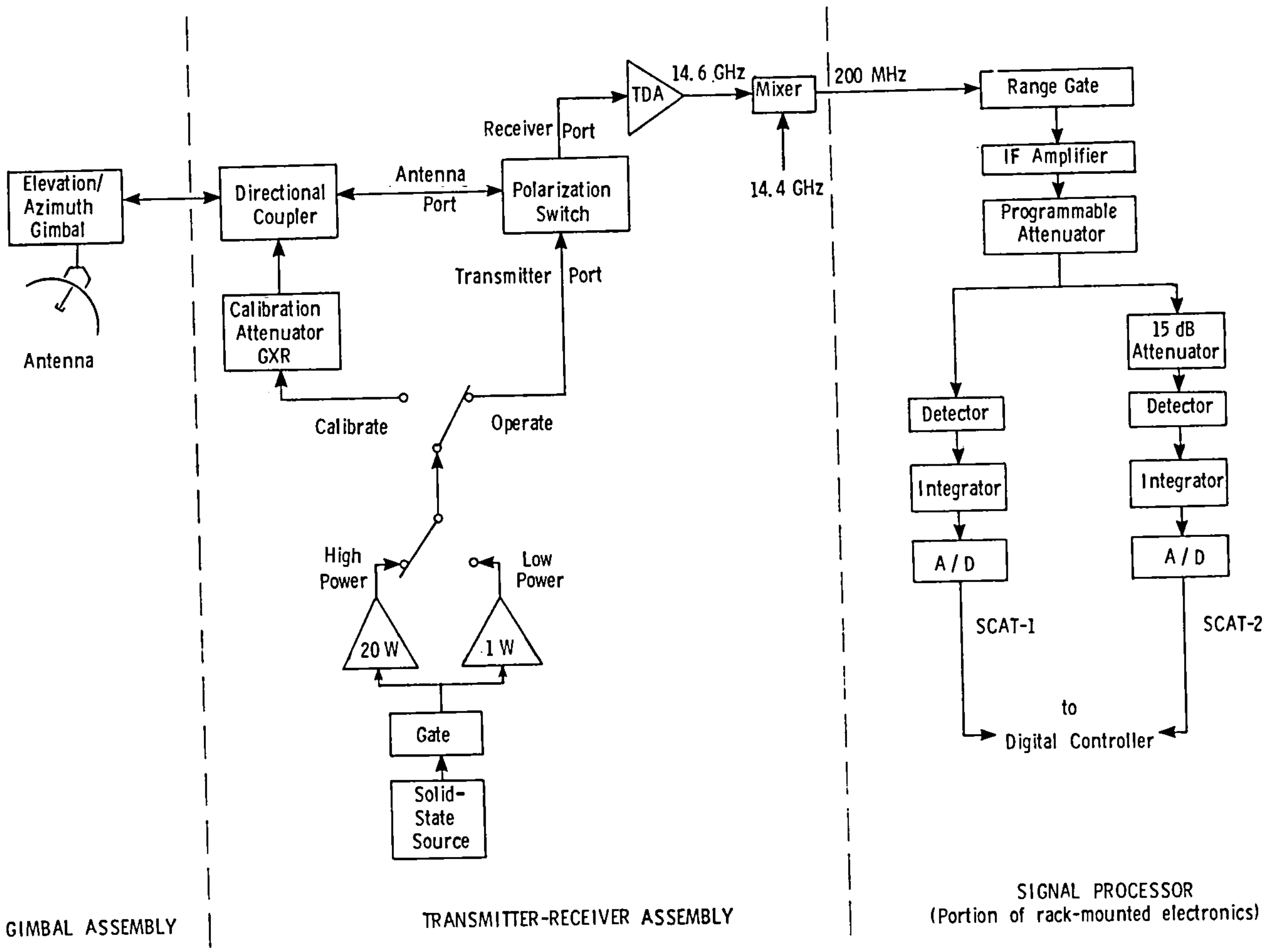

Figure 6.- Simplified block diagram of airborne microwave scatterometer. SCAT-1 indicates more sensitive channel; SCAT-2, less sensitive channel.

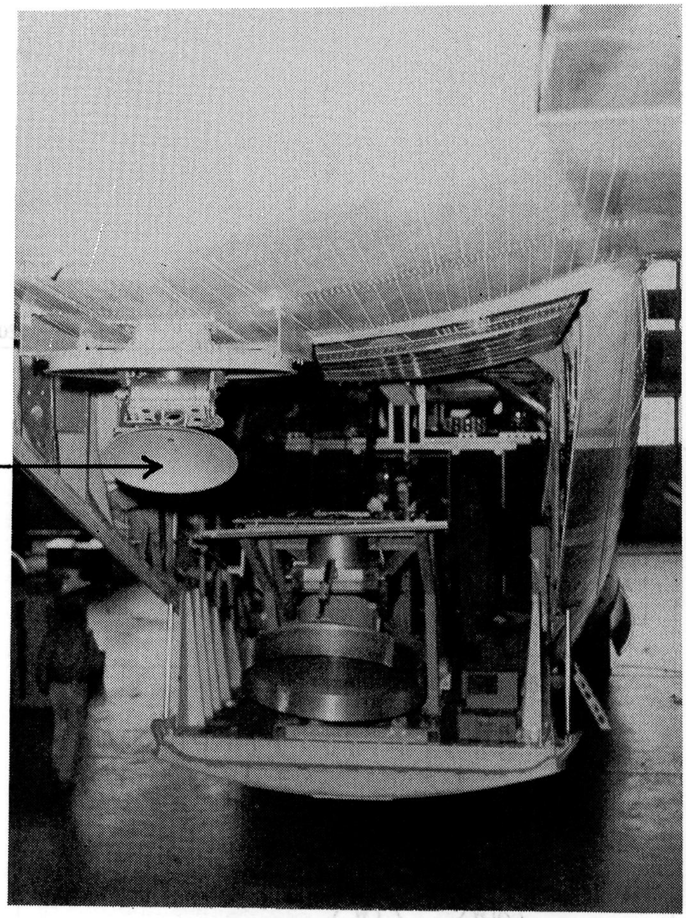

Figure 7.- Scatterometer gimbal assembly on C-130 aircraft.

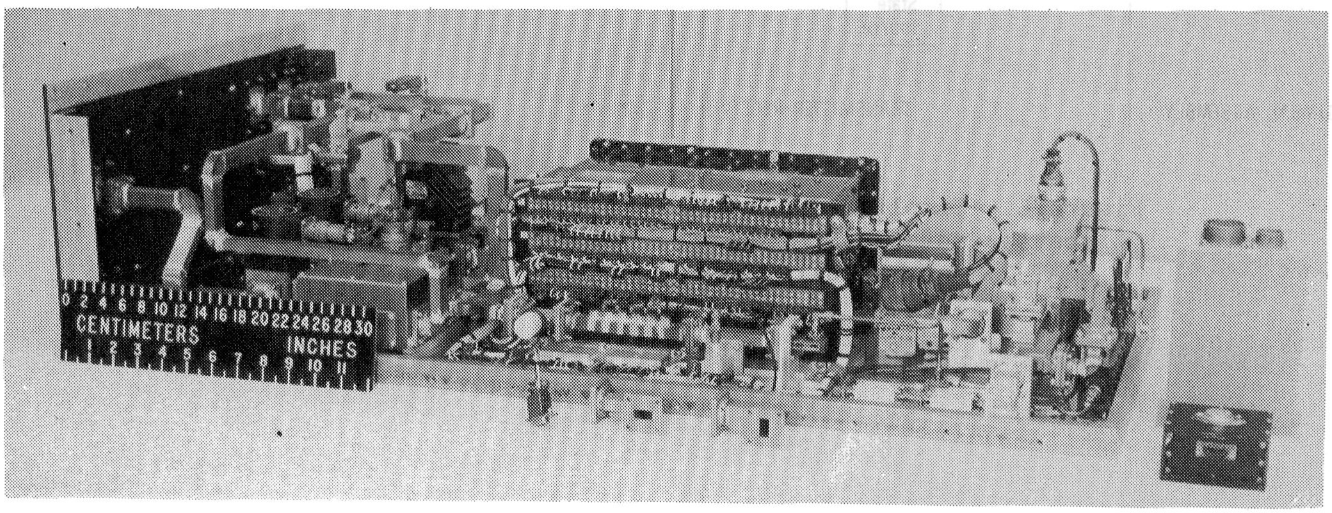

Figure 8.- Scatterometer transmitter-receiver assembly.

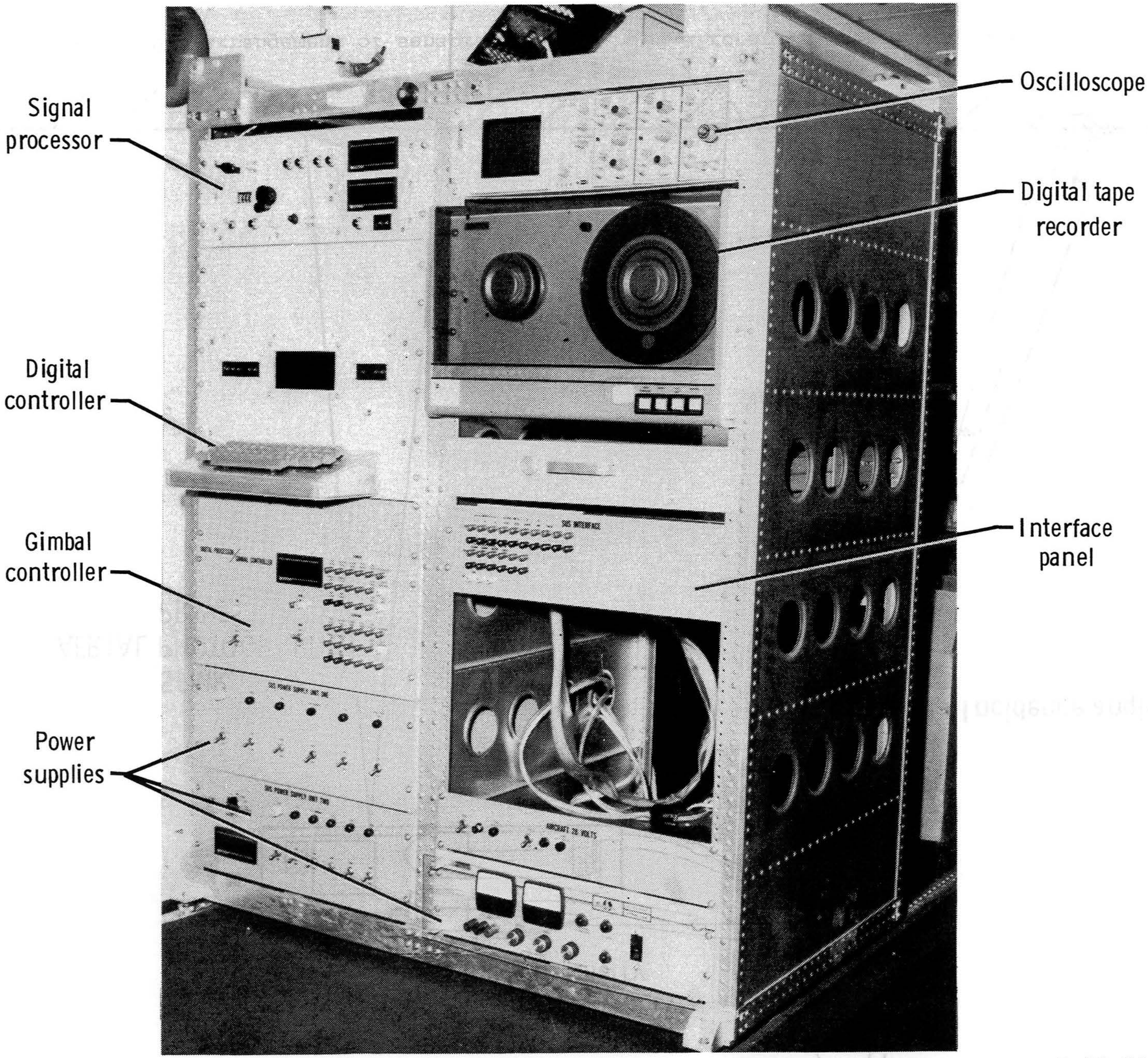

L-83-36

Figure 9.- Rack-mounted electronics for scatterometer.

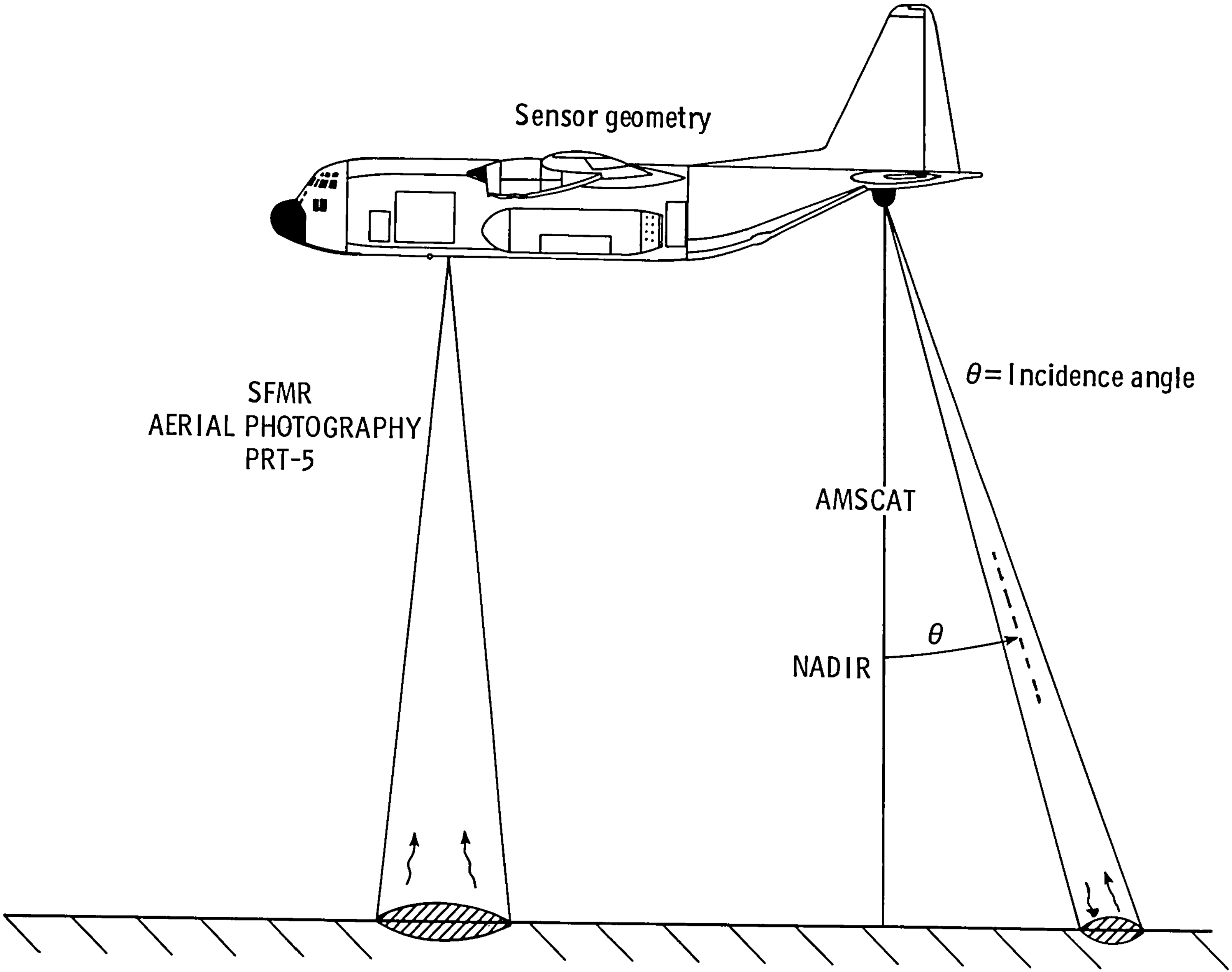

Figure 10.- Arrangement of sensors onboard C-130 aircraft. (Not drawn to scale.)

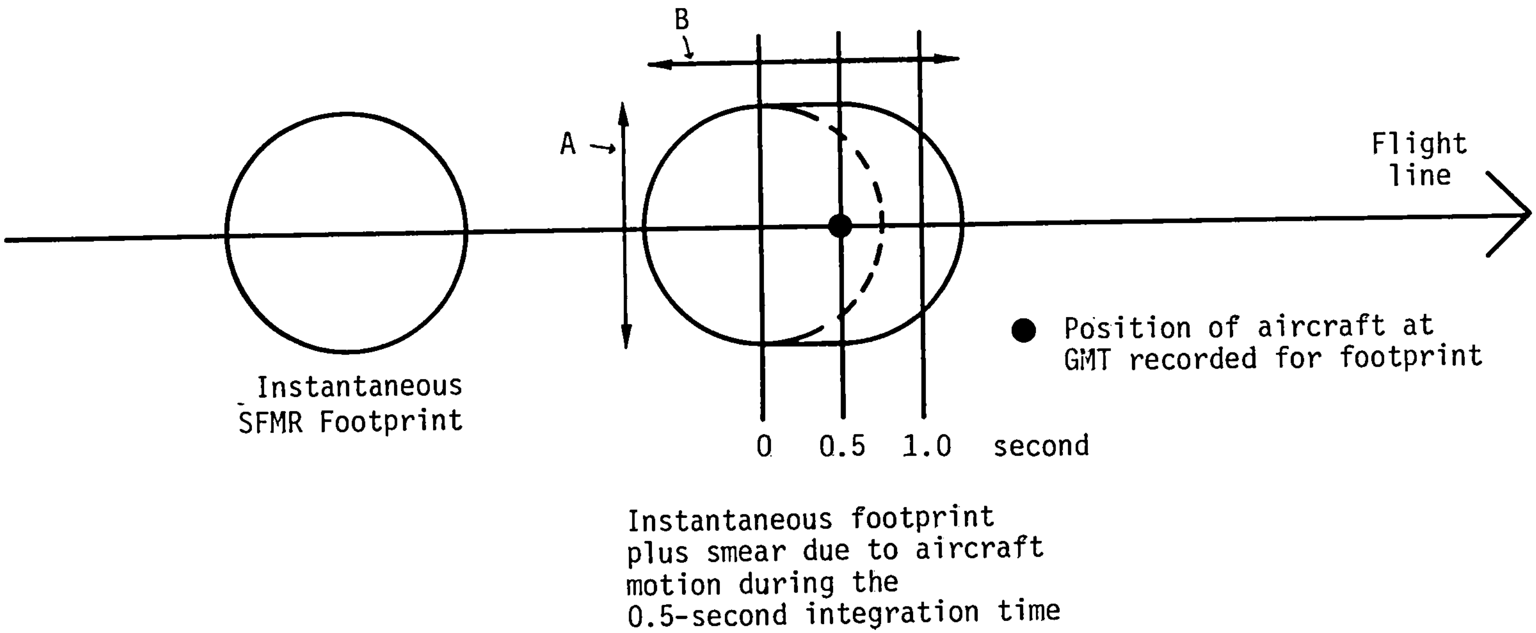

Figure 11.- SFMR footprints. (Not drawn to scale.)

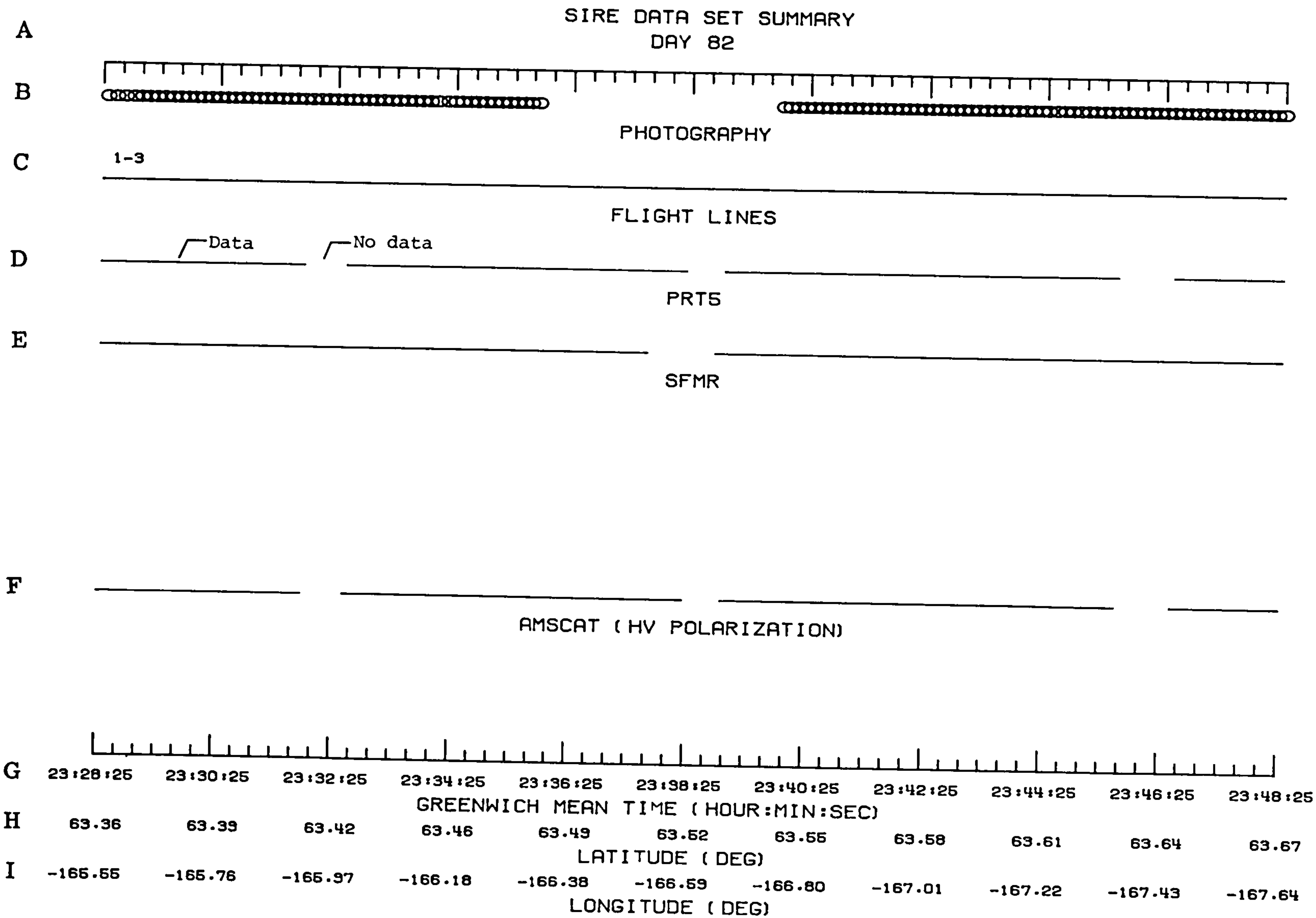

Figure 12.- Time-line plot.

1. Report No.	2. Government Accession No.	3. Recipient's Catalog No.
NASA TM-84609		

4. Title and Subtitle	
BEAUFORT/BERING 1979 MICROWAVE REMOTE SENSING DATA CATALOG REPORT - MARCH 14-24, 1979	5. Report Date: May 1983
	6. Performing Organization Code: 146-40-06-03
7. Author(s): William S. Hirstein, Harold F. Hennigar, Sally K. Schaffner, Victor E. Delnore, and William L. Grantham	8. Performing Organization Report No.: L-15554
	10. Work Unit No.
9. Performing Organization Name and Address: NASA Langley Research Center, Hampton, VA 23665	11. Contract or Grant No.
	13. Type of Report and Period Covered: Technical Memorandum
12. Sponsoring Agency Name and Address: National Aeronautics and Space Administration, Washington, DC 20546	14. Sponsoring Agency Code

15. Supplementary Notes

William S. Hirstein: Bionetics Corporation, Hampton, Virginia.
Harold F. Hennigar: Deepsea Ventures, Inc., Gloucester Point, Virginia.
Sally K. Schaffner: OAO Corporation, Hampton, Virginia.
Victor E. Delnore: Kentron International, Inc., Hampton, Virginia.
William L. Grantham: Langley Research Center, Hampton, Virginia.

16. Abstract

This report catalogs the airborne microwave remote sensing measurements obtained by the Langley Research Center in support of the 1979 Sea-Ice Radar Experiment (SIRE) in the Beaufort and Bering Seas. The remote sensing objective of SIRE was to define correlations between both active and passive microwave signatures and ice phenomena associated with practical applications in the Arctic. The instruments used by Langley during SIRE include the stepped frequency microwave radiometer (SFMR), the airborne microwave scatterometer (AMSCAT), the precision radiation thermometer (PRT-5), and metric aerial photography. Remote sensing data are inventoried and cataloged in a user-friendly format. The data catalog is presented as time-history plots of when and where data were obtained as well as the sensor configuration. All data are available on 9-track computer tapes in card-image format upon request to the National Technical Information Service (NTIS).

17. Key Words (Suggested by Author(s))	18. Distribution Statement
Microwave Remote sensing Radar signatures	Unclassified - Unlimited Subject Category 48

19. Security Classif. (of this report)	20. Security Classif. (of this page)	21. No. of Pages	22. Price
Unclassified	Unclassified	111	A06

National Aeronautics and
Space Administration

Washington, D.C.
20546

Official Business
Penalty for Private Use, $300

THIRD-CLASS BULK RATE

Postage and Fees Paid
National Aeronautics and
Space Administration
NASA-451

U.S.MAIL

NASA

POSTMASTER: If Undeliverable (Section 158 Postal Manual) Do Not Return